Final Report
NASA CR-112107
Project No. IITRI E6200
Contract No. NAS1-10716

INVESTIGATION OF THE USE OF
MICROWAVE IMAGE LINE INTEGRATED
CIRCUITS FOR USE IN RADIOMETERS
AND OTHER MICROWAVE DEVICES IN
X-BAND AND ABOVE

NASA-Langley Research Center
Hampton, Virginia

IITRI

Final Report
NASA CR-112107
Project No. IITRI E6200
Contract No. NAS1-10716

INVESTIGATION OF THE USE OF
MICROWAVE IMAGE LINE INTEGRATED
CIRCUITS FOR USE IN RADIOMETERS
AND OTHER MICROWAVE DEVICES IN
X-BAND AND ABOVE

NASA-Langley Research Center
Hampton, Virginia

Prepared by

R. M. Knox
P. P. Toulios
G. Y. Onoda

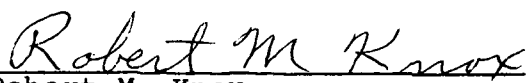IIT Research Institute
10 West 35th Street
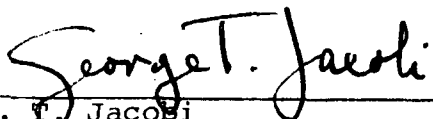Chicago, Illinois   60616

August 1972

FOREWORD

This is the Final Report on IIT Research Institute Project Number E6200, entitled, "Investigation of the Use of Microwave Image Line Integrated Circuits for Use in Radiometers and Other Microwave Devices in X-Band and Above," conducted for the National Aeronautical and Space Administration-Langley Research Center, Hampton, Virginia, under Contract NAS1-10716. The active program period was 12 April, 1971 to 26 July, 1972. Program participants included: R. Knox, project engineer, P. Toulios, G. Onoda, A. Ali, and K. Brandt. In addition to this report, various components developed during the course of the project were delivered to NASA-Langley Research Center. This report describes all significant theoretical and experimental results achieved during the project.

Respectfully submitted,

IIT RESEARCH INSTITUTE

Robert M. Knox
Research Engineer

APPROVED:

G. T. Jacobi
Assistant Director of Research
Civil Programs Office

ii

ABSTRACT

Program results are described in which the use of high permittivity rectangular dielectric image waveguide has been investigated for use in microwave and millimeter wavelength circuits. Launchers from rectangular metal waveguide to image waveguide are described. Theoretical and experimental evaluations of the radiation from curved image waveguides are given. Measurements of attenuation due to conductor and dielectric losses, adhesives, and gaps between the dielectric waveguide and the image plane are included. Various passive components are described and evaluations given. Investigations of various techniques for fabrication of image waveguide circuits using ceramic waveguides are also presented. Program results support the evaluation of the image line approach as an advantageous method for realizing low loss integrated electronic circuits for X-band and above.

TABLE OF CONTENTS

LIST OF FIGURES AND TABLES

LIST OF FIGURES AND TABLES (Cont.)

1. INTRODUCTION

Microwave integrated circuit techniques have developed rapidly in recent years in the frequency range from L- through X-band. The benefits which have resulted from MIC technology, namely savings in size, weight and cost, are also desired at frequencies above X-band. The principal form of transmission line for present MIC development has been the microstrip transmission line. However, in these higher frequency ranges the increased attenuation in microstrip makes it an undesirable choice for integration of microwave and millimeter-wave circuits.

The objective of the present program has been to investigate the use of high permittivity rectangular dielectric image waveguide for use in MIC's and to direct this investigation towards the application of image line integrated circuits in a 60-GHz switched Dicke-type radiometric receiver front-end module. This application would ultimately require the development of a ferrite switch, a preselector filter, a four-terminal hybrid, a downconverter, and a solid-state local oscillator. The approach taken in this program was to first enhance understanding of the basic transmission line properties. This activity included development of launchers from metal waveguide, measurement of attenuation, and determination of **radiation from curved waveguides**. The effects on attenuation of adhesive and gaps between the dielectric and the image plane were also investigated.

1

The development of various passive devices was also pursued. Included were a three-terminal junction, a four-terminal hybrid, a band-stop filter, and an attenuator.

Since the objective in developing the image line devices is a planar-type integrated circuit technology, considerable program activity was devoted to investigation and utilization of various ceramic waveguide fabrication methods. A final topic for investigation was incorporation of active devices in the image waveguide.

Section 2. relates the status of the image line technology as the program was initiated and also describes the benefits to be derived from this MIC approach. In Section 3. the various transmission line properties are examined. The two following sections--Sections 4. and 5.--relate program activity and results on passive components and active devices. Section 6. covers the subject of fabrication methods. The report concludes with conclusions and two Appendices describing theoretical models for the minimum radius-of-curvature analysis described in Section 3.

Many of the basic transmission line investigations were carried out in X-band. These were continued also experimentally in V-band. The activity on the band-stop filter and mixer diodes was also in V-band. These results confirm the original and fundamental premise that the image line indeed offers the opportunity for realization of very low-loss integrated circuits in the millimeter wavelength range.

2

2. BENEFITS AND STATUS OF THE MILIC TECHNOLOGY

2.1 Introduction

The status of the Microwave Image Line Integrated Circuit (MILIC) technology at the time the present program was initiated will be reviewed briefly in the subsections below. The remaining sections of this report will describe the program activity and results. The benefits of the image line approach to microwave integrated circuits will be presented in Section 2.3 below.

2.2 The Dielectric Image Line -- Historical Development

The image line was investigated as a form of waveguide in the 1940's and 1950's. The early investigations were limited to the semicircular dielectric image line in which low permittivity ($\varepsilon_r = 2.5$) materials were used.[1,2,3,4,5] Because only low permittivity materials were used, the early investigators found that the image line showed rather poor guidability; i.e., unless a rather large radius of curvature was used, the line had a tendency to radiate significant amounts of the energy it was guiding.

Early work also included investigations of passive devices. Launchers from waveguide,[4] horns,[2] wires and slots,[6] and coaxial cables[7] were designed. The image line as an antenna[8] was evaluated. Various forms of dielectric resonators[9,10,11] as well as directional couplers[12,13] were also considered. Very little of practical value was derived from the early work, primarily because of the low-permittivity materials used and the resulting tendency towards radiation at curves and discontinuities.

3

An indication that the use of higher permittivity dielectric materials would significantly improve the waveguide "guidability" can be found in the dispersion curves given by Schlesinger and King[14] in 1958. In this same publication the authors described experimental measurements of guide wavelength on various rectangular cross-section dielectric waveguides.

In 1969 Knox and Toulios[15] published an experimentally verified model for the rectangular dielectric image guide and proposed that this waveguide serve as the transmission line for low-loss microwave and millimeter-wave integrated circuits. A subsequent publication[16] provided an analysis of the dielectric and conductor losses in the rectangular image line. The theoretical attenuation factors were verified by experiment. A third publication[17] considered the application of parallel image lines to the design of a directional coupler. A directional coupler was fabricated for operation in X-band and was found to have coupling characteristics in good agreement with theoretical prediction.

The use of high permittivity image lines ($\varepsilon_r \simeq 6$ or greater) with a rectangular cross-section is essential to the Microwave Image Line Integrated Circuit* concept as formulated at IITRI

---

* In the MILIC acronym the words Microwave or Millimeter-wave are interchangeable depending on the frequency range of greatest interest in a given context.

and further developed under the present program. A unique family of distributed signal processing devices has been conceived; some of these devices have been investigated under this program. The rectangular cross-section of the dielectric image line is preferable for the planar-type hybrid integrated circuit fabrication processes which are described herein. The primary advantage of the dielectric image line is low attenuation and high-circuit component Q. A comparison has been made[18] between alumina image line and microstrip transmission line. The results of this comparison will be summarized in the following subsection.

2.3 Benefits of the MILIC Approach to MIC's

The dielectric image line offers the prospect of a low-loss planar-type transmission line for fabrication of microwave and millimeter-wave hybrid integrated circuits. Since the principal benefit of this transmission line is low attenuation, a comparison will be made with microstrip, the transmission line which is generally used for MIC design and fabrication. In this comparison it will be assumed that alumina is used for the dielectric material in both transmission line configurations.

The alumina rectangular image guide is shown in Figure 1a. The corresponding microstrip line on alumina substrate is shown in Figure 1b. The latter has served as the primary form of transmission line for microwave integrated circuits in recent years. At higher frequencies (approximately X-band) the conductor losses in the center strip become excessive and make this form of line a less desirable choice for circuit integration work.

5
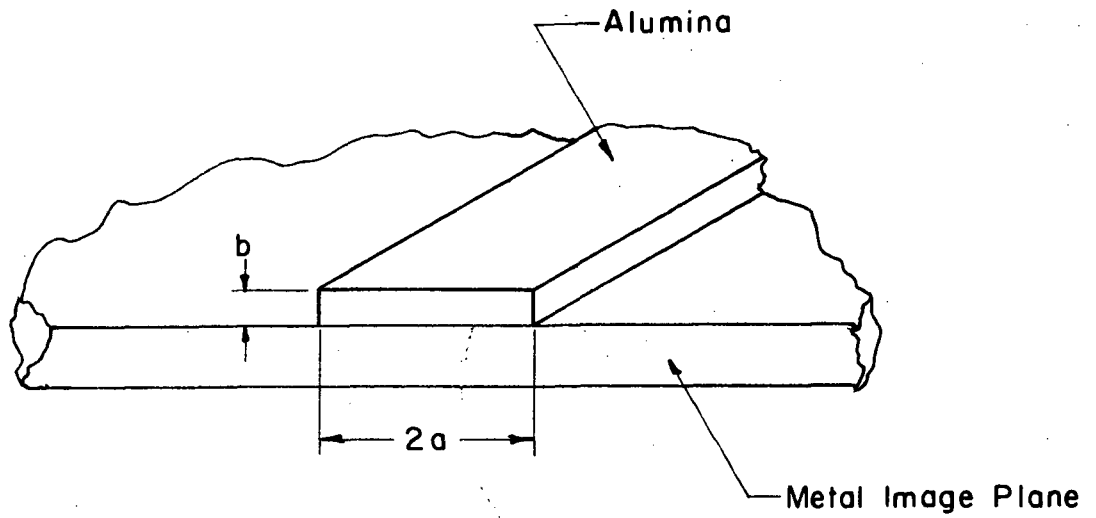
Fig. 1a   Alumina Image Guide
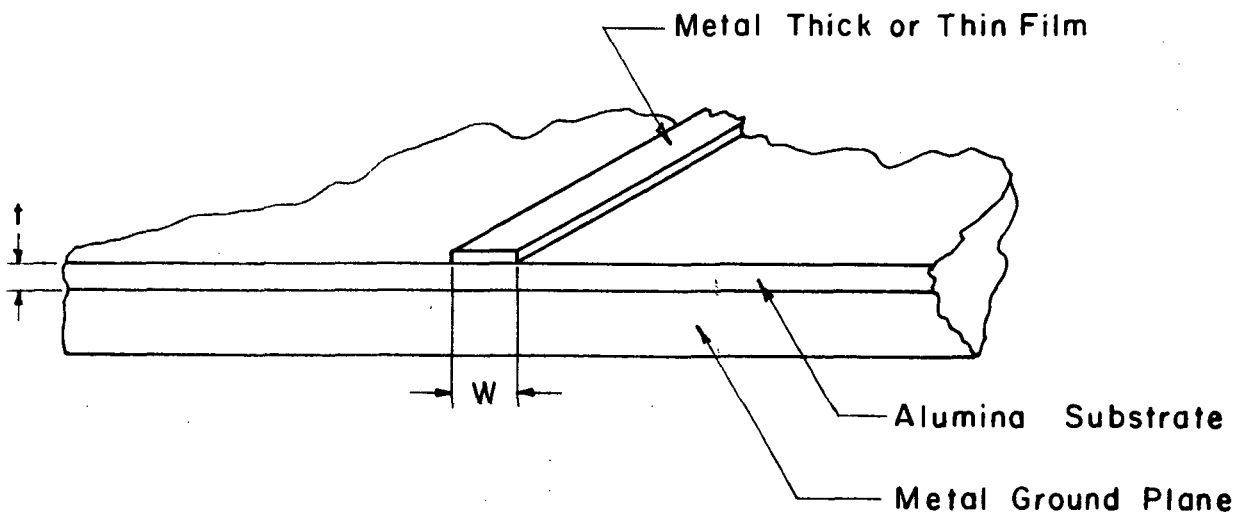
Fig. 1b   Alumina Microstrip Line

The relative dielectric constant of alumina is usually between 9 and 10. The modal dispersion solutions of the rectangular image guide for a dielectric constant of 9 are shown in Figure 2 (from Reference 15). The parameter B, the normalized height of the guide, is given by

$$B = \frac{4b}{\lambda_o} \sqrt{\epsilon_r - 1}$$

which for $\epsilon_r = 9$ is

$$B = \frac{11.3b}{\lambda_o}$$

Dispersion curves are shown for the fundamental mode E_{11}^y and the first higher order mode E_{21}^y for aspect ratios of 1 and 2. For the specified guide configuration the curves give guide wavelength as a function frequency. It can be seen that the image guide has a useful single-mode frequency range limited by higher order modes for larger values of B and poor guidability for smaller values of B.

Losses in both the alumina image guide and alumina microstrip guide are compared in Table 1. The results for an alumina image guide on an aluminum image plane are based on theoretical calculations presented earlier[16] and are for a typical operating point (B = 1.6) on the dispersion curves of Figure 2. The theoretical losses for an alumina microstrip line using gold conductors are derived from published results.[19,20] Table 2 gives theoretical losses in silver plated rectangular metal waveguide. The attenuation factor in alumina image guide is about 14 times

7
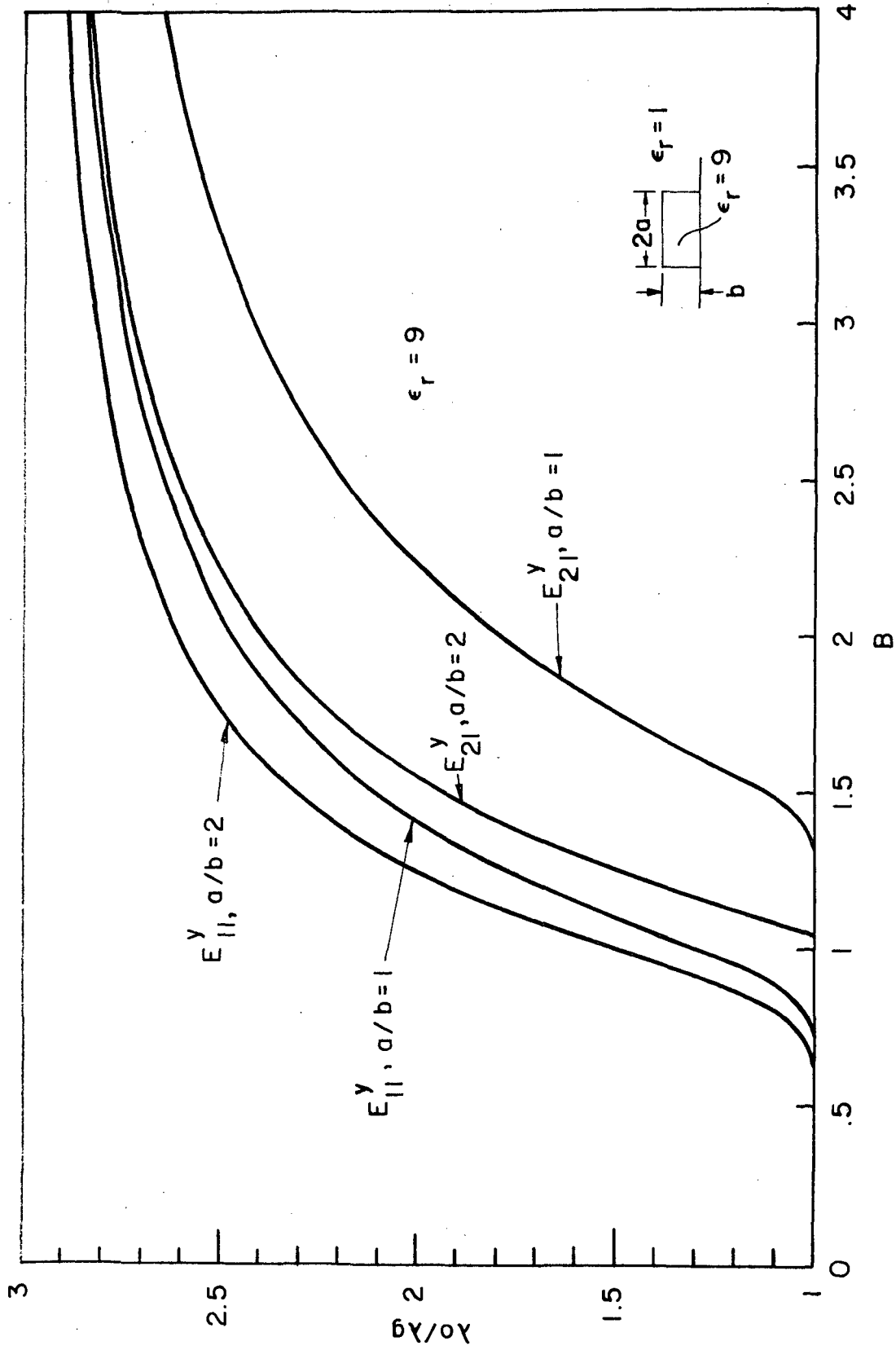
Fig. 2 GUIDE WAVELENGTH FOR VARIOUS MODES OF THE DIELECTRIC IMAGE LINE ($\epsilon_r = 9$ AND $a/b = 1, 2$)

8

Table 1

THEORETICAL ATTENUATION FACTOR AS A FUNCTION OF FREQUENCY
FOR IMAGE GUIDE AND MICROSTRIP

Frequency f (GHz)	Conductivity (Mhos/Meter)	Loss Tangent tan δ	Attenuation Factor α (dB/λ_g)	Unloaded Q* Q_u	Ratio**
		IMAGE LINE			
7.5	3.72×10^7	0.0001	0.0140	1940	14.0
15	3.72×10^7	0.0001	0.0180	1510	15.3
30	3.72×10^7	0.0001	0.0236	1150	16.4
60	3.72×10^7	0.0001	0.0317	860	17.3
90	3.72×10^7	0.0001	0.0378	720	17.5
		MICROSTRIP			
7.5	4.1×10^7	0.0001	0.196	139	
15	4.1×10^7	0.0001	0.275	99	
30	4.1×10^7	0.0001	0.388	70	
60	4.1×10^7	0.0001	0.548	50	
90	4.1×10^7	0.0001	0.662	41	

* $Q = \dfrac{27.2}{\alpha}$

** Ratio of attenuation of 50-ohm alumina microstrip line to that of alumina image line.

Table 2

THEORETICAL ATTENUATION FACTOR AS A FUNCTION OF FREQUENCY
FOR SILVER PLATED WAVEGUIDE

Frequency f (GHz)	Waveguide Designation WR ( )/μ	Guide Wavelength λ_g (In)	Attenuation Factor (dB/λ_g)	Ratio**
7.5	137*	2.075	0.0047	2.98
15	62	1.016	0.0049	3.68
30	28	0.544	0.0109	2.16
60	15	0.263	0.0104	3.04
90	10	0.174	0.0128	2.95

* Aluminum waveguide, unplated.

** Ratio of alumina image line attenuation to that of silver plated waveguide.

lower than that in alumina microstrip guide but about three times higher than in conventional waveguide at 7.5 GHz.

The ratio of microstrip to image guide losses increases slightly as frequency is increased. The lower attenuation in image guide is primarily due to the absence of the conduction losses in the center strip of the microstrip. Because of geometrical considerations the current density in the ground plane is less for the image guide, thus contributing less conductor loss than is the case for the microstrip guide.

The physical dimensions for the alumina image guide and microstrip guide are compared in Table 3. It can be seen that, if an image guide with an electrical aspect ratio of one is compared with a 50-ohm microstrip line, the image guide is about 12 times wider and about six times thicker. The larger guide dimensions for the image line not only contribute to lower ground plane losses but imply as well that dimensional tolerances will be considerably relaxed. This becomes an important consideration as frequency is increased in the millimeter wavelength range. In the X-band range the alumina image guide could be used for circuit integration where the low-loss/high-Q performance is important and the larger guide dimensions can be tolerated. Note, however, that conventional X-band waveguide is about three times the width of the image guide required for 10-GHz operation. Therefore, the alumina image waveguide offers considerable space savings with respect to conventional waveguide.

Table 3

TYPICAL DIMENSIONS AS A FUNCTION OF FREQUENCY
FOR ALUMINA IMAGE LINE AND MICROSTRIP LINE

Frequency f(GHz)	Image Line		Microstrip*	
	Height b(In.)	Width 2a(In.)	Thickness t(In.)	Strip Width w(In.)
7.5	0.22	0.44	0.036	0.036
15	0.11	0.22	0.018	0.018
30	0.055	0.11	0.009	0.009
60	0.0275	0.055	0.0045	0.0045
90	0.0183	0.0366	0.003	0.003

* Microstrip substrate thickness selected so as to be maximized (to minimize losses) and yet small enough so that the lowest order TM_o surface mode cannot be supported (Ref. 20).

These theoretical attenuation results indicate that, in the upper microwave frequency range and in the millimeter wavelength range, the alumina image line can be used for circuit integration with better than an order of magnitude improvement in performance relative to alumina microstrip. The fact that the size of the alumina image guide is several times larger than the alumina microstrip line is viewed as an advantage in the millimeter wavelength range.

3. TRANSMISSION LINE PROPERTIES

.3.1 Introduction

Various transmission line properties of the dielectric image waveguide have been investigated both prior to the initiation of this program[15,16] and during its course as well. The subsections below describe program activity relating to image waveguide transverse field distributions, attenuation in image waveguide, and excess radiation attenuation due to curvature. The first topic considered is the design of launchers from metal rectangular waveguide.

3.2 Launchers from Metal Rectangular Waveguide to Image Waveguide

A microwave or millimeter wave integrated module will usually receive one or more signals from outside the module. The incoming signal may be carried on a rectangular or circular metal waveguide, coaxial cable, or in some cases, a dielectric waveguide. Launchers from all of these forms of transmission line into the dielectric image line are therefore of interest.

The most immediate concern for the present program was launchers from metal rectangular waveguide because all test instrumentation used to characterize various image line devices operated with rectangular waveguide. Experimental investigations of these launchers in various configurations were conducted. A primary motivation was simplicity of construction consistent

with good efficiency. The designs investigated were those in which the major fabricative variations were carried out on the metal part of the launcher with only minimal shaping of the dielectric required. All launcher designs were developed for a relative dielectric constant of 9-10.

Typically, the ratio of metal waveguide transverse dimensions to those of image waveguide will be about $\sqrt{\varepsilon}$. Standard metal waveguide dimensions for X-band are 0.9 in. by 0.4 in. The image waveguide dimensions employed during this program for all X-band waveguides were 0.250 in. by 0.125 in.* Impedance matching requires that the two waveguides be made physically and electrically compatible gradually over a length of transmission line, ranging from two to six wavelengths.

Two sources of excess attenuation** were found to be important in these launchers. If complete transformation of the fields from the TE_{10} mode in the metal waveguide to the E_{11}^y mode in the image guide does not occur, then excess attenuation due to radiation will result. The second form of excess attenuation is the conduction loss in the metal walls of the launcher. Since conduction losses cannot be completely eliminated, primary emphasis of the launcher design activity was to minimize radiation losses.

---

* The dimensions chosen here were deliberately made somewhat smaller than otherwise advisable because it was of interest to operate the waveguide over the range of frequencies where guidability is poor, i.e., $B < 1.2$ for $\varepsilon = 9$ and $a/b = 1$.

** Excess attenuation implies attenuation exceeding that which is typical for the transmission line outside of the launcher.

Four types of launchers which successively increase in degree of complexity, but which do not necessarily improve in performance as the complexity increases will now be described. The general structure of these launchers is shown in Figure 3. This particular drawing most closely resembles the launcher designated type B below. The specific construction and dimensional designations will be given in subsequent figures for each of the four types.

The first launcher design, herein designated type A, is shown in Figure 4. No changes in the walls of the metal waveguide were made. The dielectric image waveguide was tapered to a point over a length ℓ. The end of the taper region was located with respect to the output end of the metal waveguide at the distance d. Five variations of this configuration were measured with ℓ ranging from 1 to 2 in. and d ranging from +0.25 in. to -0.25 in. The best result was obtained with $\ell = 1.5$ in. and d = 0.25 in. The test line was a "U" waveguide for X-band operation as shown in Figure 5.* The radii of the curves were 2.0 in. The measured

---

*This same waveguide was also used for field distribution measurements, the fields being probed through the holes in the image plane. The image waveguide was attached with Eastman 910 adhesive.

16

Metal Waveguide Flange

Metal Waveguide

Base Plate

Metal Taper Insert

Dielectric Waveguide
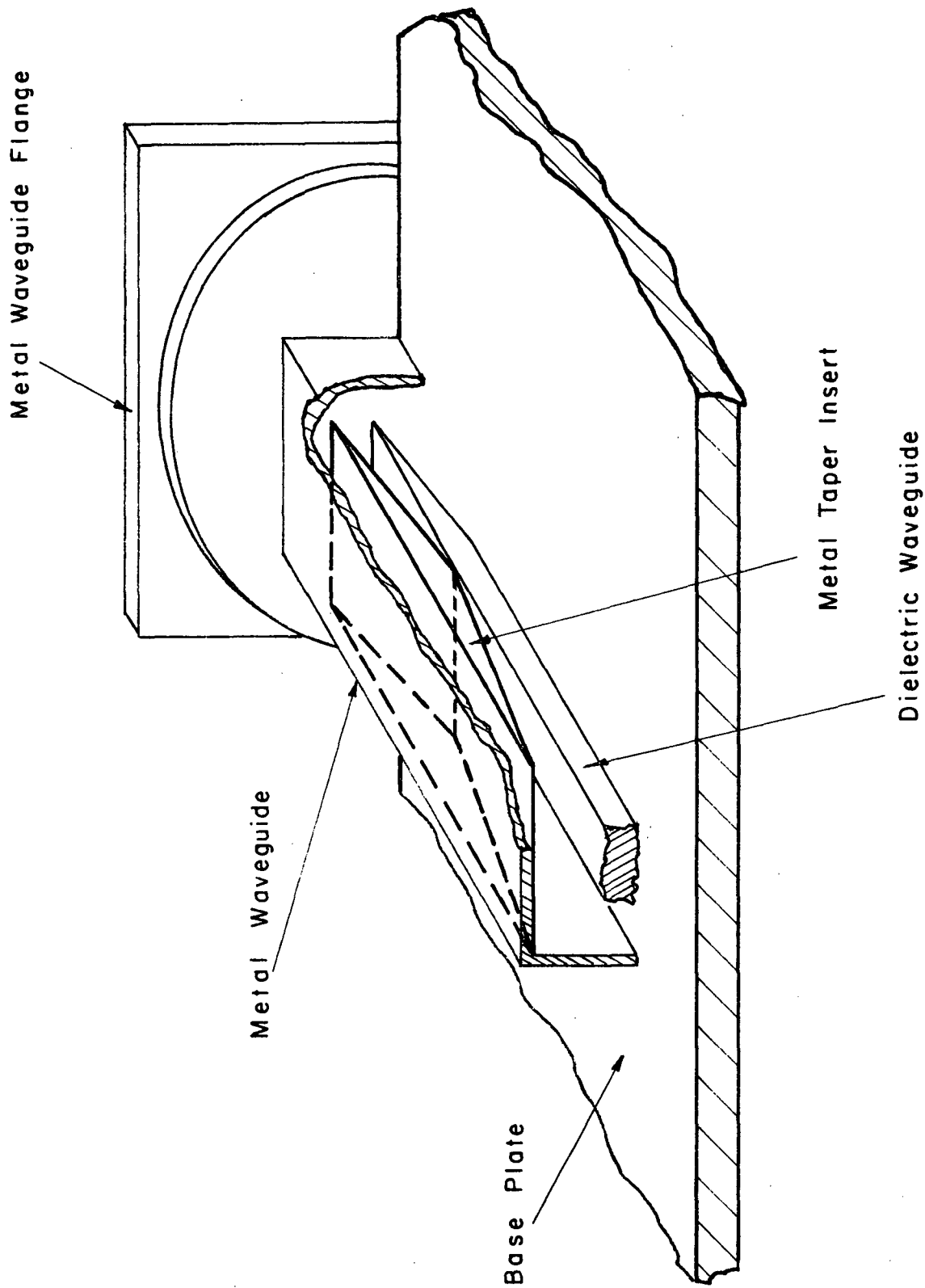
Fig. 3   DETAIL OF GENERAL STRUCTURE OF THE LAUNCHER
         DESIGNS FOR METAL WAVEGUIDE

17

Image Plane

Image Waveguide

Metal Waveguide

d

ℓ

TOP VIEW

Image Waveguide

Metal Waveguide

Image Plane

SIDE VIEW
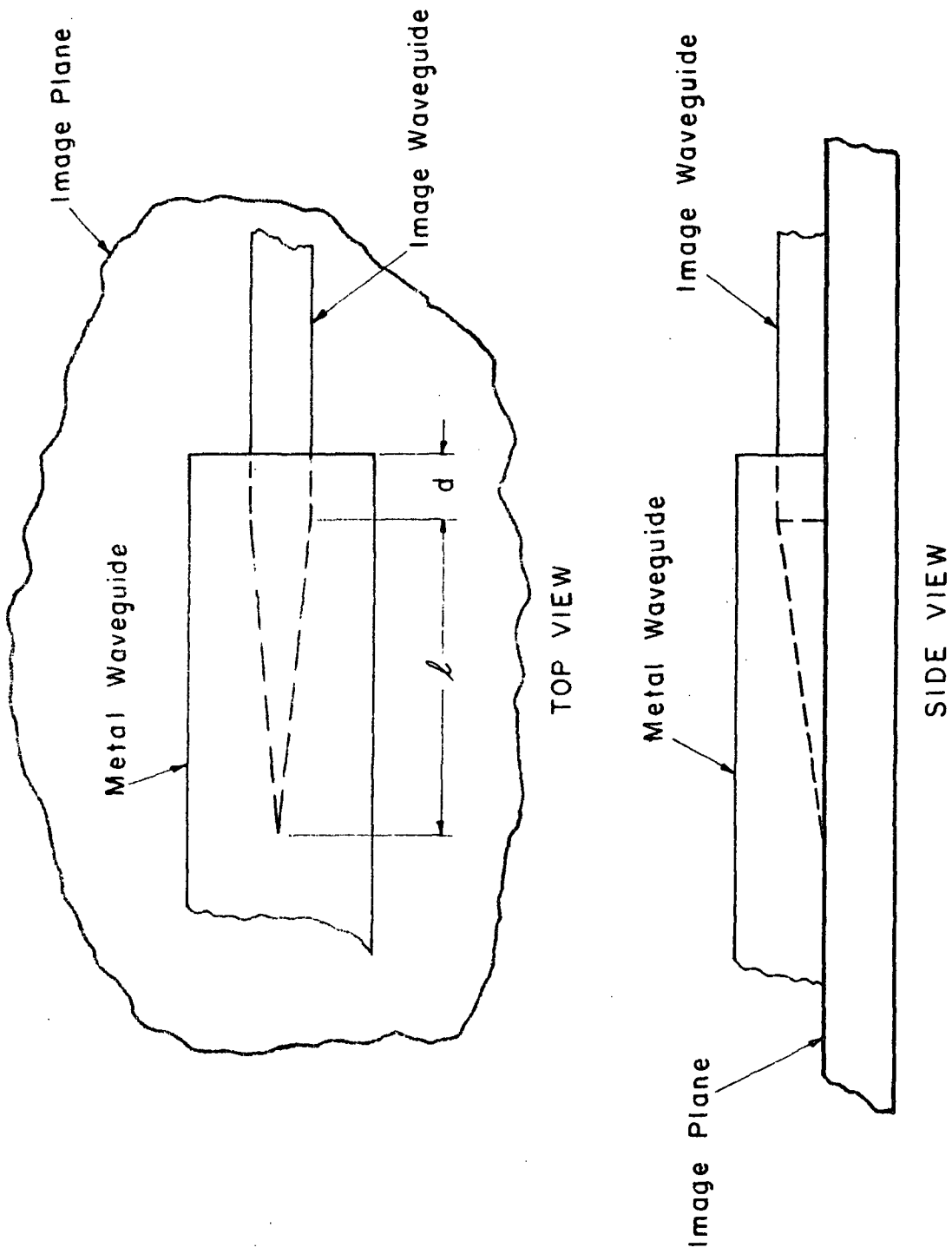
Fig. 4   TYPE A LAUNCHER CONFIGURATION

18
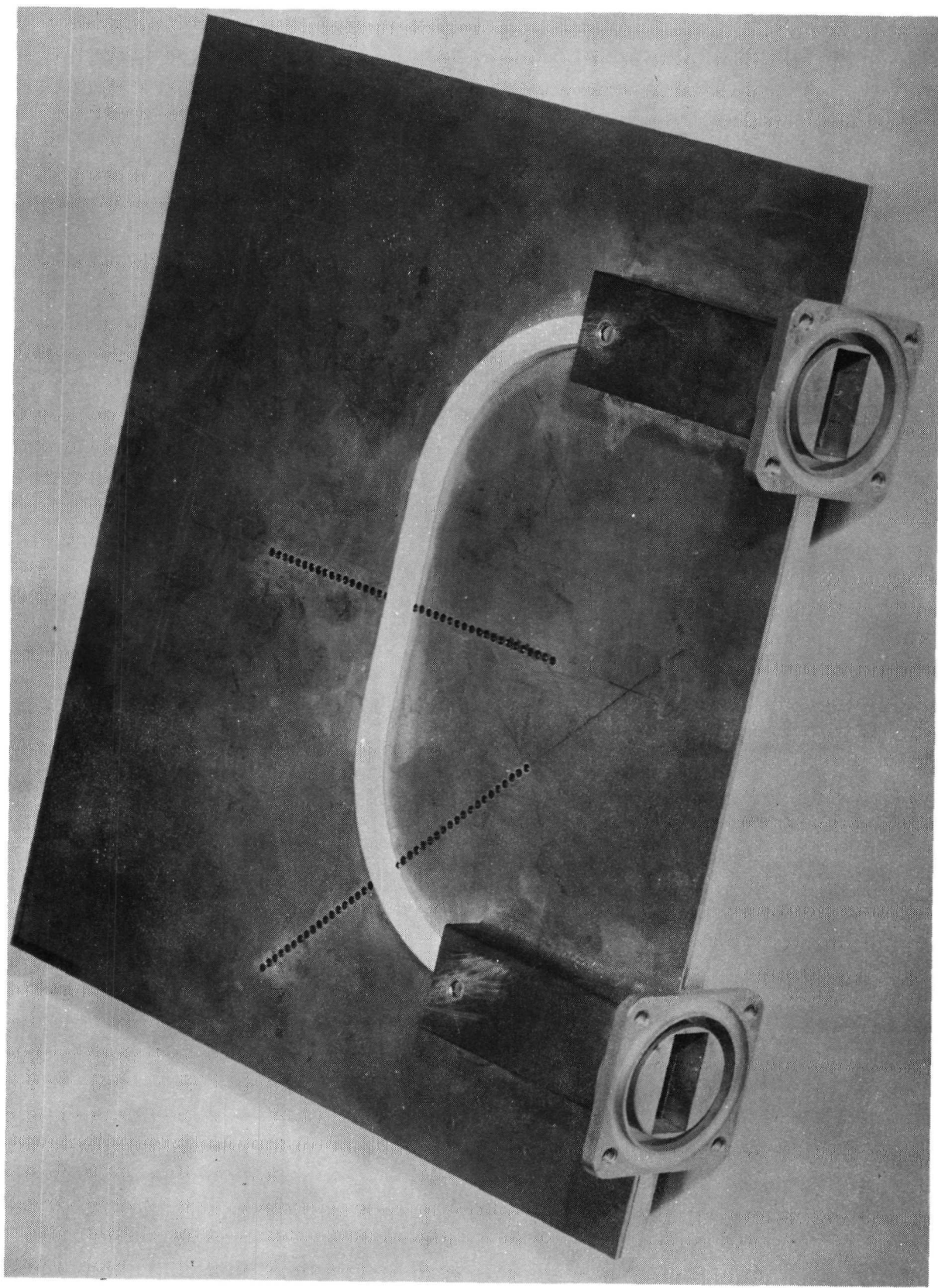
Fig. 5   X-BAND "U" WAVEGUIDE FOR EVALUATION OF LAUNCHERS

results for this type A launcher are shown in Figure 6. The excess attenuation below 10 GHz was due to radiation from the two curves on the "U" waveguide. Above 10 GHz typical attenuation was 2.7 to 3.0 dB with the minimum total attenuation being 2.6 dB, of which 1.6 dB was determined to be losses in the image waveguide (see Section 3.3). Therefore, the attenuation per launcher was 0.5 dB. The maximum input VSWR for this "U" waveguide was 1.6:1 with typical values 1.3:1 or less, as shown in Figure 5.

The next launcher configuration investigated involved introducing tapers in the top wall of the metal waveguide for the purpose of improving the mode coupling between the two types of waveguide. This configuration, designated type B, is shown in Figure 7 (see also Figure 3). The dielectric image line was given a uniform 1.0-in. taper in both planes to a point. A metal insert with double tapers was provided with the shape described by the dimensions ℓ,d, and s, shown in Figure 7.

Several variations of this launcher were tried with ℓ and d ranging from 1.0 to 2.0 in. in various combinations and various values of s. Results for three of these variations are shown in Figures 8-10. The low VSWR but high attenuation,for s = 0.128 in., shown in Figure 8, indicates excess radiation loss which increased considerably between 10 and 12 GHz.* The

---

* Excess loss below 10 GHz is once again attributable to radiation from the curves of the "U" waveguide.
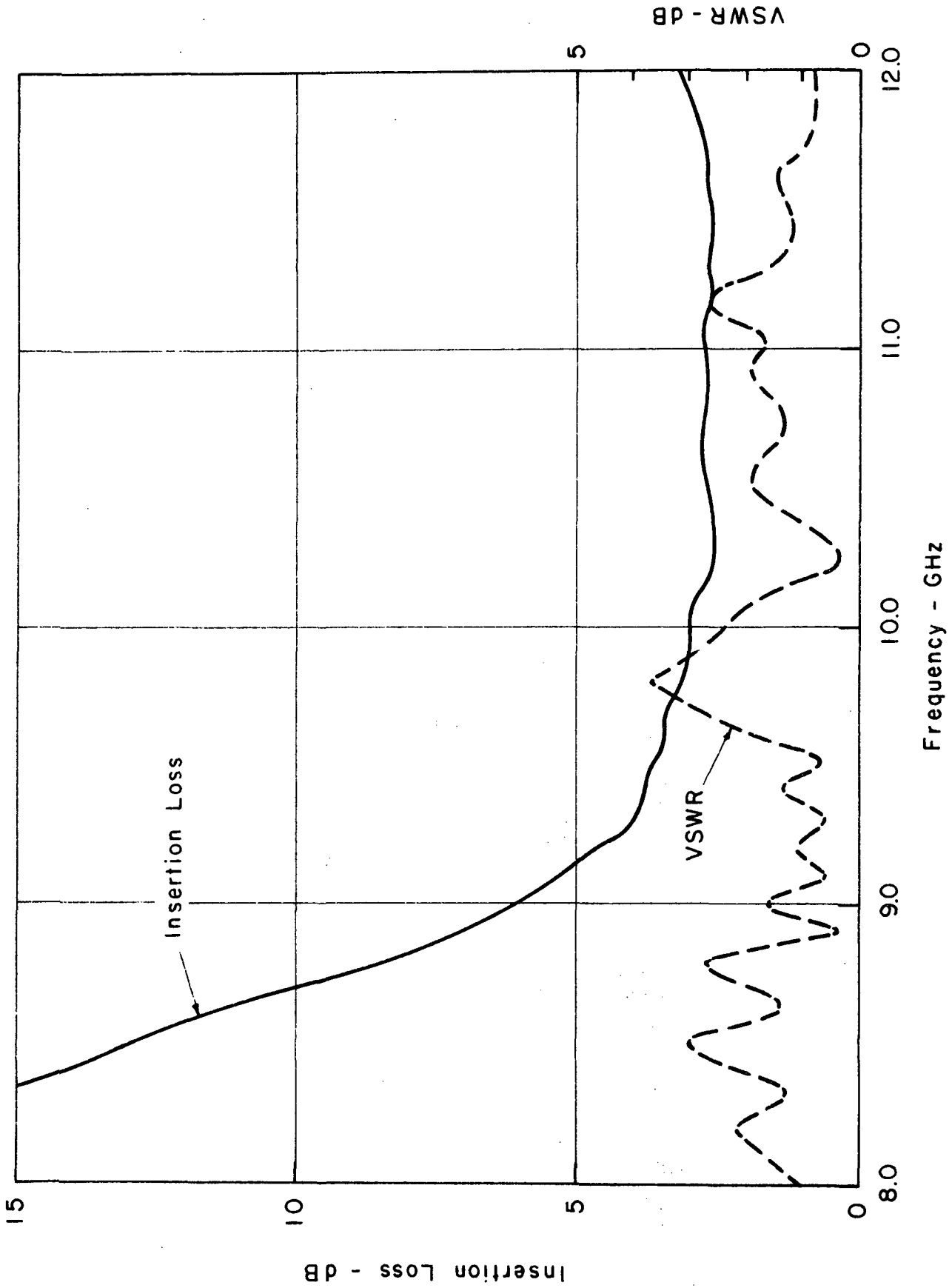
Fig. 6   MEASURED LOSS AND VSWR FOR THE TYPE A LAUNCHER WITH $\ell = 1.5$ in AND $d = 0.25$ in.

21

Fig. 7   TYPE B LAUNCHER

Labels in figure (top view):
Image Plane
Image Wavequide
Metal Wavequide
Metal Taper
TOP VIEW

Labels in figure (side view):
Image Wavequide
Image Plane
Metal Wavequide
SIDE VIEW
d
ℓ
s
1.0 in
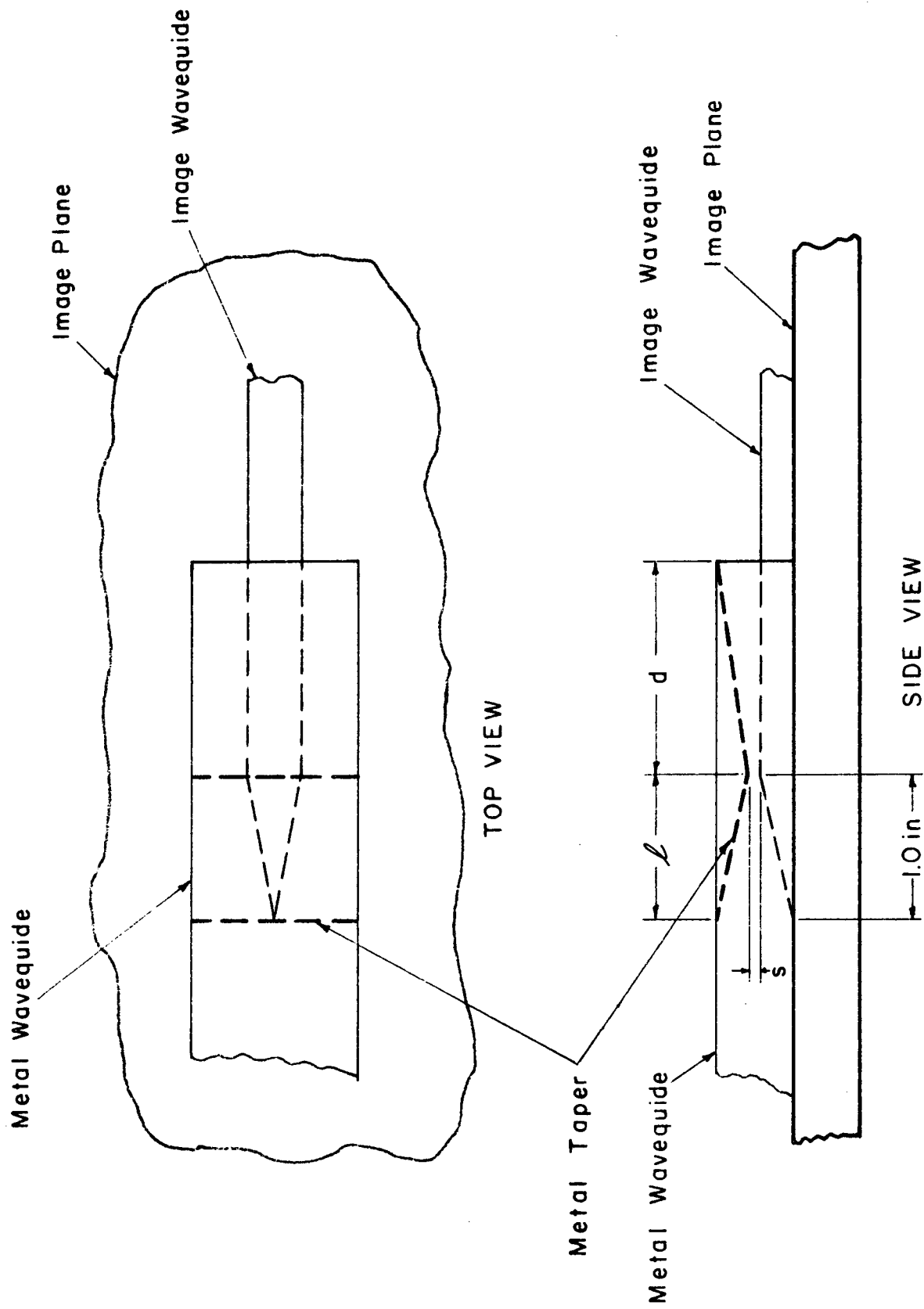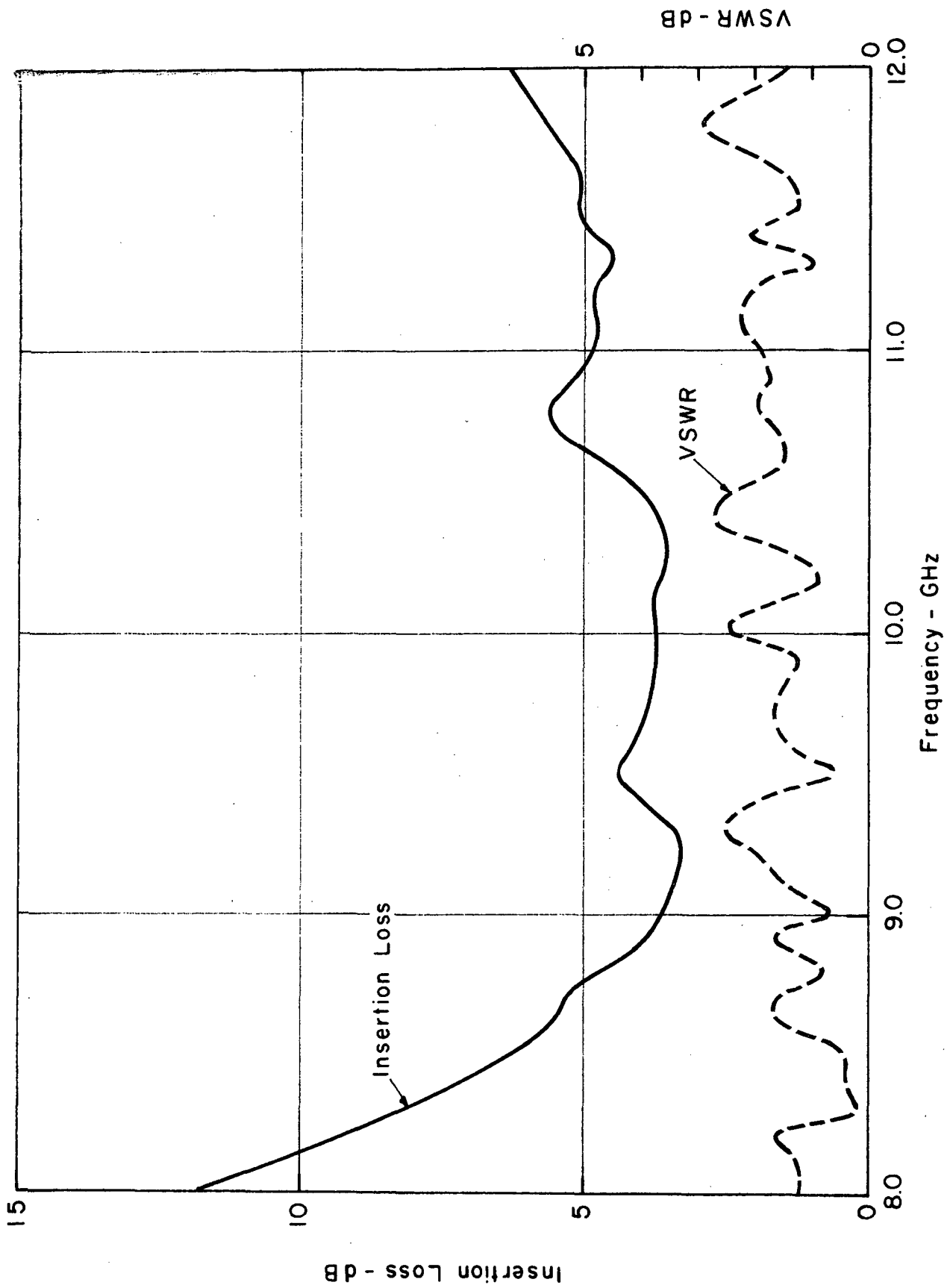
Fig. 8   MEASURED LOSS AND VSWR FOR THE TYPE B LAUNCHER WITH
$\ell = 2.0$ in., $d = 1.0$ in. AND $s = 0.128$ in.

23
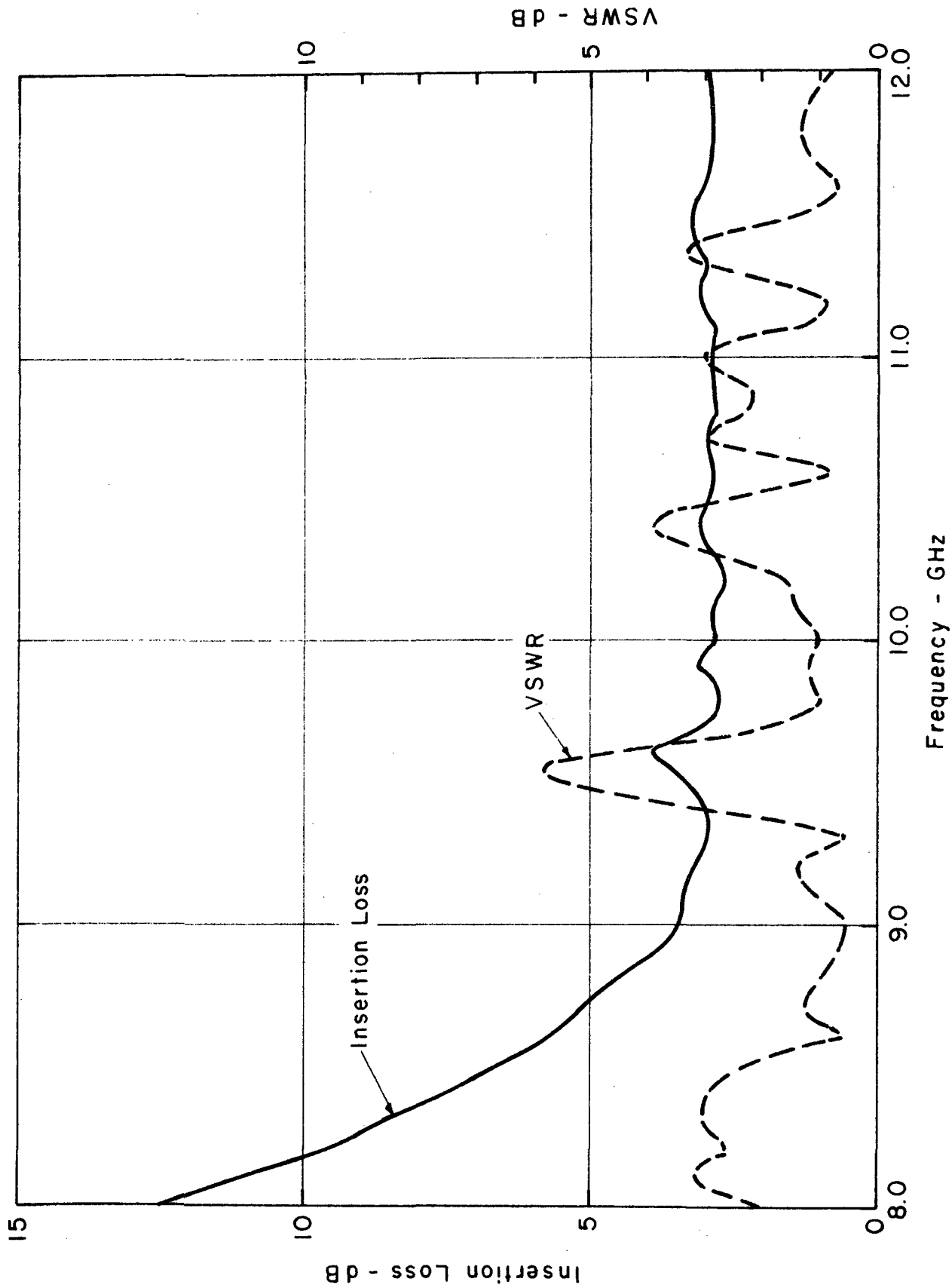
Fig. 9 MEASURED LOSS AND VSWR FOR THE TYPE B LAUNCHER WITH
ℓ = 2.0in , d = 1.0in And s = 0in.

24
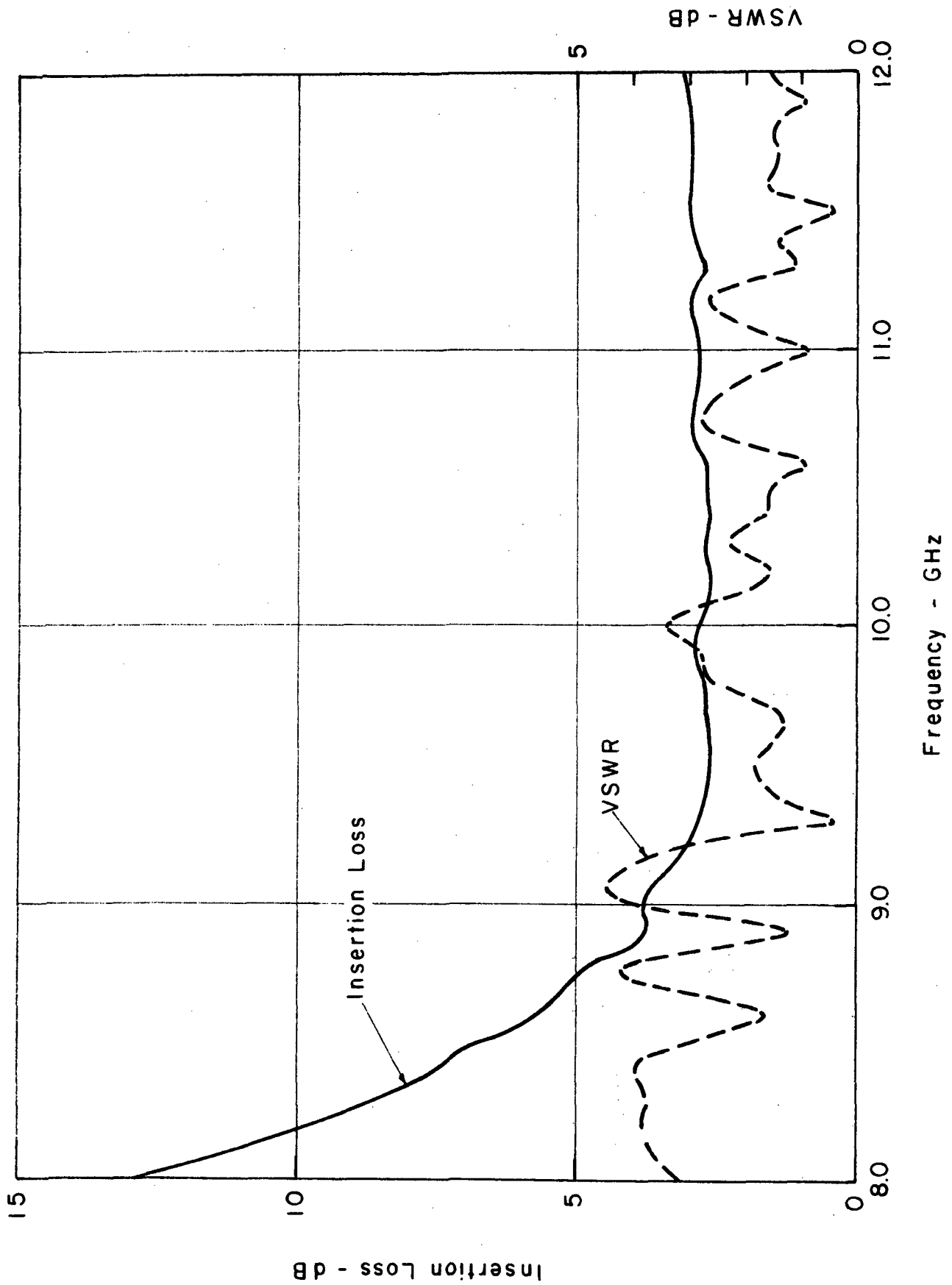
Fig. 10 MEASURED LOSS AND VSWR FOR THE TYPE B LAUNCHER WITH
$\ell = 1.0$ in, $d = 1.0$ in AND $s = 0$ in.

25

minimum attenuation was 3.3 dB, indicating an attenuation of 0.85 dB per launcher assuming once again line losses of 1.6 dB.*

The mode coupling was improved and more uniform in frequency when the gap between the metal taper and the image line was reduced to zero, as shown in Figure 9. Attenuation was consistently about 2.9 dB with minimum loss being 2.6 dB. The launcher reflections were increased, however, by the tighter mode coupling. This mismatch was improved when the taper of the metal insert were shortened to match that of the dielectric taper, as shown in Figure 10. The minimum total attenuation was 2.6 dB with the increase in attenuation between 10 and 12 GHz smaller than in the previous case. The minimum attenuation per launcher was 0.5 dB.

The conclusions drawn from the results presented thus far are as follows:

(1) The use of top-wall, double metal tapers provides more uniform launcher coupling with frequency but does not reduce the minimum attenuation.

(2) The metal taper should contact the top of the dielectric image waveguide to get maximum coupling.

(3) The metal and dielectric tapers should be the same length and be located at the same position in the launcher to get the best impedance match.

An additional series of launcher measurements was conducted on a different "U" waveguide in which the "U" was completely circular,** rather than having two 90-degree curves connected by a

---

* The adhesive, as before, was Eastman 910.

** The total line length was reduced by 2.0 in.

straight section. This waveguide is shown in Figure 11 and will be henceforth designated the "C" waveguide.

The type B launcher configuration was measured once again using the "C" waveguide; the results are shown in Figure 12. The minimum total attenuation was 1.75 dB in the 10-to-11-GHz range and increased to 2.25 dB above 11 GHz. Assuming line attenuation of 0.72 dB (see Section 3.3.3), the minimum attenuation per launcher was 0.51 dB.* A variation of the type B launcher was to introduce a flat section in the double metal taper as shown in Figure 13. The tapers were the same as those in the type B launcher. The attenuation of the "C" waveguide with this launcher, designated type C, is shown in Figure 14. The results were virtually identical to those of the type B launcher with the minimum attenuation again 1.75 dB.

In the fourth type of launcher metal tapers were also introduced in the horizontal plane. The type D launcher is shown in Figure 15. The intended purpose of the tapers in the horizontal plane was to force the horizontal field distribution in

---

* The "C" waveguide was attached with a low-loss temperature
  sensitive adhesive, Crystalbond 509 by Aremco, Briarcliff
  Manor, New York.
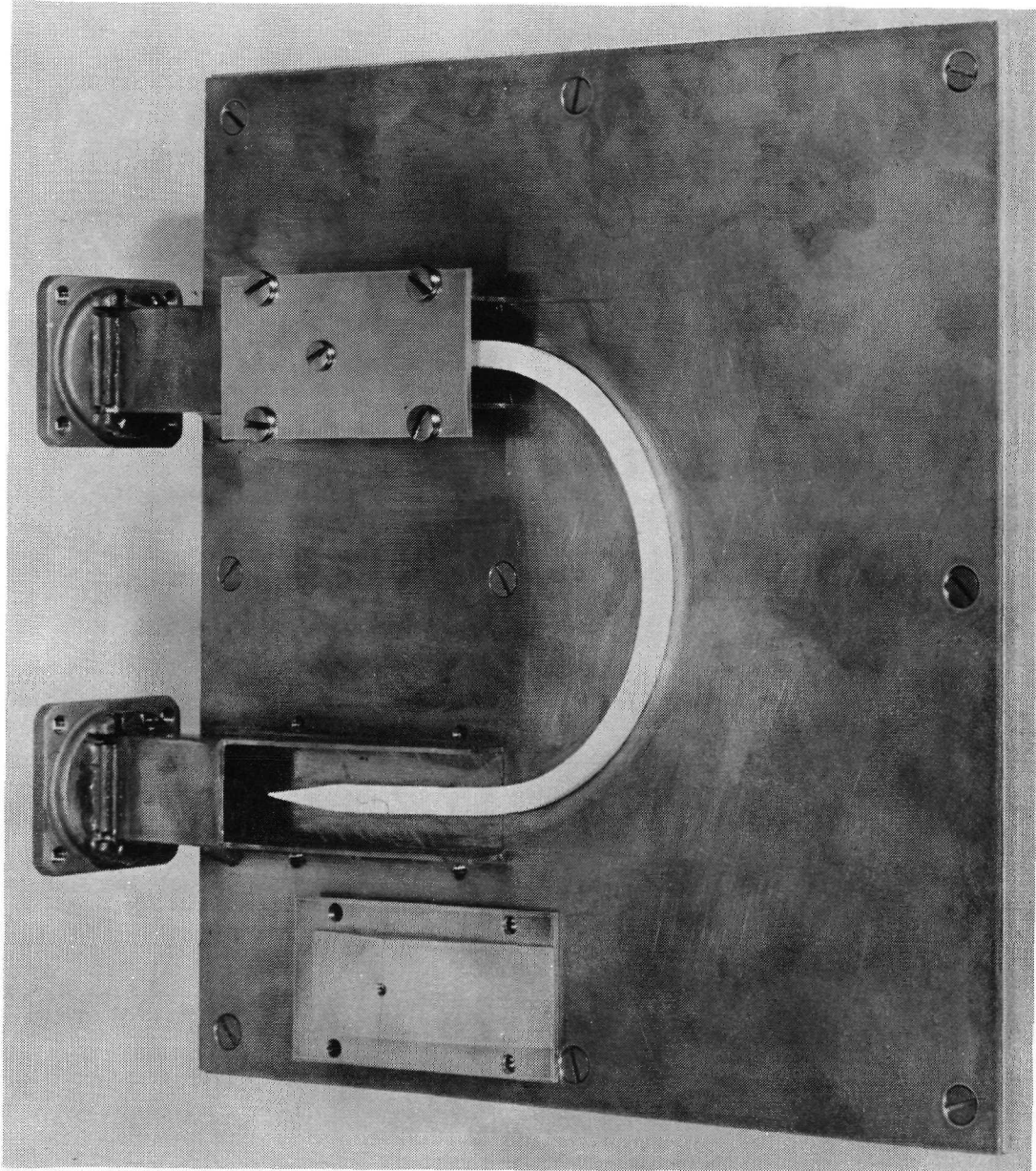
Fig. 11 A CIRCULAR "U" WAVEGUIDE USED FOR ADDITIONAL
LAUNCHER STUDIES
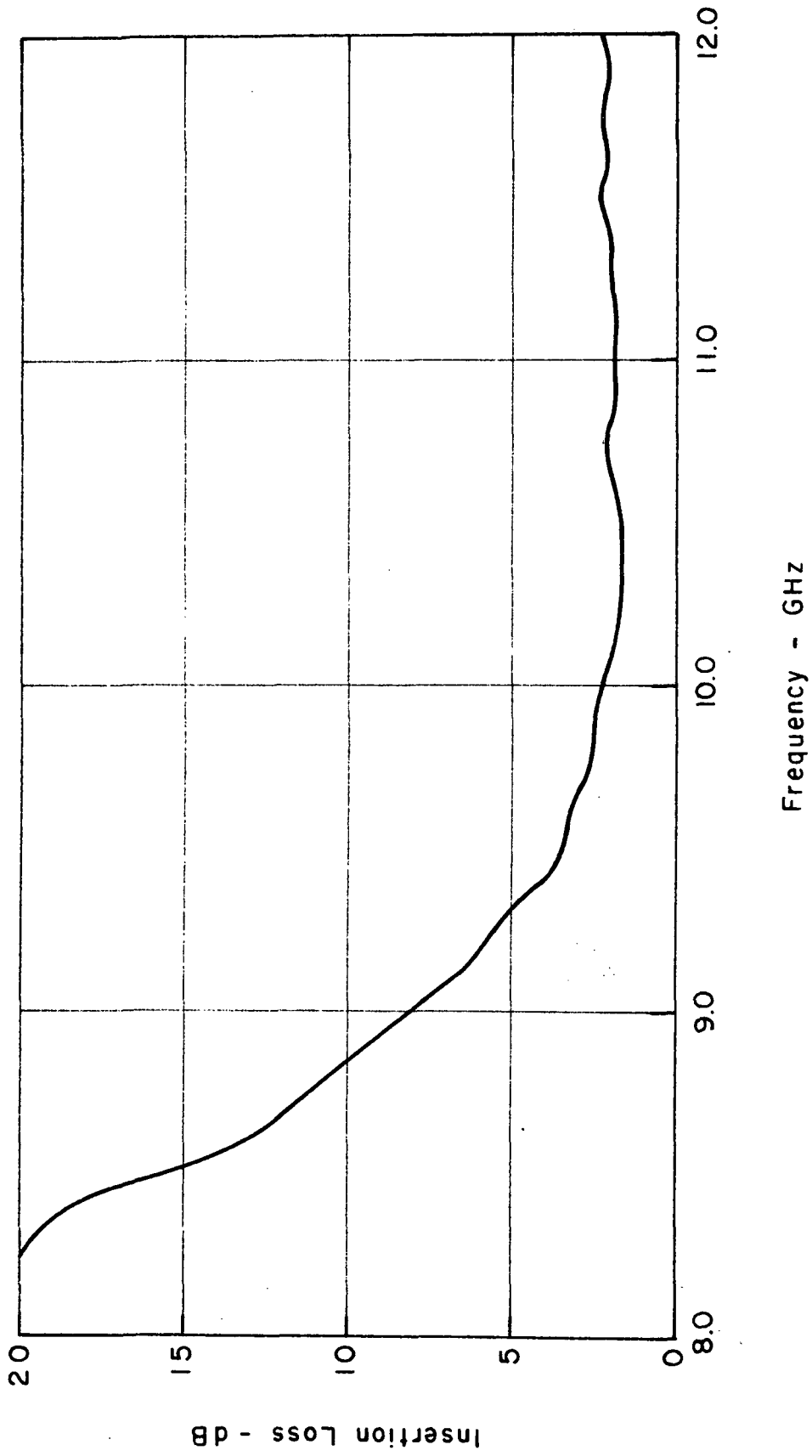
Fig. 12 ATTENUATION OF THE "C" WAVEGUIDE WITH THE TYPE B LAUNCHER

29

Image Plane

Image Wavequide

Metal Wavequide

TOP VIEW

Metal Taper

Image Wavequide

Image Plane

d

1.0 in

ℓ

s

Metal Wavequide

1.0 in

SIDE VIEW
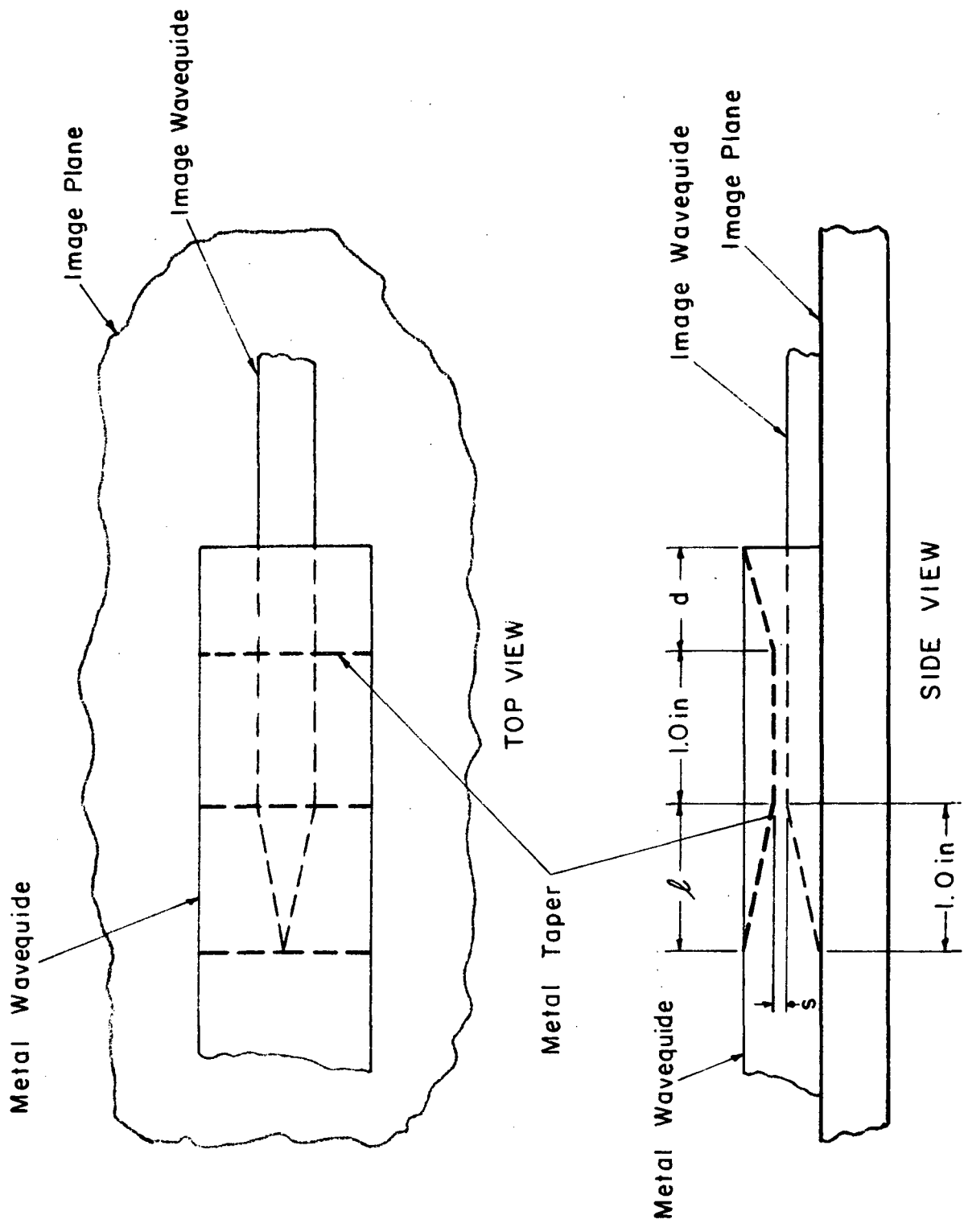
Fig. 13   THE TYPE C LAUNCHER WHICH HAS A FLAT SECTION IN THE METAL TAPER

30

Fig. 14   ATTENUATION OF THE "C" WAVEGUIDE WITH THE TYPE
C LAUNCHER

31
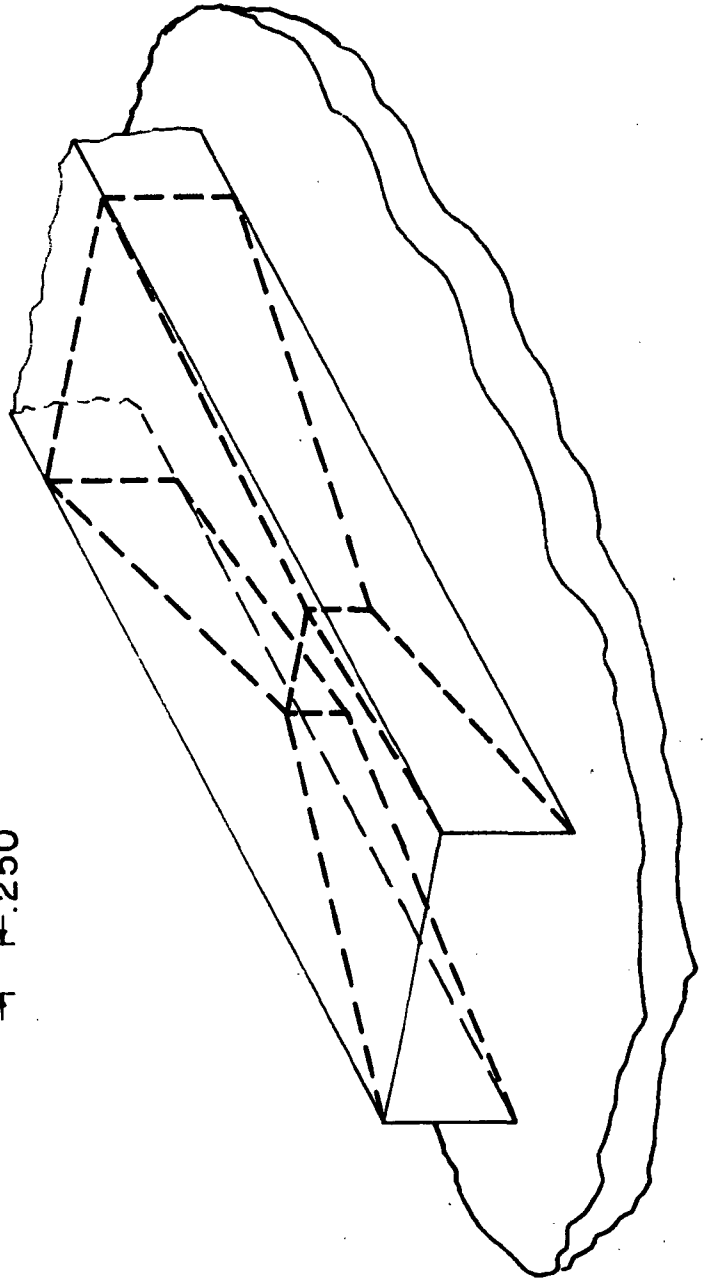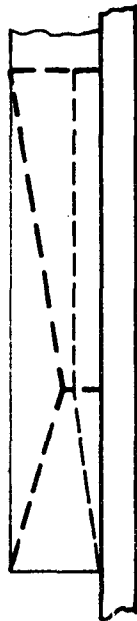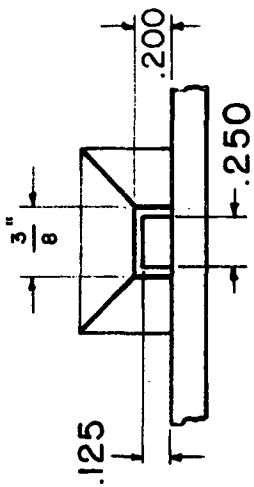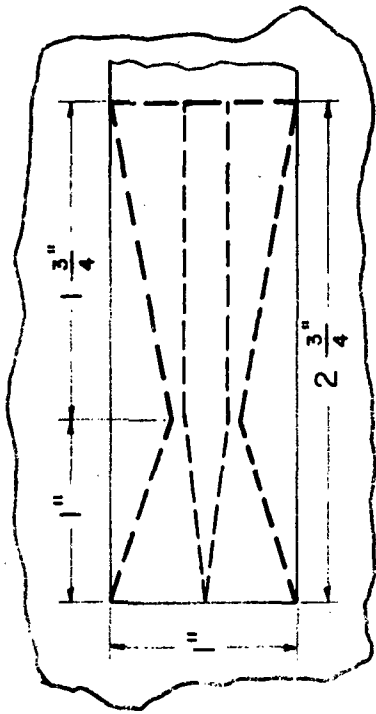
Fig. 15   THE TYPE D LAUNCHER WITH TAPERS IN BOTH HORIZONTAL AND VERTICAL PLANES

32

the metal waveguide to match that of the image waveguide and reduce the effective aperture from which the metal waveguide might radiate. The modification did not have the intended effect, as shown in Figure 16. The minimum total attenuation increased to about 2.25 dB, an increase of 0.5 dB over the type B launcher. It is likely that the 0.25 dB per launcher increase was due to increased conductor losses which was not compensated by a reduction of mode conversion loss. In fact, for all of the launcher designs the general conclusion to be drawn is that mode conversion was not the major problem, but rather reduction of conductor losses in the metal structure.

As stated at the outset of this subsection, the design of these launchers was predicated largely on achieving mode conversion through manipulation of the dimensions and shape of the metal part of the launcher structure. An alternate approach is to expand the cross-sectional dimensions of the dielectric waveguide. This allows higher order modes to exist locally in the launcher and should provide high efficiency in mode transformation. This approach is also likely to reduce conductor losses because of lower current densities. This approach may be worthy of future investigation in order to reduce the launcher **attenuation below the 0.5 dB achieved in present** launcher designs.
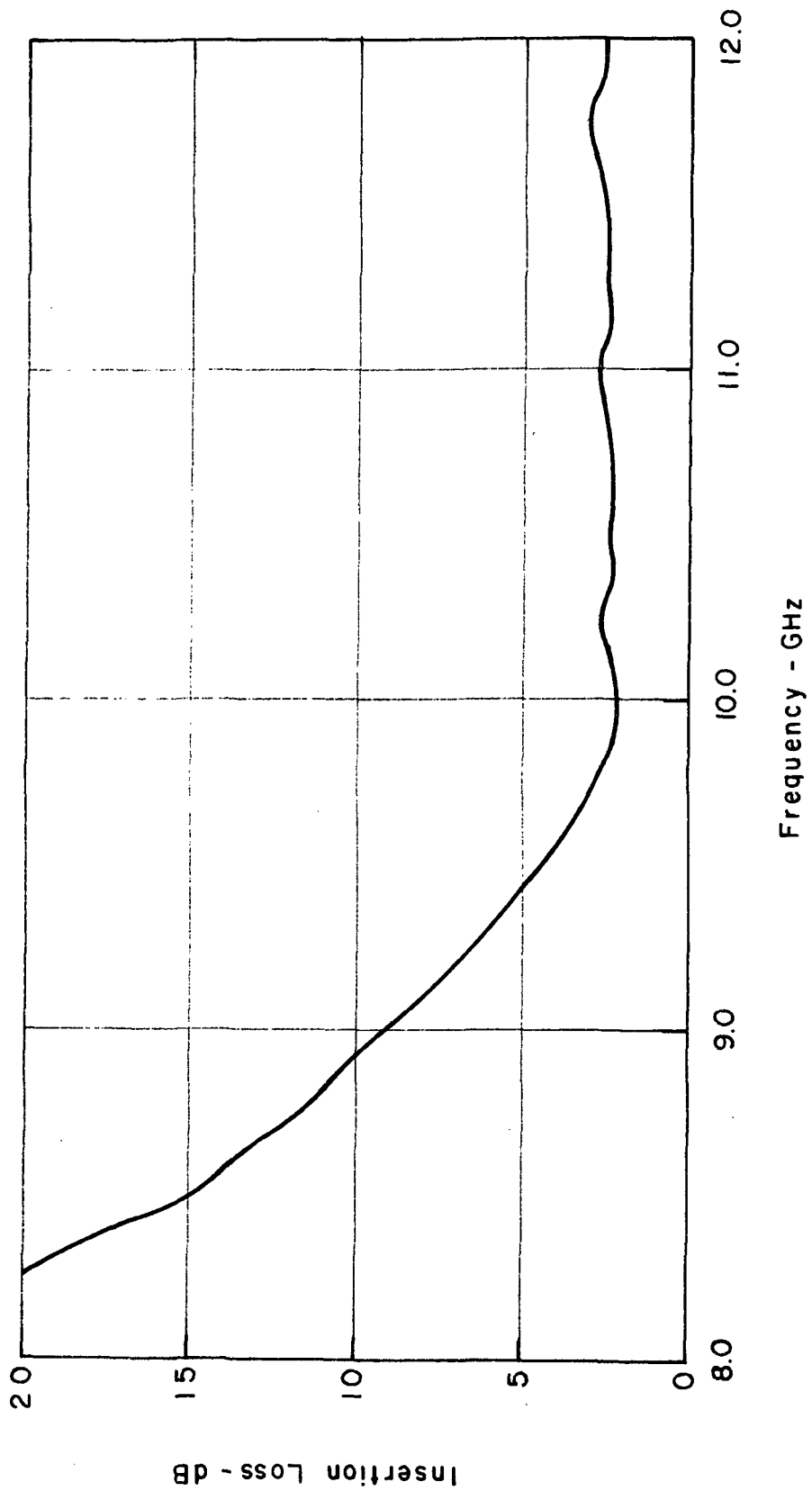
Fig. 16   ATTENUATION OF THE "C" WAVEGUIDE WITH THE TYPE
          D LAUNCHERS

3.3 Attenuation in Image Waveguide

3.3.1 Introduction

The "U" waveguide structures, described in the previous sub-section, are useful in measuring image line attenuation, especially the excess attenuation due to radiation from the curves. A second method of determining waveguide attenuation is to measure the Q of a resonant section of image waveguide. This sub-section will consider image waveguide attenuation in X-band (8 to 12 GHz) and V-band (50 to 75 GHz) as derived from "U" waveguides and the Q of ring resonators.

3.3.2 Loss Mechanisms

Attenuation in the dielectric image waveguide was found to originate in several different loss mechanisms. These sources of attenuation are:

    (1)   Absorption losses in the dielectric material

    (2)   Ohmic losses in the image conducting plane

    (3)   Losses in the adhesive

    (4)   Losses due to surface roughness of the conductor

    (5)   Radiation losses from curves due to the gap between the dielectric and conductor.*

The first two are well-known loss mechanisms and have been described theoretically.[16] Various results relative to (3) and

---

* The mechanism in this case is that the gap shifts the dispersion curve to a higher B which increases the guide wavelength (and velocity) for a given frequency and leads to higher radiation from curved waveguides.

(4) will be considered in the subsections below. The possible

influence of gaps on the results is most pertinent to excess

radiation attenuation from curves and will be considered in

Section 3.6.

The next two subsections will consider experimental results

of measurements in X-band and V-band, respectively.

3.3.3 Attenuation Calculation and Measurements in X-Band

The useful range of measurement for attenuation in straight

image waveguides will be 10 GHz and above. Below 10 GHz excess

attenuation, due to radiation from the curves, was obtained.

A modest increase in attenuation with frequency is expected,

but with only a 20% range of measurement (10 to 12 GHz) any

attempt to determine these small variations experimentally would

be frustrated by lack of measurement precision. Therefore, the

present consideration will be limited to relating various loss

mechanisms to measurements at 10.5 GHz where attenuation was

generally found to be minimum and well above the region of excess

radiation from curves.

All of the X-band image waveguides were constructed identi-

cally. They were designed to have an aspect ratio of 1:1 with

a = b = 0.125 in. (The physical aspect ratio was therefore 2:1,

giving a guide width of 0.250 in.) The dielectric material was

a ceramic-filled plastic.* The dispersion curves of Figure 2 were used to determine that, at 10.5 GHz (corresponding to $B = 1.26$), the ratio λ_0/λ_g is 1.78. The guide wavelength is therefore 0.632 in. The theoretical dielectric and conductor attenuation factors were obtained using the results presented in Ref. 16. At 10.5 GHz the dielectric loss was calculated to be $\alpha_d = 0.085$ dB/in. The image plane for all X-band waveguides was brass and the theoretical conductor loss was calculated to be $\alpha_c = 0.025$ dB/in.** Then the total theoretical attenuation at 10.5 GHz is

$$\alpha_t = \alpha_c + \alpha_d$$
$$= 0.110 \text{ dB/in.}$$

The length and total theoretical attenuation for the two waveguides described previously are given below.

	Length (inches)	Theoretical Attenuation dB
"U" Waveguide	8.28	0.915
"C" Waveguide	6.28	0.695

---

* Custom high-K 707L manufactured by Custom Materials, Inc., Chelmsford, MA. $\varepsilon_r = 9.2$, tan $\delta \leq 0.001$ at 10 GHz.

** The curves for conductor attenuation in Figure 11 of Ref. 16 are not accurate for a value of $B = 1.26$. Therefore a value has been assumed as follows:

$$\lambda_g \ \sigma \ \delta \ \alpha_c \times 10^2 = 3.5$$

The effect of possible inaccuracy in this assumption is small because, for this waveguide and frequency, the dielectric losses dominate the conductor losses.

The two remaining attenuation mechanisms to be considered for frequencies above 10 GHz are dielectric absorption in the adhesive and ohmic attenuation due to surface roughness. Surface roughness at X-band can contribute to excess conductor attenuation if the surface roughness exceeds approximately 10 μin.* The surface roughness of the brass plates on which the image lines were fabricated was measured to be 10 to 12 μ. Therefore, an approximate increase in conductor attenuation of 10% was added to the theoretical value, making it 0.0275 dB/in.

The "U" waveguide was attached with the type 910 adhesive, and the "C" waveguide was attached with the type 509 adhesive. To compare the attenuation introduced by these adhesives, a second set of data was measured on the "C" waveguide with type D launchers (see Figure 15) but with the type 910 adhesive rather than the type 509. The results are shown in Figure 17. The minimum was 2.75 dB compared with 2.25 dB when the type 509 adhesive was used. Thus, in all "U" waveguides an excess attenuation due to adhesive loss of 0.08 dB/in. was included. The adhesive loss in the "C" waveguides at X-band was considered to be very small and was neglected in determining total attenuation.

---

* For a detailed consideration of the effects of surface roughness in microwave integrated circuits the reader should review Refs. 21-23. A theoretical increase in conductor loss of 12% is predicted in microstrip line at 10 GHz by Sobol (Ref. 21) for a surface roughness of 10μin. This corresponds to a ratio of Δ/δ of 0.4, where Δ is rms surface roughness and δ is the skin depth. Since δ varies as the reciprocal of $\sqrt{f}$, then in V-band (60 GHz) the 10% excess attenuation would occur for Δ approximately 4 μin.
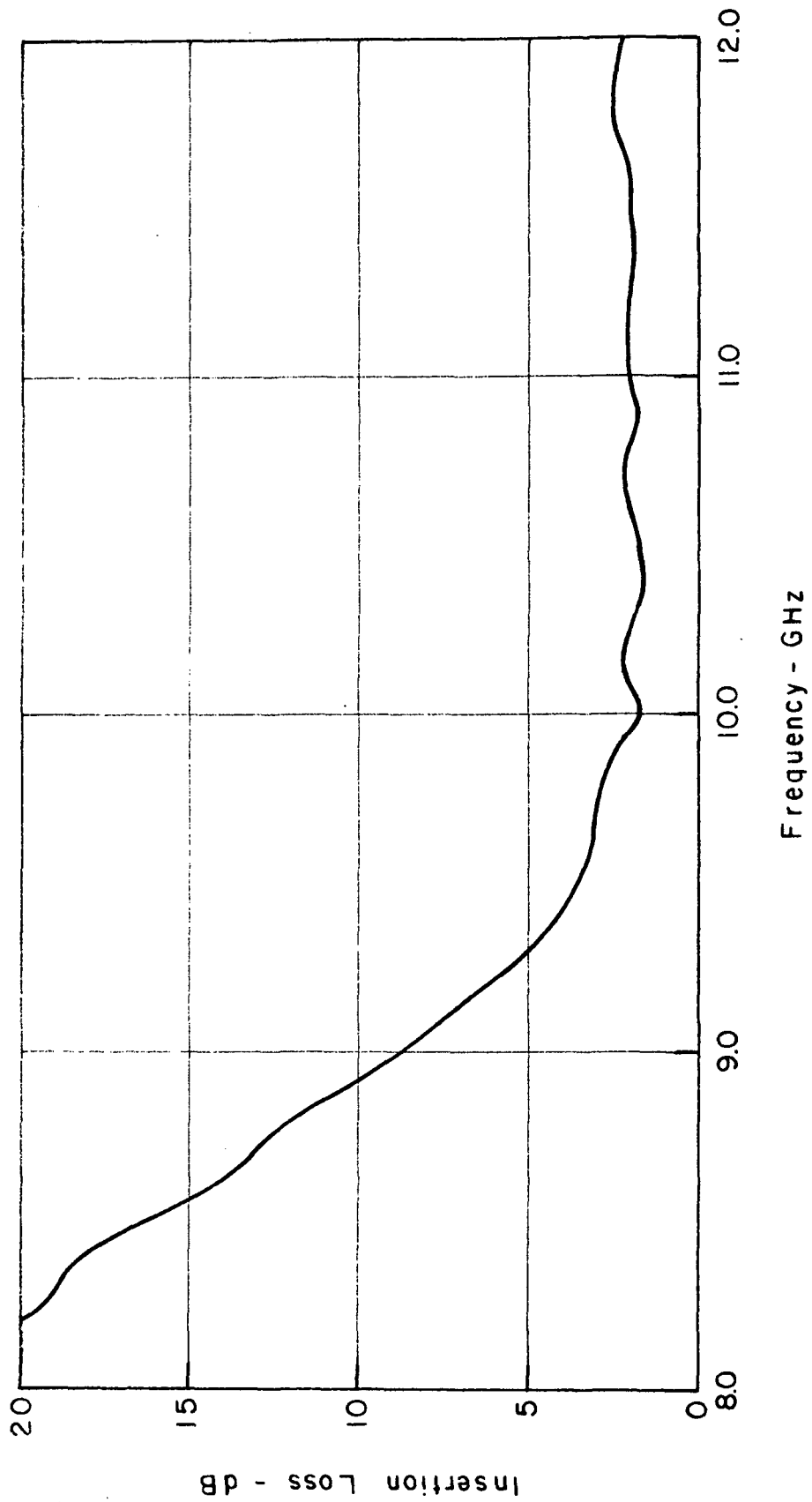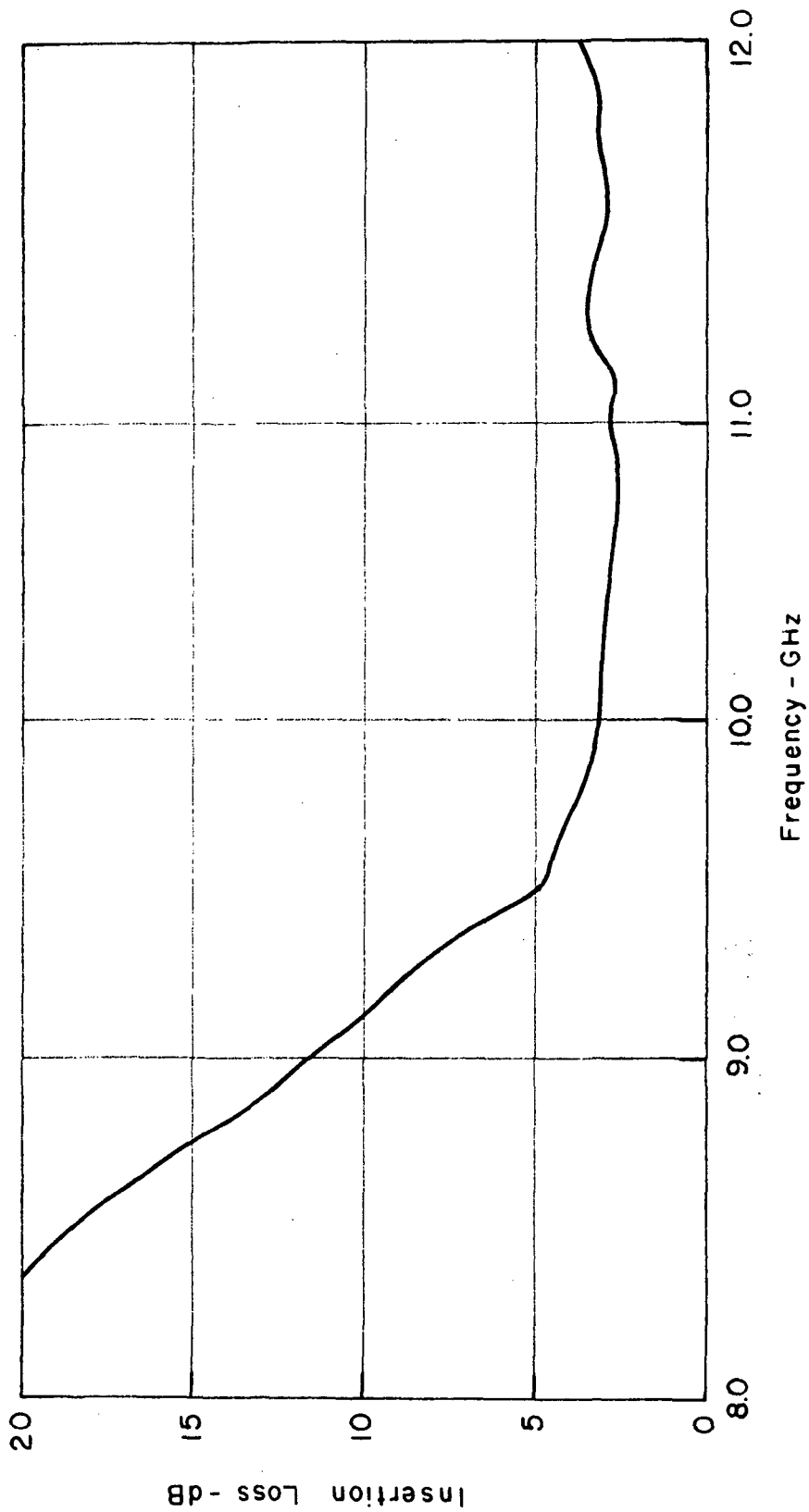
Fig. 17   ATTENUATION OF THE "C" WAVEGUIDE WITH TYPE D
LAUNCHERS AND TYPE 910 ADHESIVE

The total attenuation in the "U" and "C" waveguides including the excess attenuation due to surface roughness and lossy adhesive was then predicted. Reviewing the X-band experimental results as presented in the previous section, it was then possible to determine the minimum launcher attenuation. The results of these calculations and measurements are presented below.

Launcher Type	Minimum Measured Waveguide Attenuation (dB) Waveguide		Theoretical Line Attenuation (dB) Waveguide		Per Launcher Attenuation (dB) Waveguide	
	U	C	U	C	U	C
A	2.6		1.6	0.72	0.5	
B-C	2.6	1.75	1.6	0.72	0.5	0.51
D		2.25	1.6	0.72		0.76

3.3.4 Attenuation Calculations and Measurements in V-band

Experimental measurements in V-band of waveguide attenuation were performed on two different waveguide structures. The first of these was the "U" waveguide similar to that used extensively in X-band. Attenuation measurements were also obtained by measuring the Q of a ring resonator. These results are reported in Section 4.5. The fabrication of these experimental circuits will first be described and the measurements then presented.

A decision was made early in the program to use only high-purity alumina waveguides for the V-band experiments because the

properties of the ceramic-filled plastic are unknown at V-band
and measuring them would be in itself a major program task.
Secondly, the experience to be gained in designing and fabrica-
ting ceramic alumina waveguides was viewed as an important element
of the program.

Two approaches to fabrication of the V-band "U" waveguides
were developed in parallel. One of these was the use of green
alumina tape machined to appropriate dimensions (to allow for
shrinkage during firing) and subsequently sintered into final
form. Details of this fabrication procedure are given in Sec-
tion 6.4.3.

In anticipation that sintering of green ceramic tape might
not yield useful test waveguides, the second approach to fabri-
cating waveguides was the use of abrasive machining, described
in Section 6.3.3.2. Two precision templates were manufactured
to be used in making the "U" waveguides. One of these is shown
in Figure 64. The success of the sintering method made it unne-
cessary to use this method. However, the abrasive machining
method was used to make a waveguide for one of the band-stop
filters, described in Section 4.5 below.

Four each of two different "U" waveguide designs were machined
for sintering. Four of the eight had cross-bars to provide sta-
bility during firing. The machined green tapes are shown in Fig-
ure 18. The four pieces without cross-bars bowed so as to
be unusable. A view of the parts after firing is shown in Fig-
ure 67. Two of the parts are also shown in Figure 19. The pointed

41
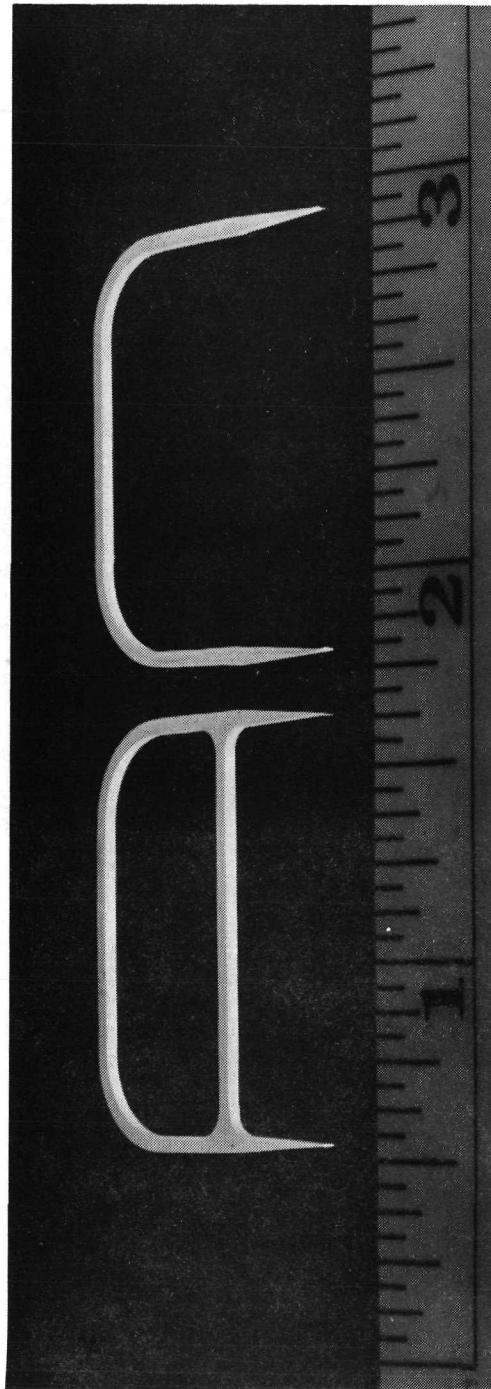
Fig. 18 "U" WAVEGUIDES MACHINED FROM GREEN TAPES SHOWN PRIOR TO FIRING
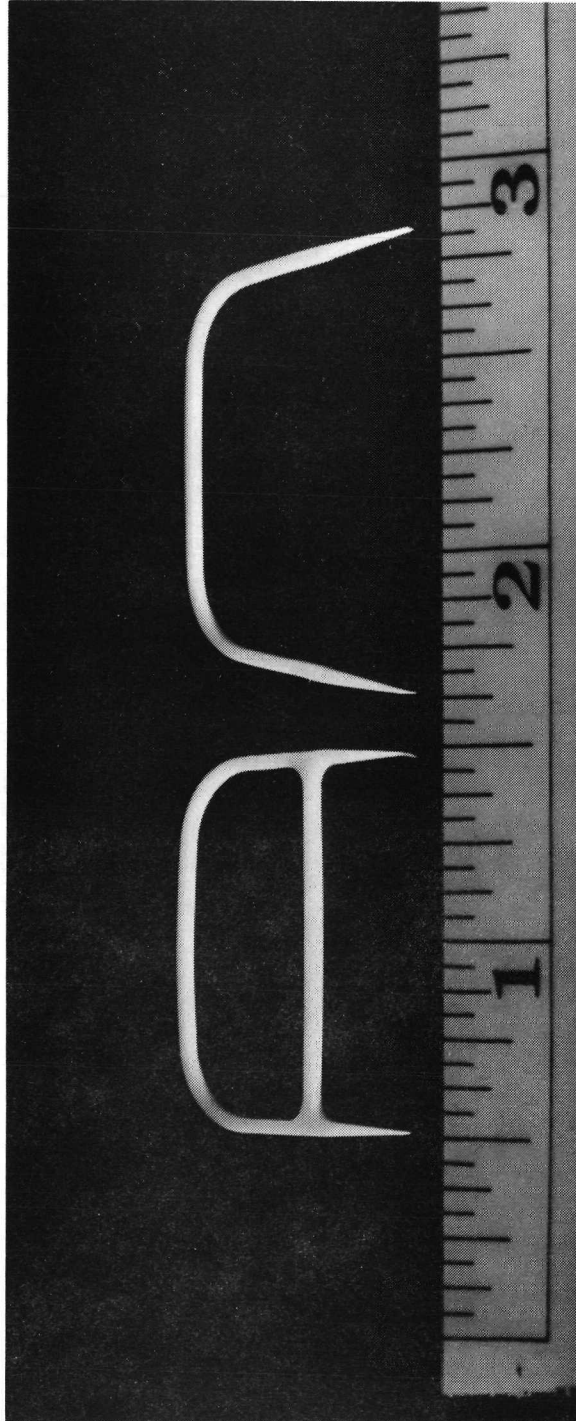
Fig. 19 "U" WAVEGUIDE PARTS SHOWN AFTER FIRING

ends of four guides having cross-bars warped upward slightly.
These four pieces were refired at a slightly lower temperature
with ceramic disks used as weights to flatten the tips. Unfortu-
nately, fusing occurred between the waveguide tips and the disks
on two of the four pieces. The tips broke off when an attempt
was made to remove the waveguides from the disks.

These waveguides represented two different designs. These
designs are described by the dimensions in the following.

	"U" Waveguide	
	No. 1	No. 2
Width 2a (in.)	0.050	0.038
Height b (in.)	0.025	0.025
Mean Radius of Curvature (in.)	0.275	0.210
Length of Tapers (in.)	0.300	0.300
Length of Straight Section (in.)	0.400	0.530

The broken tips occurred on both specimens of line No. 1.
However, it was decided to fabricate new tips and concentrate
on measurement of this waveguide because it had an aspect ratio
of 2:1 for which theoretical modeling and numerical results were
readily available. The No. 1 waveguide and tips were polished
on the lower side to a surface finish of 2 to 4 μin. The waveguide

and tips were installed in the aluminum base-plate assembly as shown in Figure 20. Viewed from the input/output side, the assembly appears as in Figure 21. The base-plate surface was also polished to a surface of 2 to 4 μin.

The launcher designs were similar to those designated type B in Section 3.2 above. The top wall of the metal waveguide was tapered linearly over 0.3 in. to a low point and then tapered linearly upward over 0.3 in. The tapered tip of the alumina waveguide was colocated with the downward taper of the top wall of the launcher. Detail of the launcher construction is shown in Figure 22. In this view, one of the launchers has been removed and inverted to show the metal tapers.

The cross-sectional surfaces where the tips and waveguide were joined were cut and polished flat so that, when the tips were placed against the "U" waveguide, no gap of any consequence to the measurements was present. When the alumina waveguides were attached to the polished alumina surface, weights were used in order to assure intimate contact between the alumina and aluminum. Measurements were made under two conditions of adhesive application to "U" waveguide No. 1. In the first case, the type 509 heat sensitive adhesive was applied uniformly over the entire undersurface of the alumina waveguide and tips. In the second case, the adhesive was applied very sparingly to about 25% of the undersurface of the alumina waveguide. Measurements of attenuation of the "U" waveguide for these two cases are shown in Figures 23 and 24, respectively.
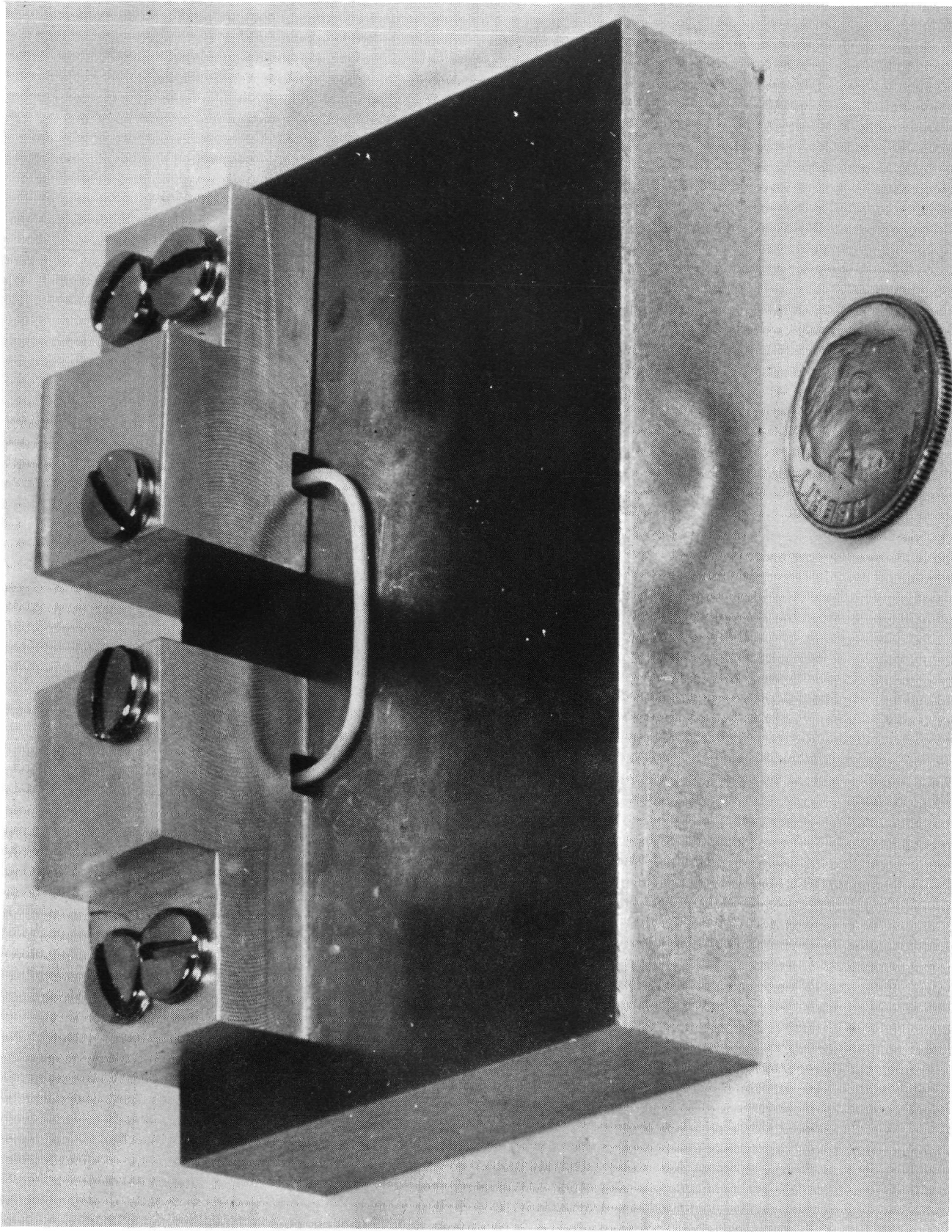
Fig. 20 ALUMINA WAVEGUIDE "U" MOUNTED ON A BASEPLATE
FOR MEASUREMENTS IN V-BAND
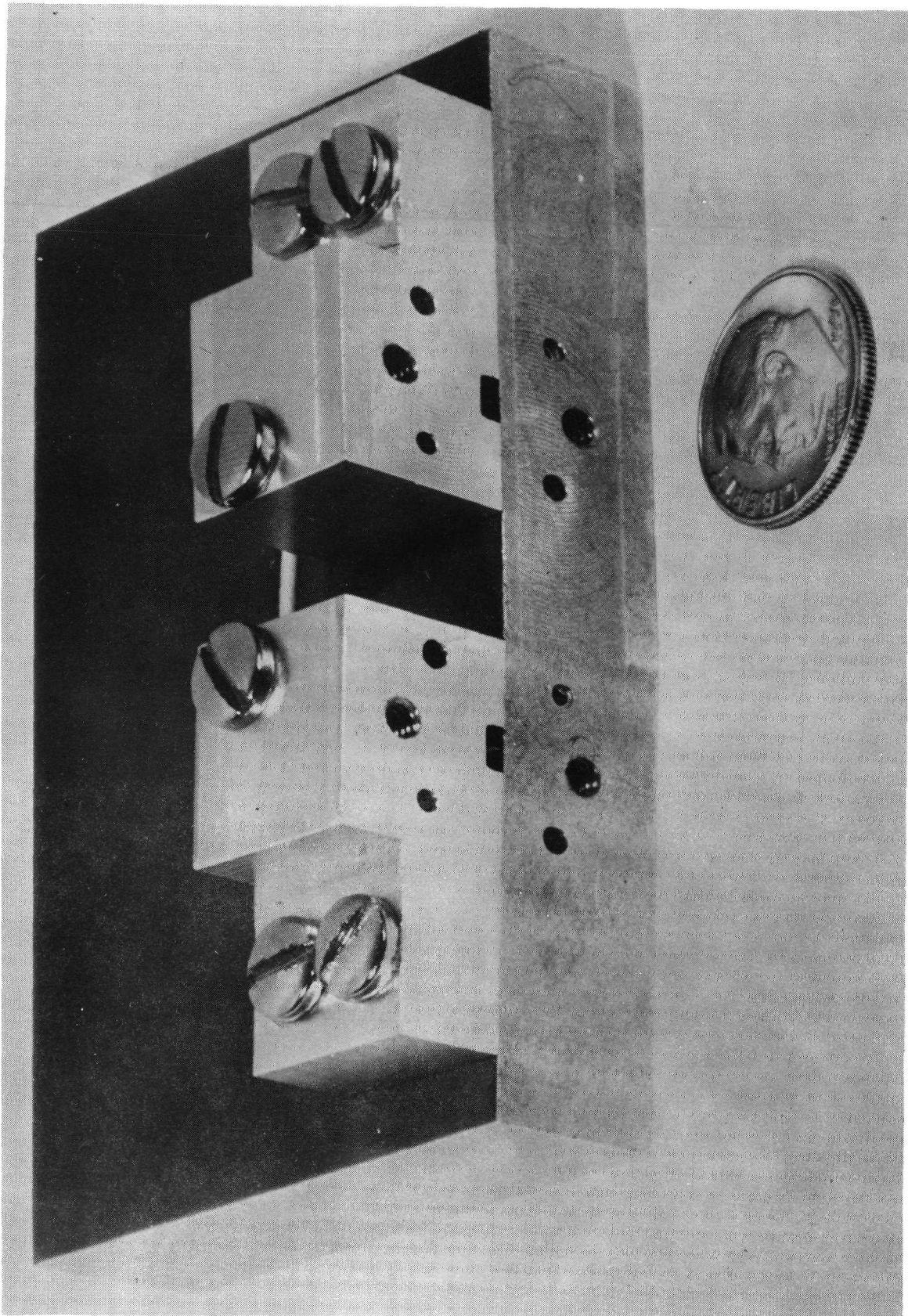
Fig. 21 V-BAND "U" WAVEGUIDE, BASEPLATE AND LAUNCHERS
VIEWED FROM THE INPUT/OUTPUT TERMINALS
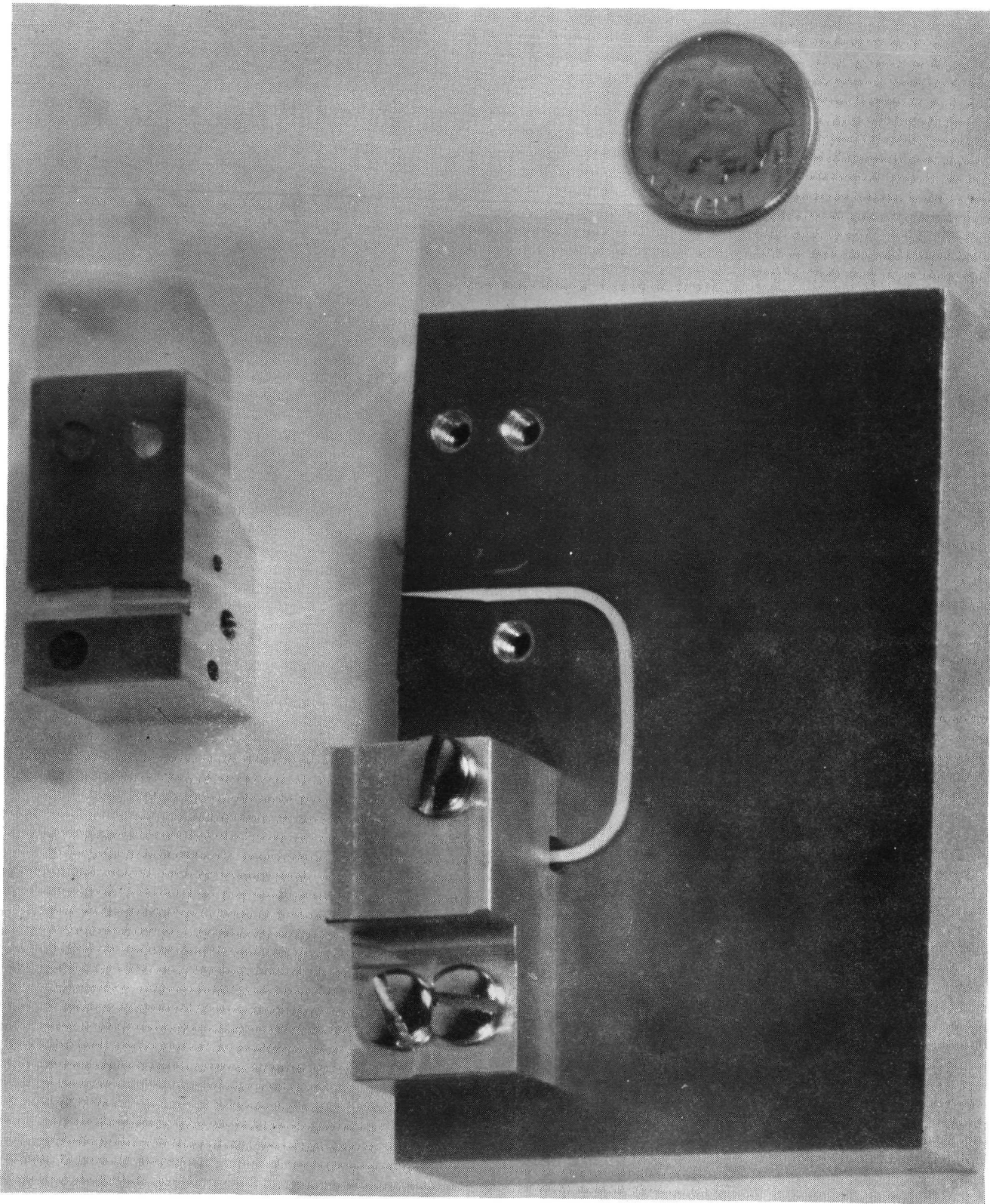
Fig. 22   V-BAND "U" WAVEGUIDE ASSEMBLY PARTIALLY DISASSEMBLED
TO SHOW LAUNCHER CONSTRUCTION
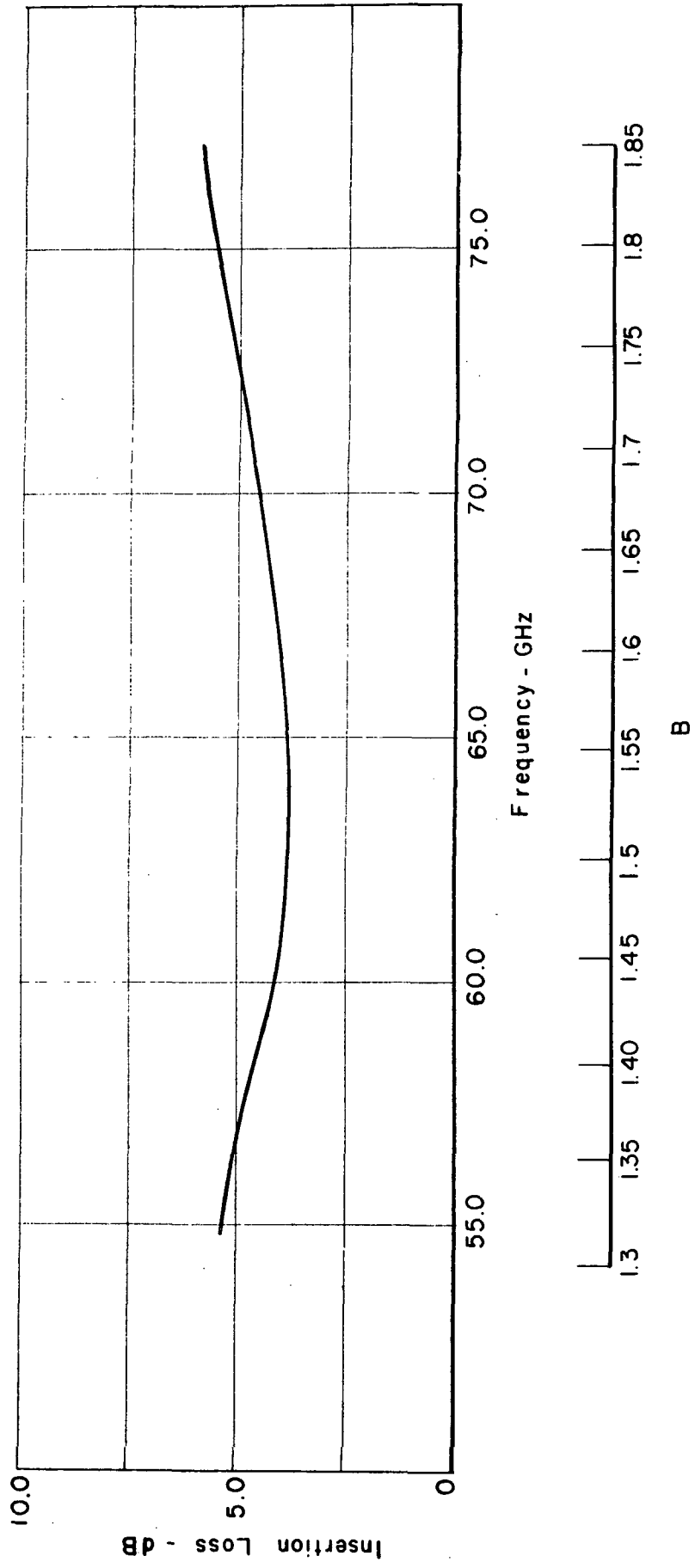
Fig. 23   ATTENUATION IN V-BAND OF "U" WAVEGUIDE NO I WITH TYPE 509 ADHESIVE APPLIED TO 100% OF THE ALUMINA UNDERSURFACE
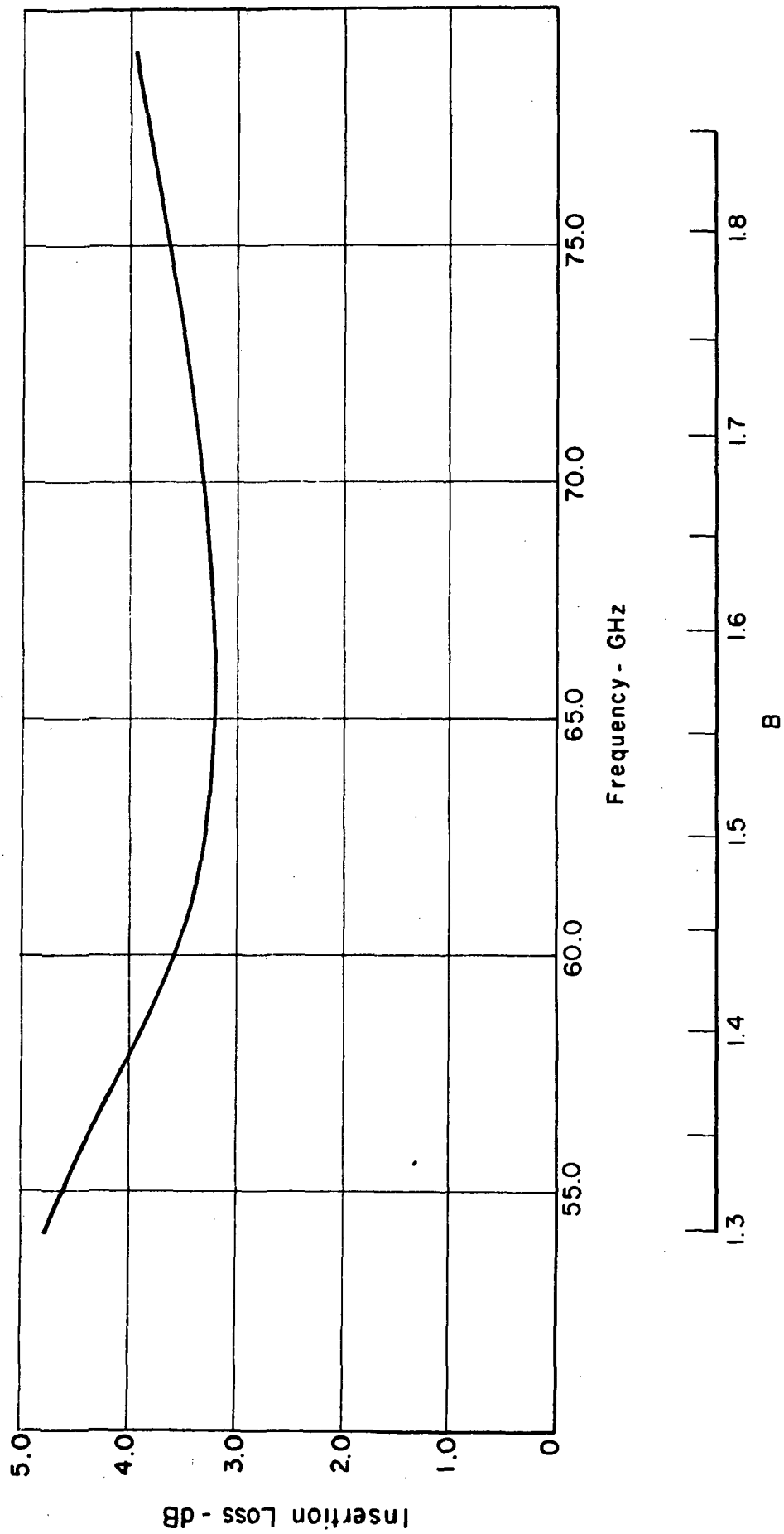
Fig. 24 ATTENUATION IN V- BAND OF "U" WAVEGUIDE NO I WITH TYPE 509 ADHESIVE APPLIED TO 25% OF THE ALUMINA UNDERSURFACE

50

Both attenuation curves showed a minimum at about 65 GHz.
The increase in attenuation above 65 GHz was attributed to an increase in excess radiation from the launcher due to a gap between the ceramic and the metal taper. Details on this gap radiation are given subsequently in this subsection.

The increase in radiation below 65 GHz may have been due to radiation from the curves in the waveguide. In the X-band measurements curvature radiation was observed for values of B less than 1.25. The R/2a* value was 8.5. The R/2a ratio in the V-band line No. 1 was 5.5. Since the radius of curvature was reduced and the aspect ratio a/b was the same, the curvature radiation would occur at higher values of B.

Calculations of dielectric and conductor losses** were performed at 65 GHz (B = 1.56). The dielectric attenuation, assuming ε_r = 9.6 and tan δ = 0.0002,*** was calculated to be 0.107 dB/in. or 0.009 db/λ_g. The conductor attenuation was calculated to be 0.298 dB/in. or 0.025 db/λ_g. The total theoretical attenuation was therefore 0.405 dB/in. or 0.034 dB/λ_g.

---

*   R/2a is the ratio of the mean radius of curvature to the waveguide width.

** Derived from Ref. 16; see also Section 3.3.3 above.

*** Data from American Lava Corp., Chattanooga, Tenn., supplier of the type 772 alumina green tape, indicates tan δ = 0.0001 and ε_r = 9.8 at 25 GHz. The values assumed in the calculations allow for changes as the frequency is increased to 60 GHz.

In extrapolating the previously determined launcher attenuation from X-band to V-band, (see Section 3.3.3) an assumption was made about the division of the total attenuation between conductor loss, dielectric loss, and radiation loss. The portion of the total 0.5 dB attenuation attributable to conductor loss in the type B launcher was assumed to be 0.35 dB.* Since the conductor losses increase according to $\sqrt{f}$ between the two frequencies of calculation (10.5 and 65 GHz), the conductor losses were expected to increase to about 0.875 dB per launcher. Because of tolerances in fabrication, the spacing s between the metal taper and the alumina was 0.010 in. rather than zero as intended. On the basis of earlier measurements on the type B launcher,** and the existence of a gap s approximately equal to $b/2$, it was assumed that the excess radiation attenuation at 65 GHz was 0.2 dB per launcher.

The length of the ceramic waveguide within the launcher was 0.6 in. The assumed dielectric attenuation within the launcher was therefore 0.06 dB per launcher. Adding together the per-launcher attenuation factors, 0.875 dB conductor attenuation, 0.2 dB radiation attenuation, and 0.06 dB dielectric attenuation, the total expected attenuation for two launchers was 2.27 dB.

---

* Since the dielectric attenuation factor for the image wave-guide was calculated to be 0.085 dB/in, the dielectric attenuation within each launcher would be about 0.15 dB.

** Figure 8 shows that, when a gap of 0.128 in. ($\approx$ b) was introduced, the excess radiation loss was 0.35 dB per launcher.

The line attenuation due to dielectric and conductor losses was calculated to be 0.512 dB for a line length of 1.265 in. Total expected attenuation, not considering losses in the adhesive, was therefore 2.78 dB. The measured attenuation was about 3.2 dB at 65 GHz, as shown in Figure 23. The attenuation due to adhesive was therefore about 0.4 dB when about 25% coverage was used. When 100% adhesive coverage was used, the expected increase in attenuation was therefore an additional 1.2 dB. Comparing Figures 23 and 24 the measured increase due to added adhesive was about 1.3 dB at 65 GHz. Thus, the total attenuation due to adhesive, when 100% coverage was employed, was about 1.6 dB or 1.26 dB/in. Therefore, the adhesive, which apparently contributed negligible attenuation in X-band, became a serious contributor to attenuation in V-band.

Measurement of attenuation with "U" waveguide No. 2 is shown in Figure 25. All measurement conditions were indentical to those for waveguide No. 1. The minimum attenuation was 3.0 dB, about 0.2 dB lower than with waveguide No. 1. A slightly lower attenuation would be expected because the cross-sectional area was smaller and dielectric attenuation would be reduced. However, other variables could also account for changes in the minimum attenuation as well. Since adhesive attenuation was high, variations in the amount applied could influence results. Also, the positioning of the waveguide within the launcher region could influence launcher attenuation.
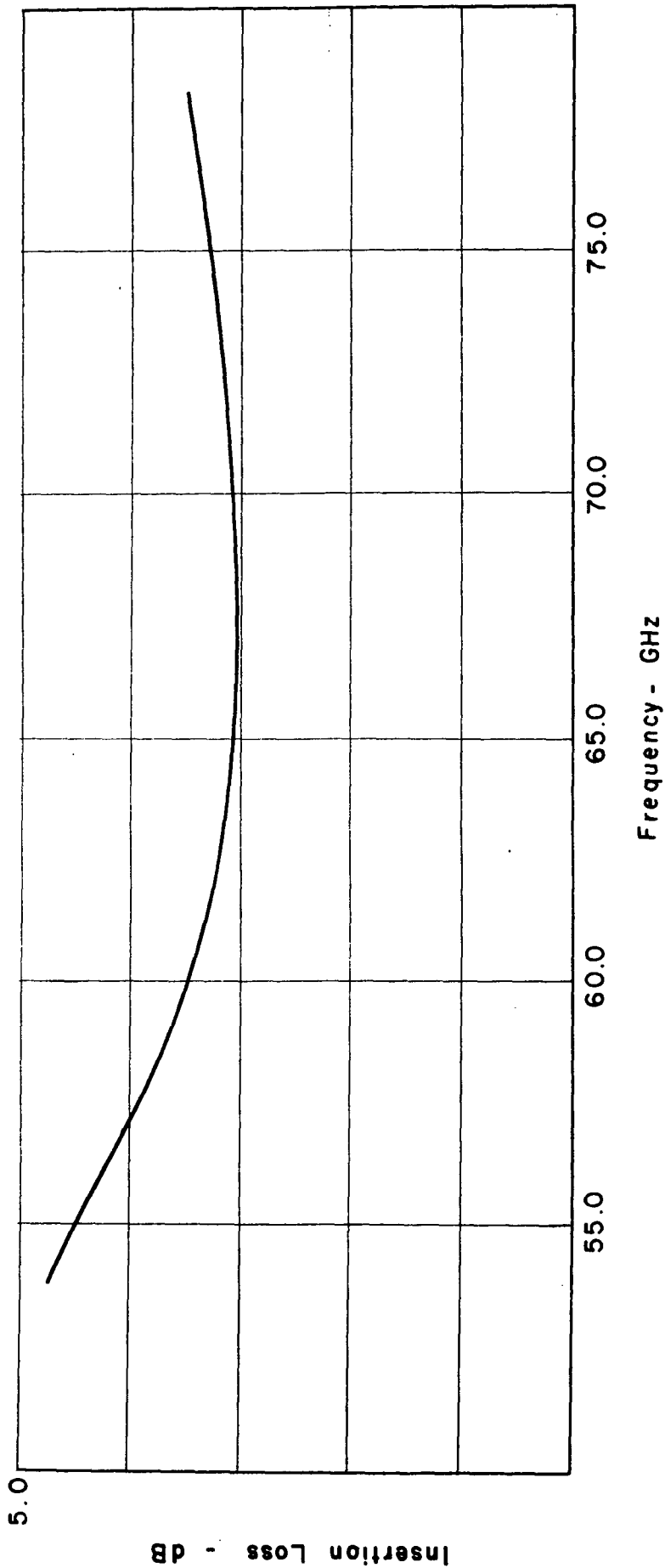
Fig. 25 ATTENUATION IN V-BAND OF "U" WAVEGUIDE NO 2 WITH TYPE 509 ADHESIVE
APPLIED TO 25% OF THE ALUMINA UNDERSURFACE

54

The above results clearly indicate that many factors contribute to excess waveguide attenuation and can seriously degrade the performance of components requiring low attenuation. Other factors that can affect attenuation were also investigated and will be discussed in the following subsection.

3.3.5 Effects of Surface Preparation and Metal Films on Attenuation

The additional measurements of attenuation presented in this subsection relate to excess loss mechanisms in the V-band alumina image waveguides. **The alumina "U" waveguide designated No. 2** was measured on a second base plate. This base plate, shown in Figure 26 was made of brass and plated with gold.* The launchers were of the same type as in the aluminum base plate described earlier. The primary difference in the two base plates was that, in the gold plated brass version, no attempt was made to achieve a very flat or highly polished surface. Measurement of attenuation in "U" waveguide No. 2 on the gold plated brass base plate (100% coverage of the type 509 adhesive) is shown in Figure 27. The increase in attenuation compared with Figure 22 was 1 dB or more which was attributed to lack of flatness and/or surface roughness. A further increase in attenuation was noted when the alumina waveguide was attached with the type 509 heat-sensitive adhesive but without benefit of weights during the cooling of the adhesive. The increase

---

* Thickness was greater than 0.0001 in. The skin depth in gold at 60 GHz is 0.000016 in. Therefore, the plating thickness exceeded the skin depth by more than six times.
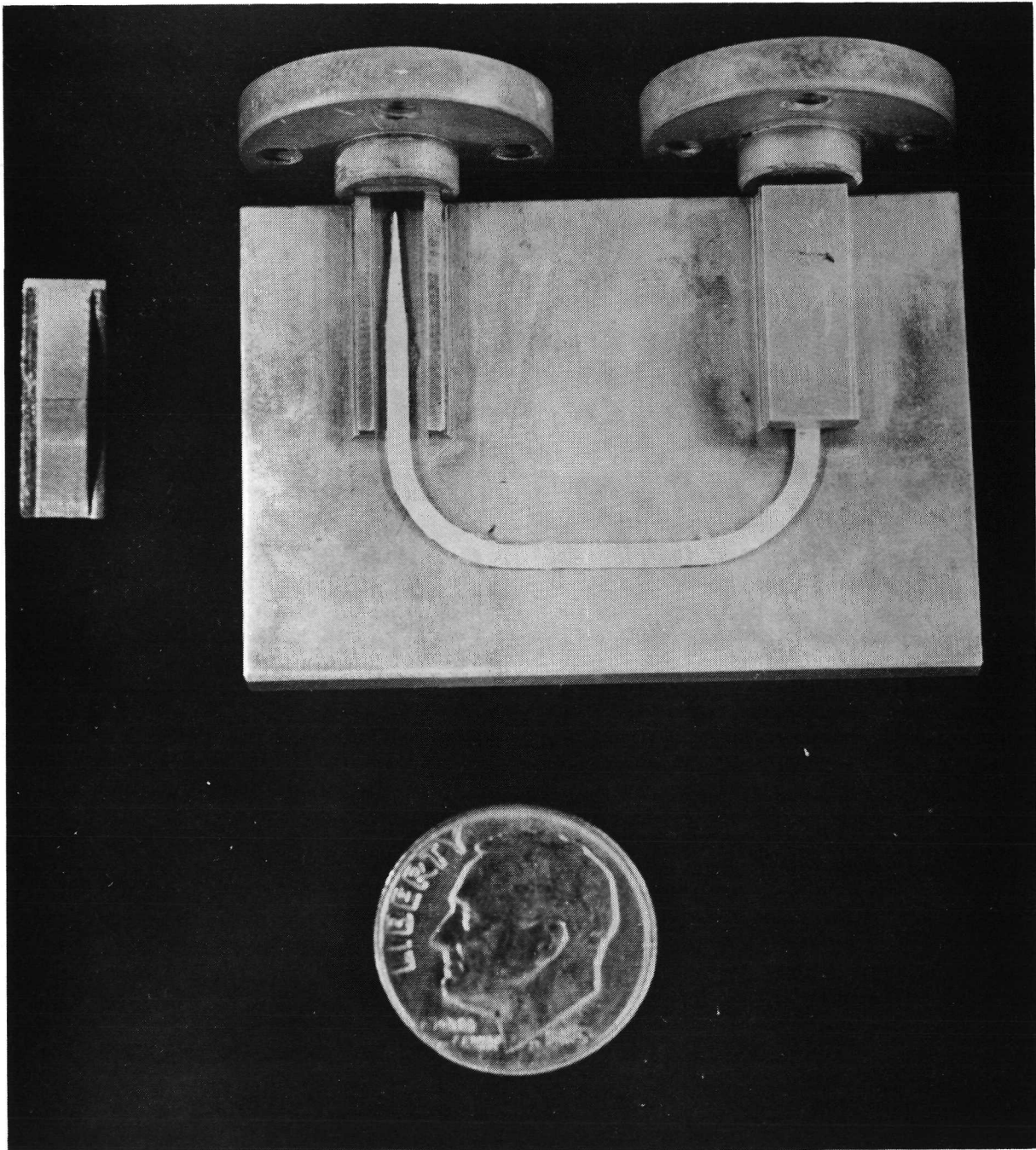
Fig. 26 GOLD PLATED BRASS BASEPLATE AND LAUNCHERS FOR
V-BAND MEASUREMENTS

56
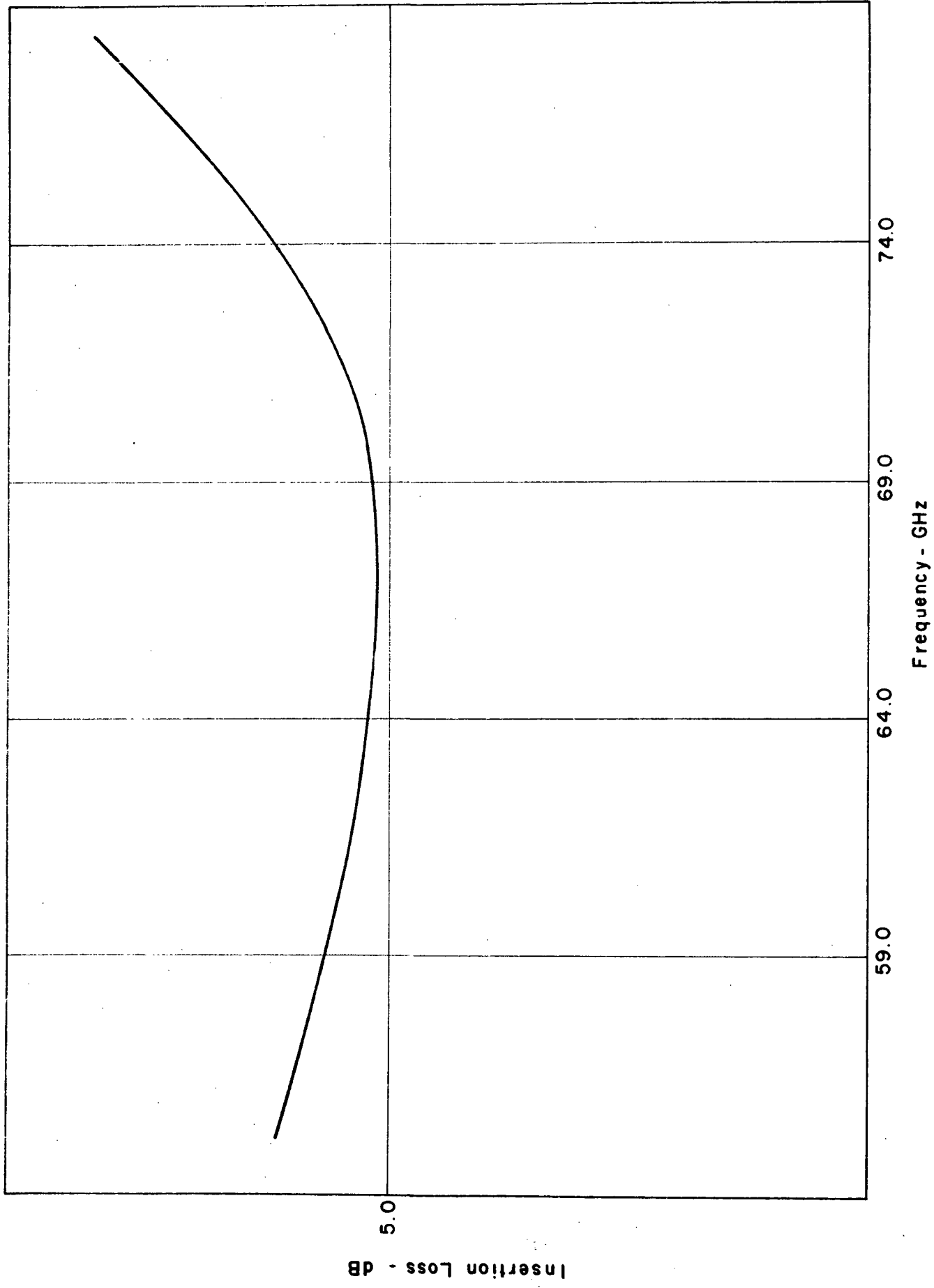
Fig. 27 ATTENUATION OF "U" WAVEGUIDE NO 2 ON A GOLD / BRASS BASE PLATE

57

in attenuation was typically 2 dB, shown in Figure 28. The attenuation increase in this case was attributed to a larger gap between the alumina and the base plate which would contain a larger volume of adhesive.

It is evident from these results and those of the previous subsection that adhesive losses are of primary concern in the fabrication of image waveguide integrated circuits. A method was investigated for eliminating the adhesive losses. The deposition of a conducting metal film on the undersurface of the alumina waveguide would require the conduction currents immediately below the alumina to flow in the film rather than in the base plate. If the adhesive were placed between the base plate and the film, it is expected that the capacitive coupling between the two metal surfaces would prevent dielectric losses in the adhesive.

Two attempts to verify this theory were made. The use of films in conjunction with the band-stop filter was successful with Q values of 1000* achieved in one measurement and 660 in a second measurement. Details of these results are given in Section 4.5.

---

* If this Q of 1000 is assumed to be the unloaded Q, then the corresponding attenuation factor would be $\alpha = 0.027$ db/λ_g. This compares favorably with the value of 0.025 dB/λ_g calculated for the image waveguide at 65 GHz (see Section 3.3.4).
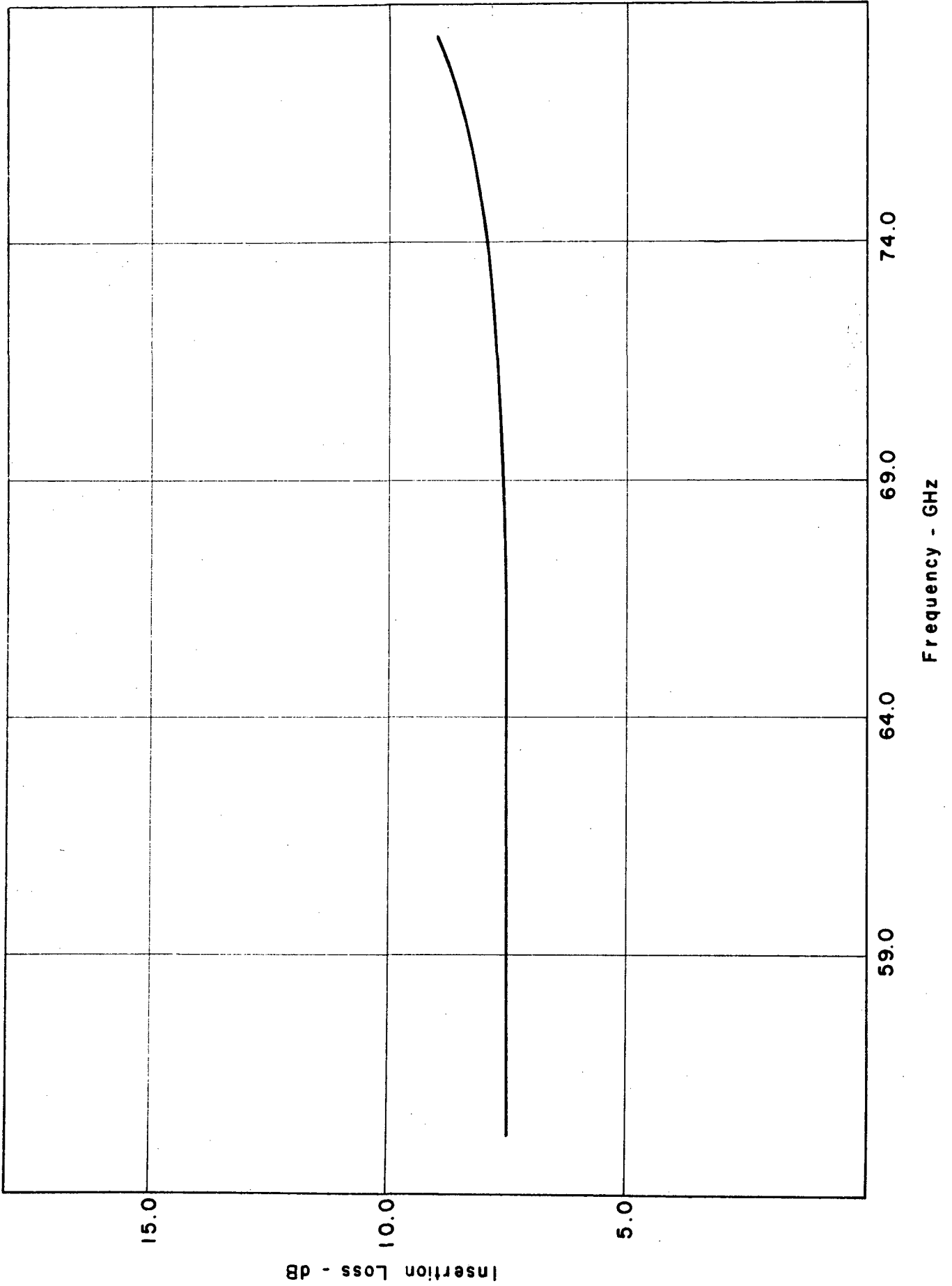
Fig. 28 ATTENUATION OF "U" WAVEGUIDE NO 2 ON THE GOLD / BRASS BASEPLATE - ALUMINA
WAVEGUIDE NOT WEIGHTED DURING ATTACHMENT

59

An aluminum film of 0.000078 in.* was plated on the polished undersurface of the alumina "U" waveguide No. 2. The alumina waveguide was attached to the gold/brass base plate with the type 509 adhesive. The attenuation of the "U" waveguide with the film is shown in Figure 29. The attenuation curve indicated excess radiation or absorption for all frequencies below 70 GHz. The attenuation above 70 GHz was excessive, but was attributable to one of the mechanisms described earlier (adhesive loss, excess conductor loss) because this waveguide was not weighted during attachment (see Figure 28). The result strongly suggested that the dispersion curve, shown earlier in Figure 2 for $\varepsilon_r = d$ and a/b = 1, was not applicable and that the wave velocity increased below 75 GHz to the point where radiation from the curves in the waveguide was possible. If a gap existed below the film, as was evidenced by the excess attenuation above 70 GHz, then the waveguide indeed conformed to a rather different model than the image waveguide. The waveguide model with the gap would be as shown in Figure 30 where the film-to-image plane spacing is designated **g**. The influence of the gap g would be to increase the velocity for any given value of frequency (B). This point is taken up further in Section 3.6.

The results of this subsection clearly indicate the need for a method of attachment of the ceramic waveguide to the image plane which does not introduce additional attenuation or cause a change

---

* The skin depth in aluminum at 60 GHz is 0.000016 in. Therefore, the film thickness exceeded the skin depth by five times.
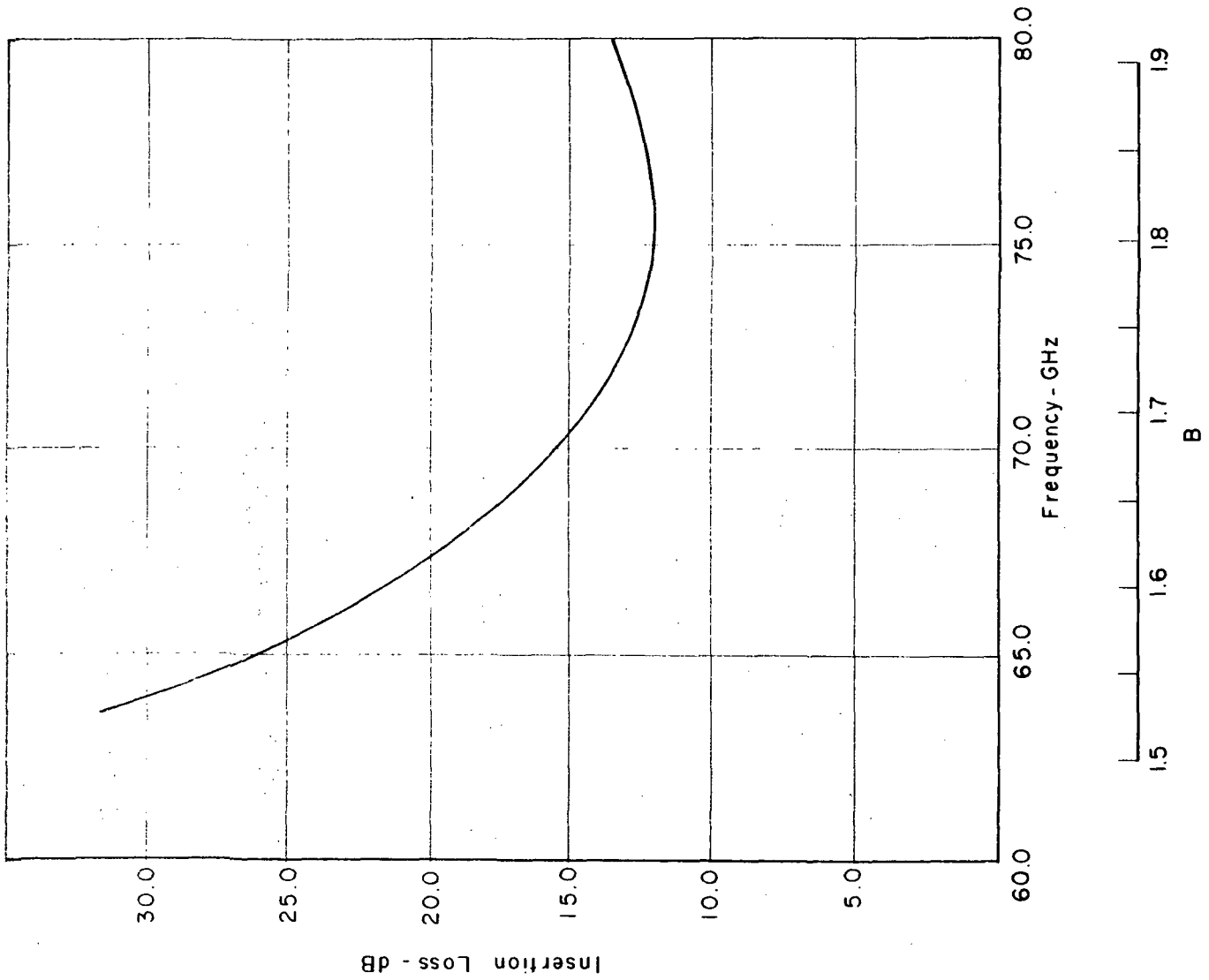
Fig. 29 ATTENUATION OF "U" WAVEGUIDE NO 2 WITH
ALUMINUM FILM PLATED ON THE UNDER
SURFACE

61
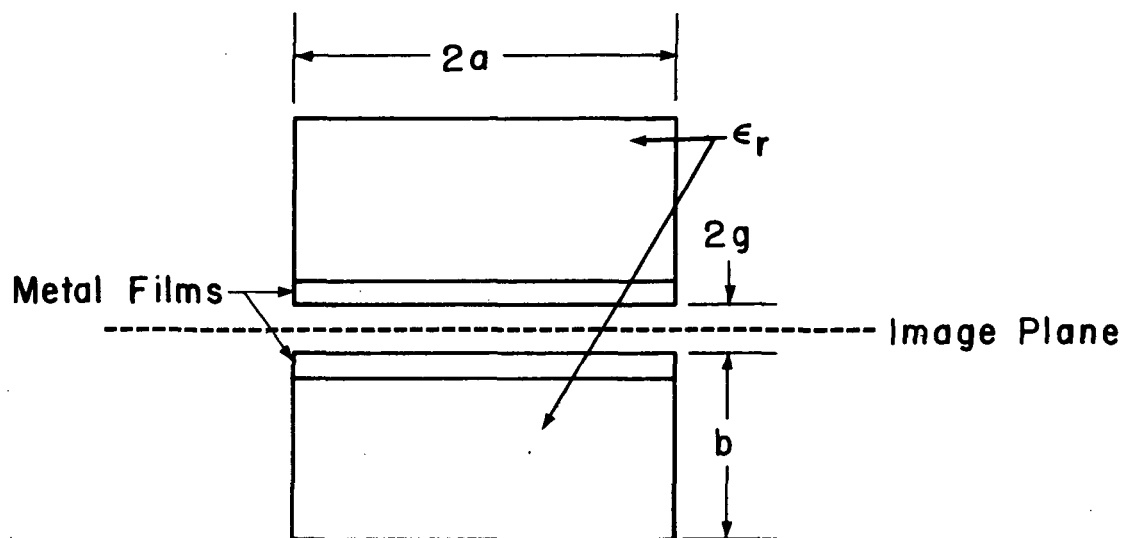
Fig. 30   MODEL   OF THE IMAGE WAVEGUIDE PLATED WITH
METAL   FILM   AND HAVING A GAP g BETWEEN THE
FILM   AND THE IMAGE PLANE

in the waveguide dispersion properties. While the results of

investigations using films were favorable, further understanding

of this approach is required before any conclusions are drawn.

The use of solder or braze appears to be an approach with consid-

erable merit in that it would eliminate any possible gap. The

constituents must be selected carefully so as not to introduce

an increase in conduction losses. Attachment of the ceramic

waveguide to the image plane is considered further in Section 6.3.4.

3.4 Field Distribution in the Image Waveguide

3.4.1 Introduction

The field distributions in the image waveguide have been pre-

dicted theoretically.[15] When the image waveguide is straight,

the field distribution must be symmetrical about the center line

of the dielectric. However, when the waveguide is curved, the

field distribution changes across the waveguide. Also when an

image waveguide couples to another, field distributions must change

due to the effects of mutual coupling. In the following subsec-

tions measurements of the field distributions in a curved guide

and in a three-terminal Y junction will be described.

3.4.2 Field Distribution a Curved Waveguide

The X-band "U" waveguide, shown in Figure 5, was used

for measurement of field distribution. The linear array of small

holes in the image plane allowed the insertion of a short electric

field probe into the fields of the image waveguide and adjacent

areas. Probing of the fields along the straight section of the

image waveguide indicated, as expected, symmetry of the fields at all frequencies in X-band. The field distribution radially along the 2-in. radius of the curved section of waveguide is shown in Figure 31(a) through (f) for various frequencies between 8 and 12 GHz. In these figures zero distance is at the center of the dielectric. Negative distances represent radial measurements toward the center of the waveguide curvature. Positive distances represent measurements radially outward from the center of curvature. The ordinate is power level in dB relative to the maximum.

In Figure 31(a) the field distribution at 8.0 GHz was found to be highly asymmetrical with distribution shifted radially outwards due to radiation from the curve.* The radiation from the curves was clearly evident in the results shown earlier in Figure 6 for frequencies below 10 GHz (see also Section 3.5). The asymmetry in the central field lobe continued but diminished as the frequency was increased from 8 to 10 GHz. This is shown in Figures 31(b) through (e). Note that even within the dielectric material the peak of the field distribution was shifted outward from the center line.

In Figure 31(f) the field distribution at 11 GHz was very nearly symmetrical in the central lobe. Unfortunately, the probe pickup, apparently due to excess radiation from the launchers,

---

* The sidelobe fields, which were typically 15 to 20 dB down from the peak value, are difficult to interpret because of stray fields from the launcher.
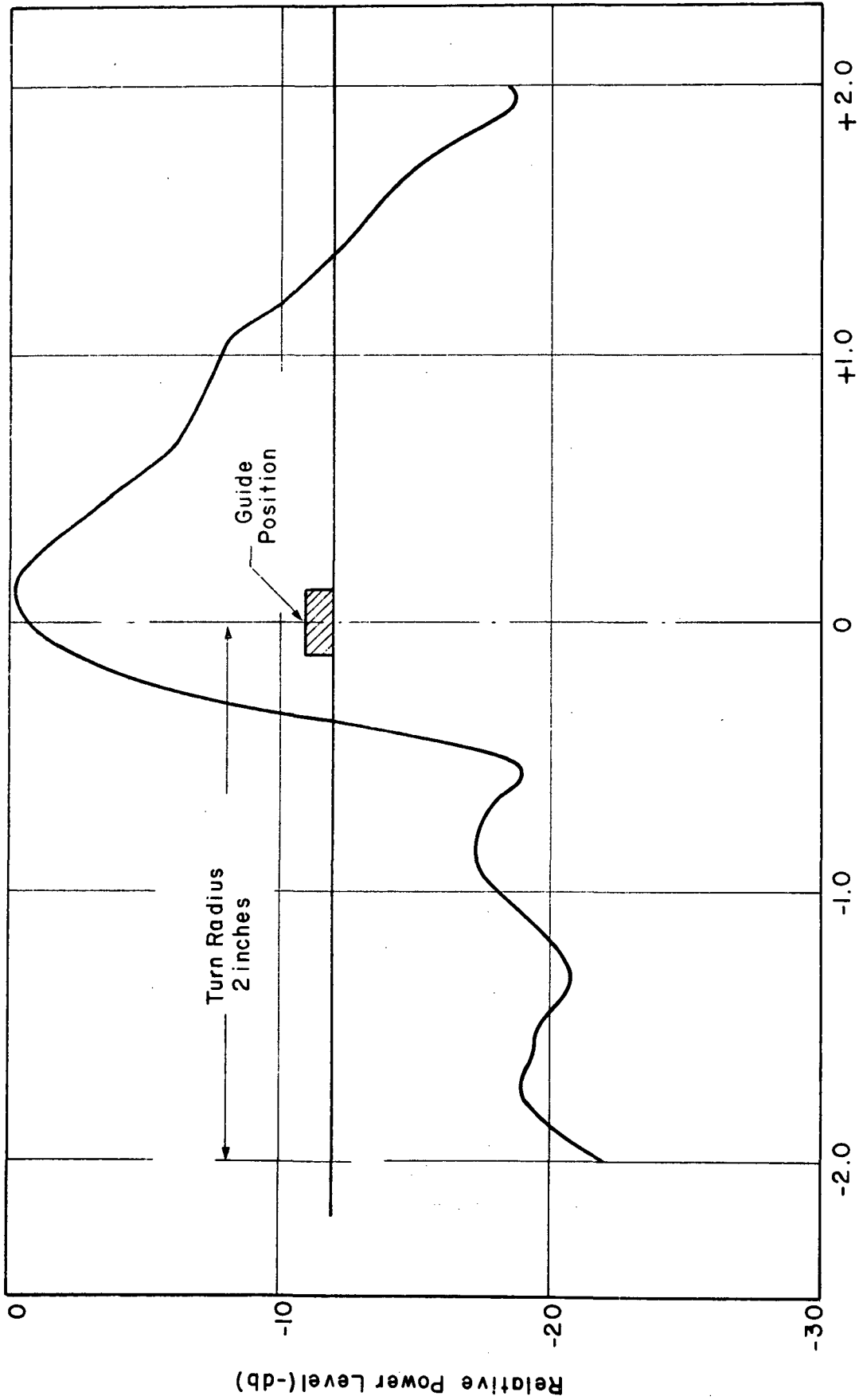
Fig. 31a FIELD DISTRIBUTION IN A CURVED WAVEGUIDE, FREQ = 8.0 GHZ

65
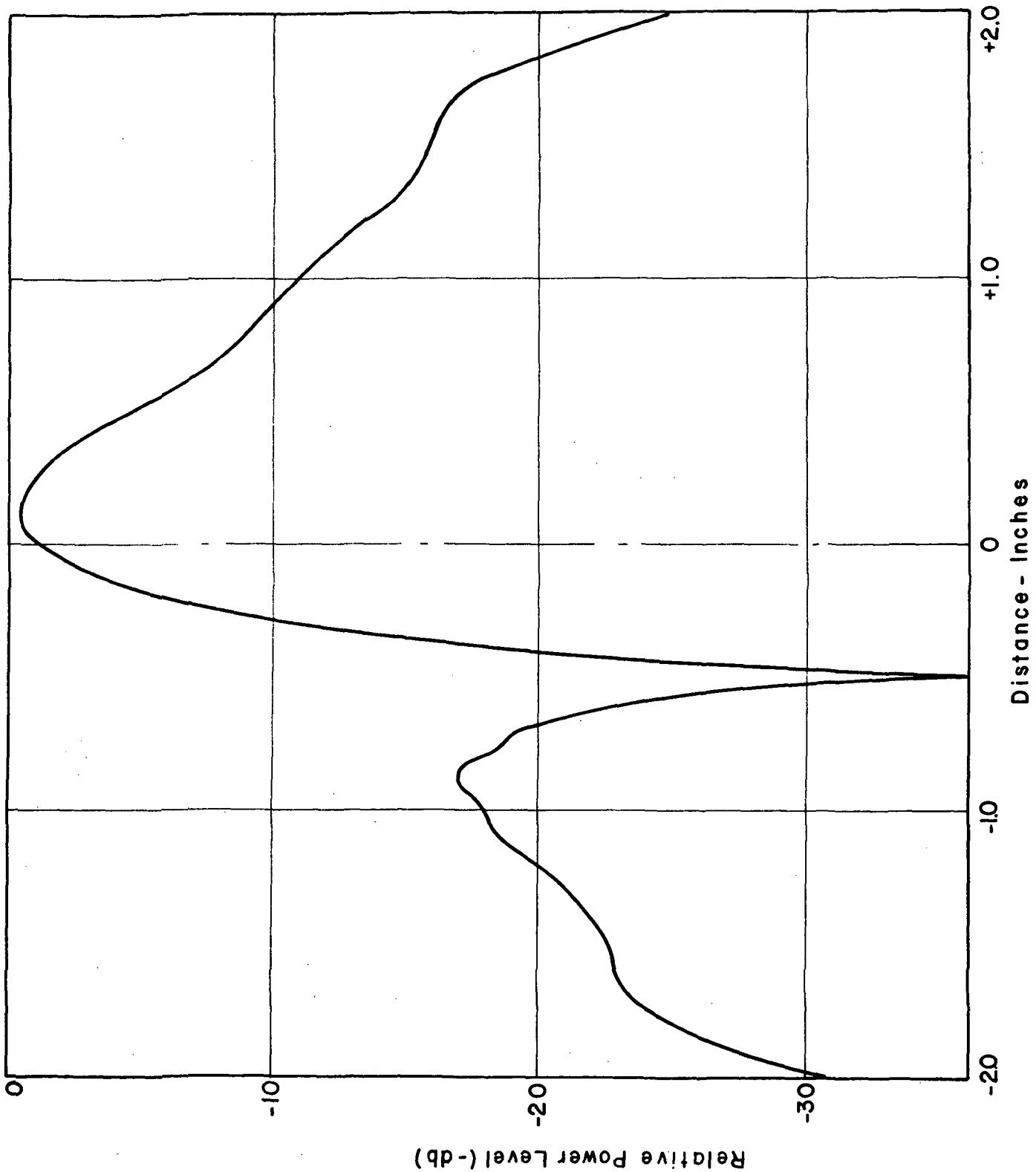
Fig. 31b FIELD DISTRIBUTION IN A CURVED WAVEGUIDE, FREQ=8.5 GHZ

Distance - Inches

Relative Power Level (-db)

66
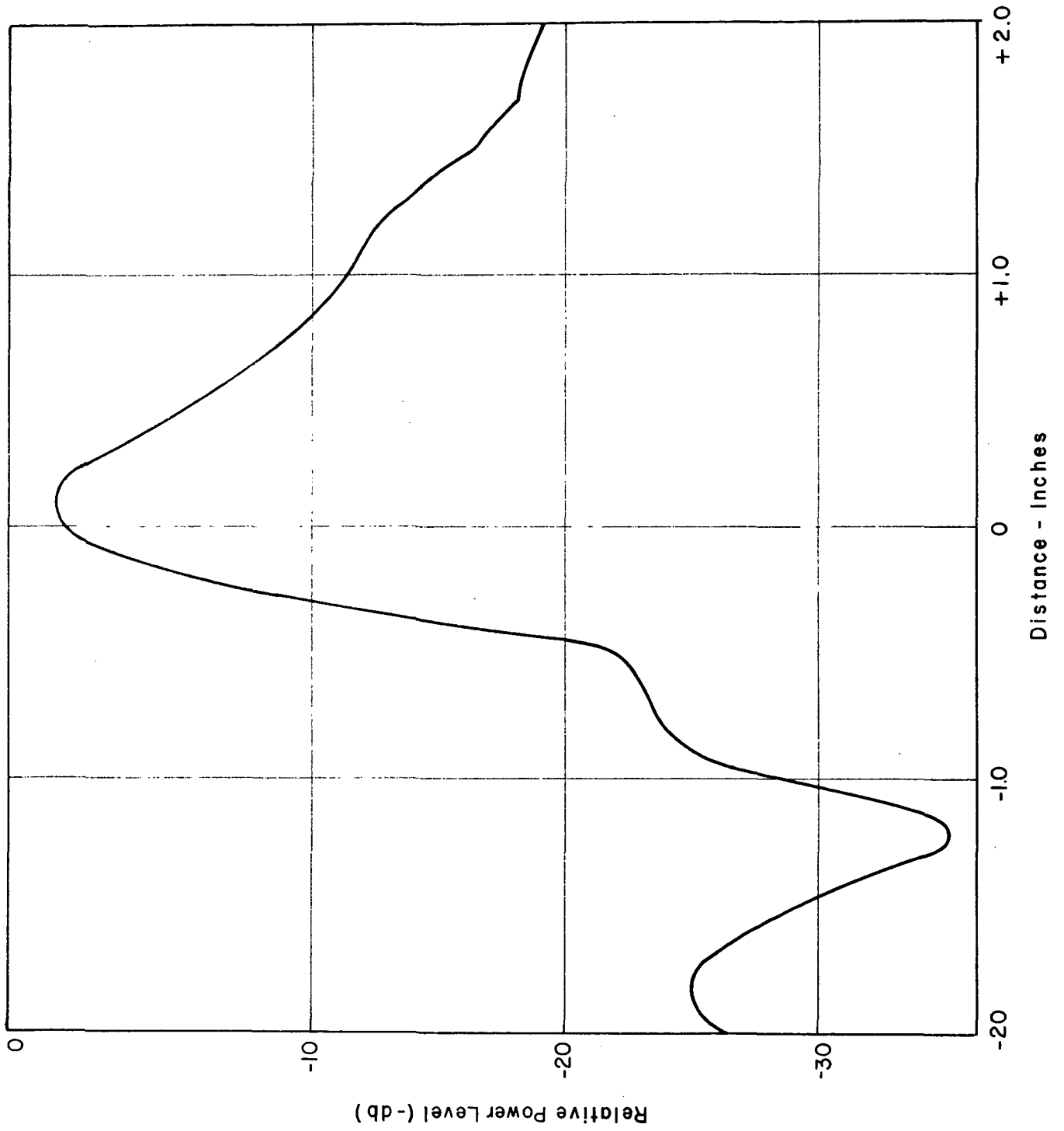
Fig.31c FIELD DISTRIBUTION IN A CURVED WAVEGUIDE, FREQ = 9.0 GHZ

Distance – Inches

Relative Power Level (-db)

Fig.31d FIELD DISTRIBUTION IN A CURVED WAVEGUIDE, FREQ=9.5 GHZ

Distance - Inches

Relative Power Level (-db)
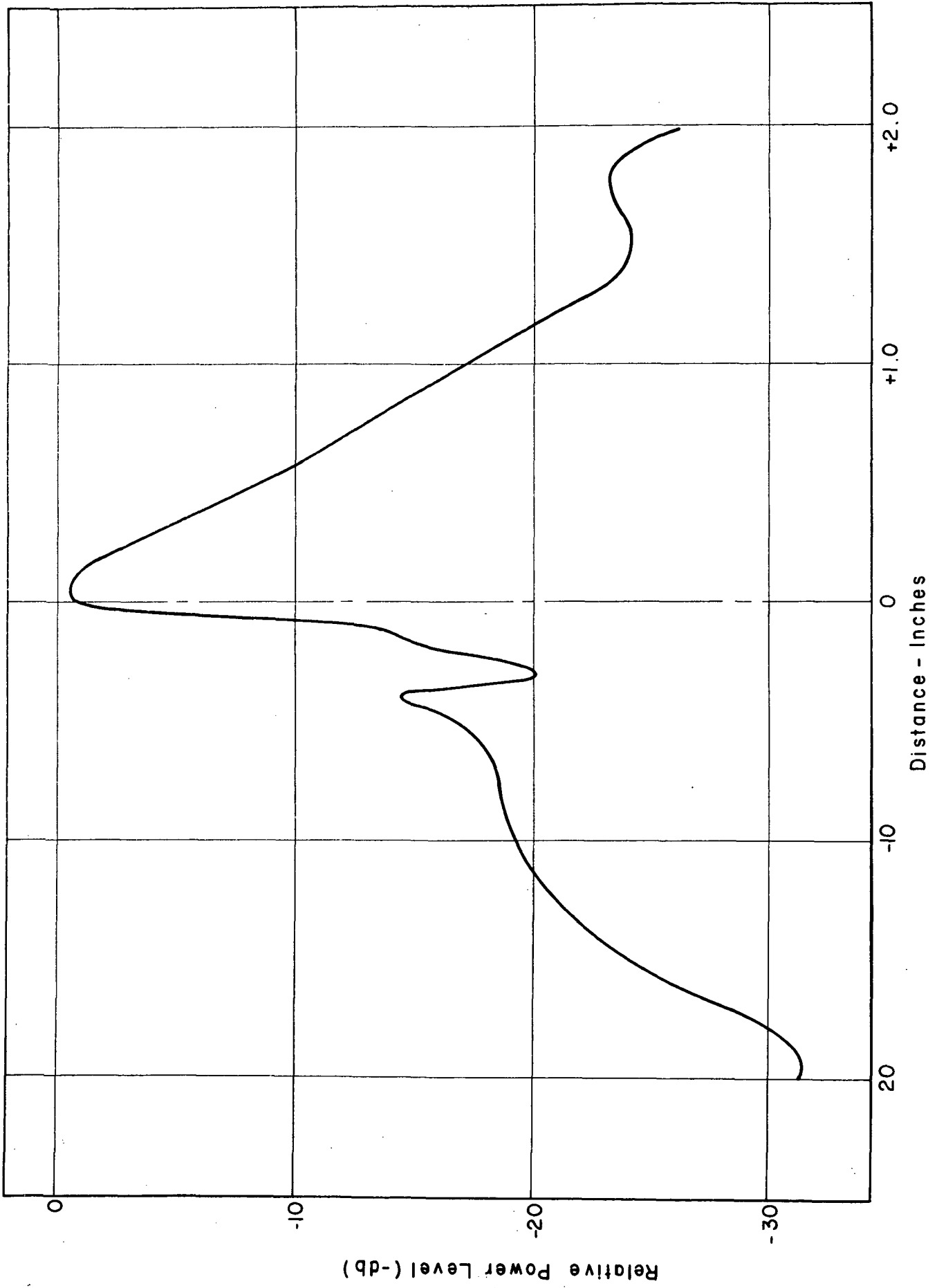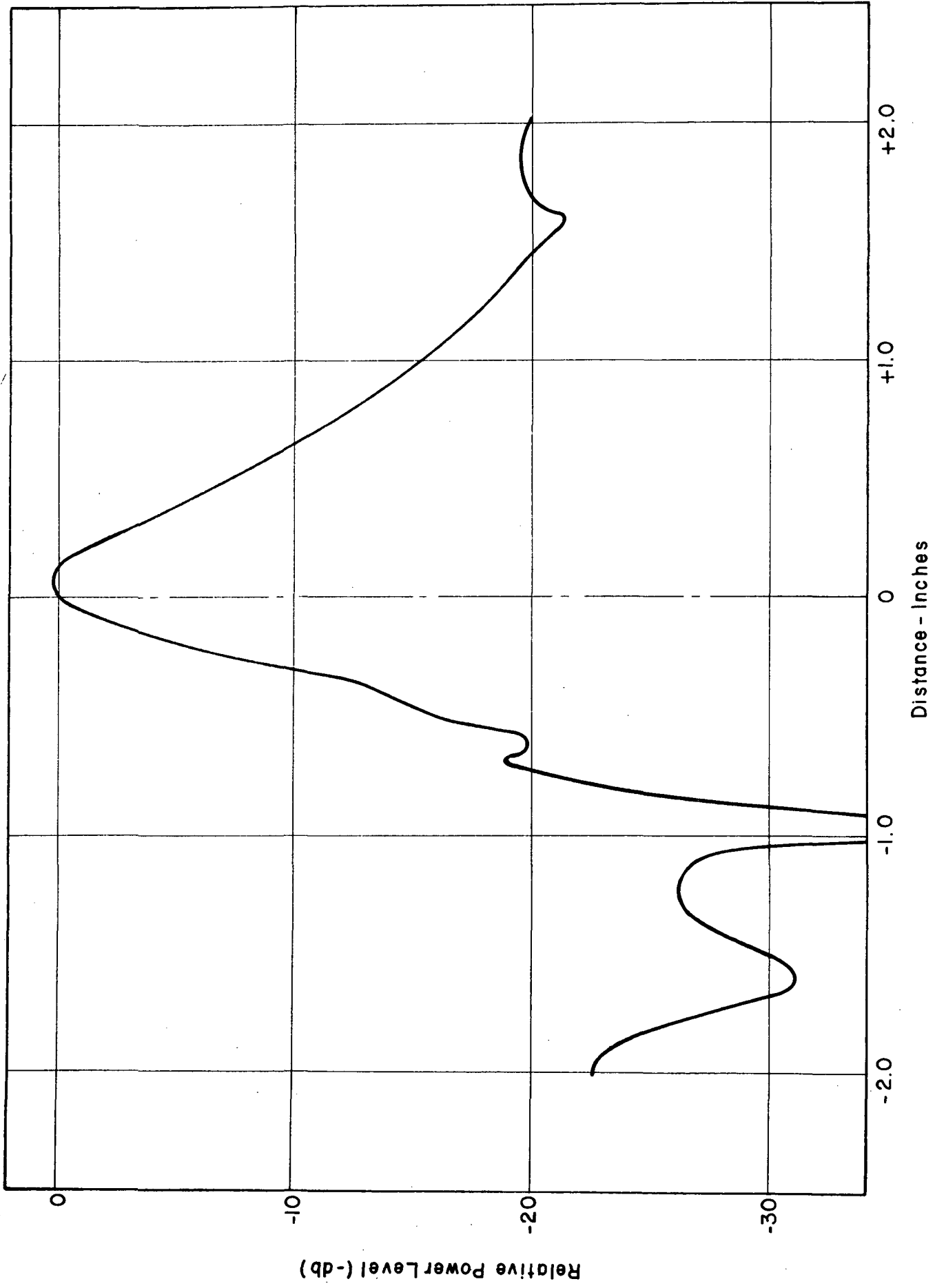
Fig. 31e FIELD DISTRIBUTION IN A CURVED WAVEGUIDE, FREQ = 10.0 GHZ

Distance – Inches

Relative Power Level (-db)

69
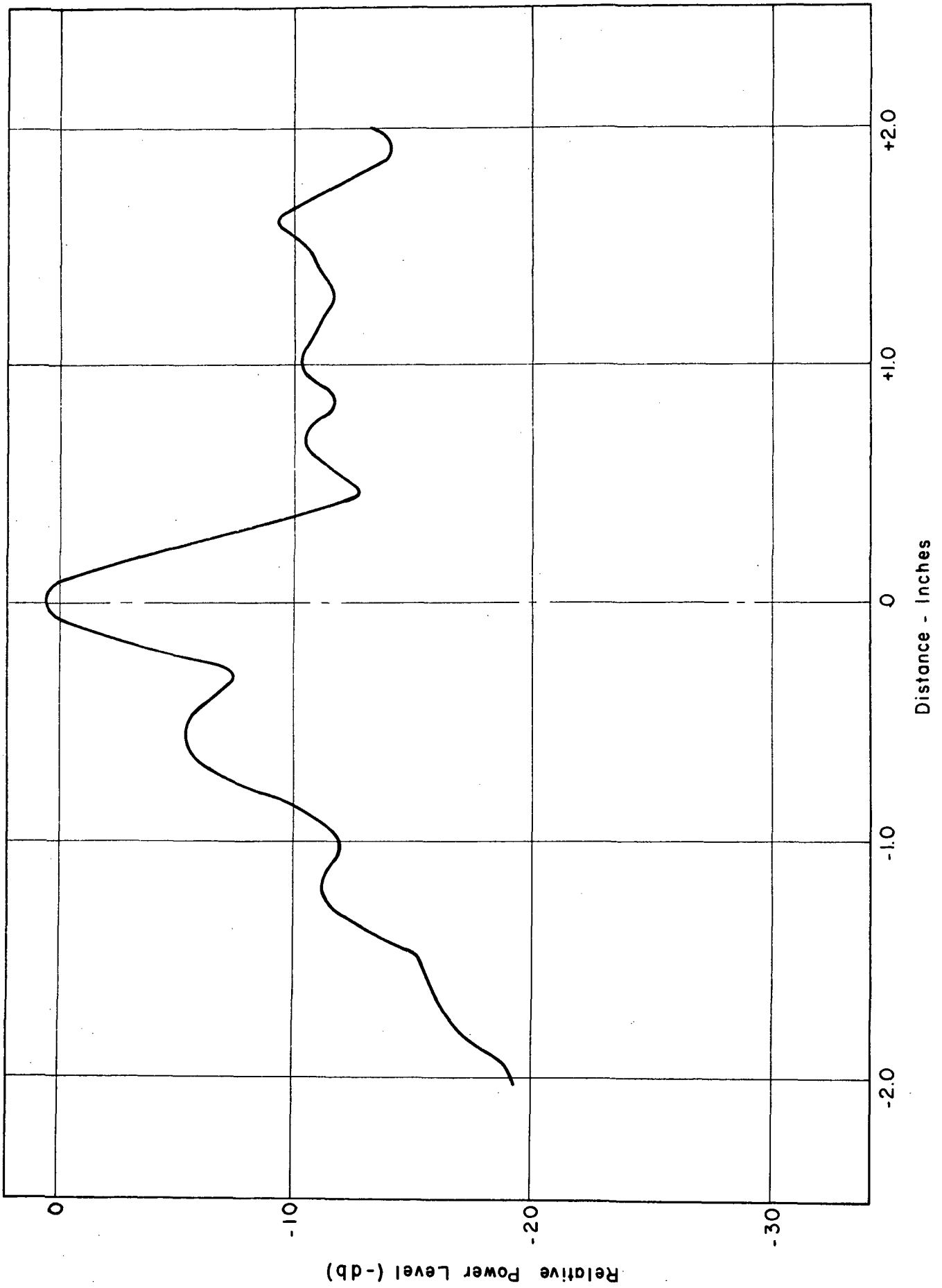
Fig. 31f FIELD DISTRIBUTION IN A CURVED WAVEGUIDE, FREQ = 11.0 GHZ

Distance - Inches

Relative Power Level (-db)

70

caused an increase in the sidelobe levels. As the frequency was further increased, the pickup dominated the measurement, and the fields within the waveguide were not discernible. It should be noted that these measurements were performed prior to the time in the program that launcher efficiencies were improved and the excess attenuation due to adhesive loss became apparent.

The distribution measurements correlate well with the attenuation measurements given in Section 3.3.3 in that they show a shift in the field distribution radially outward as radiation attenuation increased. The broadening and shifting of the central field lobe with decreasing frequency is an indication of degradation in the guidability of the image waveguide.

3.4.3 Field Distributions in the Y Junction

Field distributions were also measured on the three-terminal junction designated Y-1 and shown in Figure 42. Small holes in the image plane, located 0.1 in. apart, were drilled in two linear patterns as shown in Figure 32. The relative field distribution at various frequencies between 8.5 and 12.0 GHz in junction Y-1 are shown in Figure 33(a) through (e). The line of measurement marked $\mathcal{E}$ passes through the center of the junction, a null is expected at a distance 0 in., and peaks are expected at approximately $\pm$ 0.4 in. Examination of the $\mathcal{E}$ distribution at lower frequencies (8.5 through 10.0 GHz) shows that three distinct peaks are found and that the null at 0 in. is not very deep. The first peak, which occurs at -0.2 in., coincides
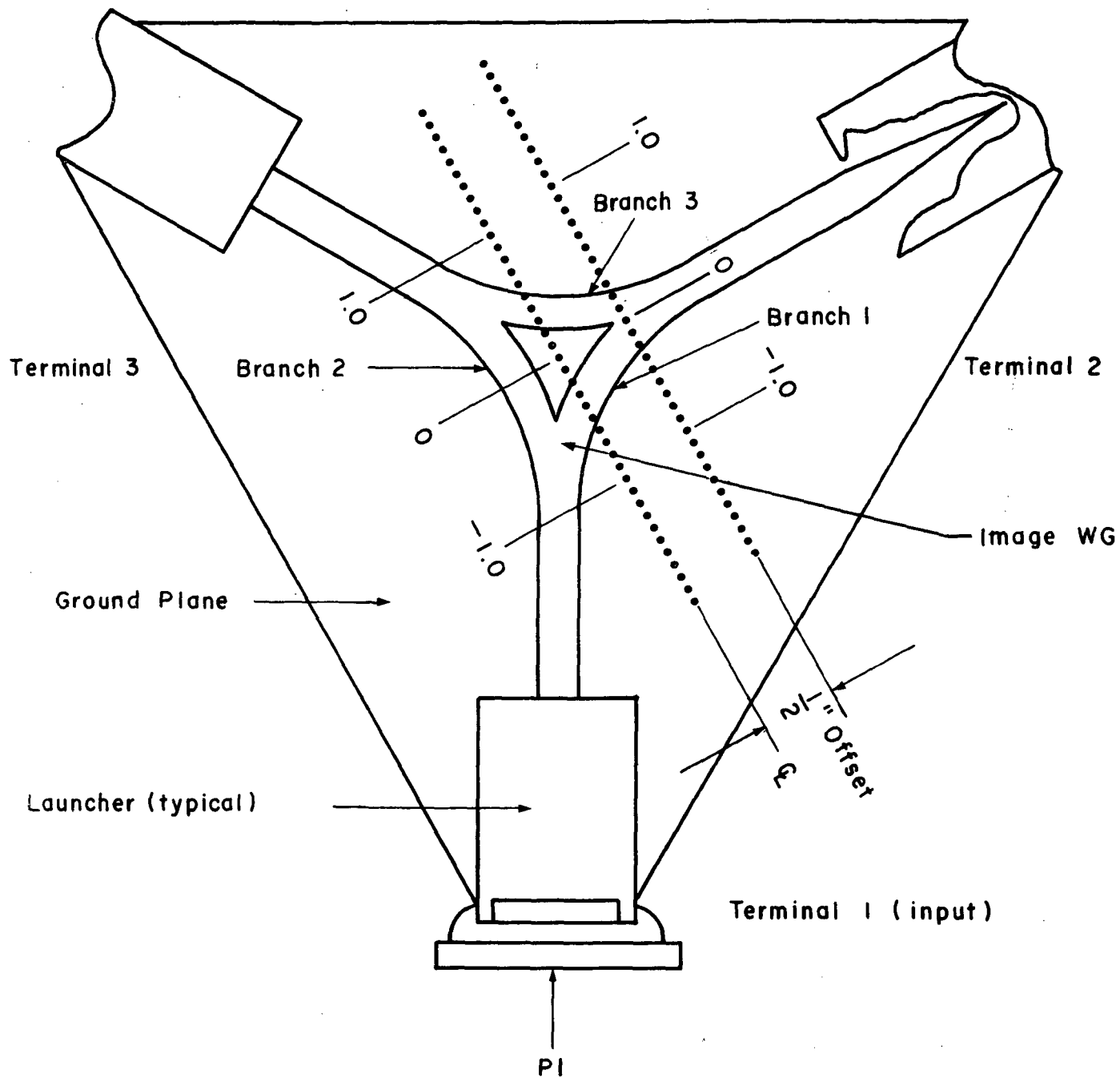
Fig. 32   JUNCTION Y-1 SHOWING HOLES FOR INSERTING
FIELD PROBES
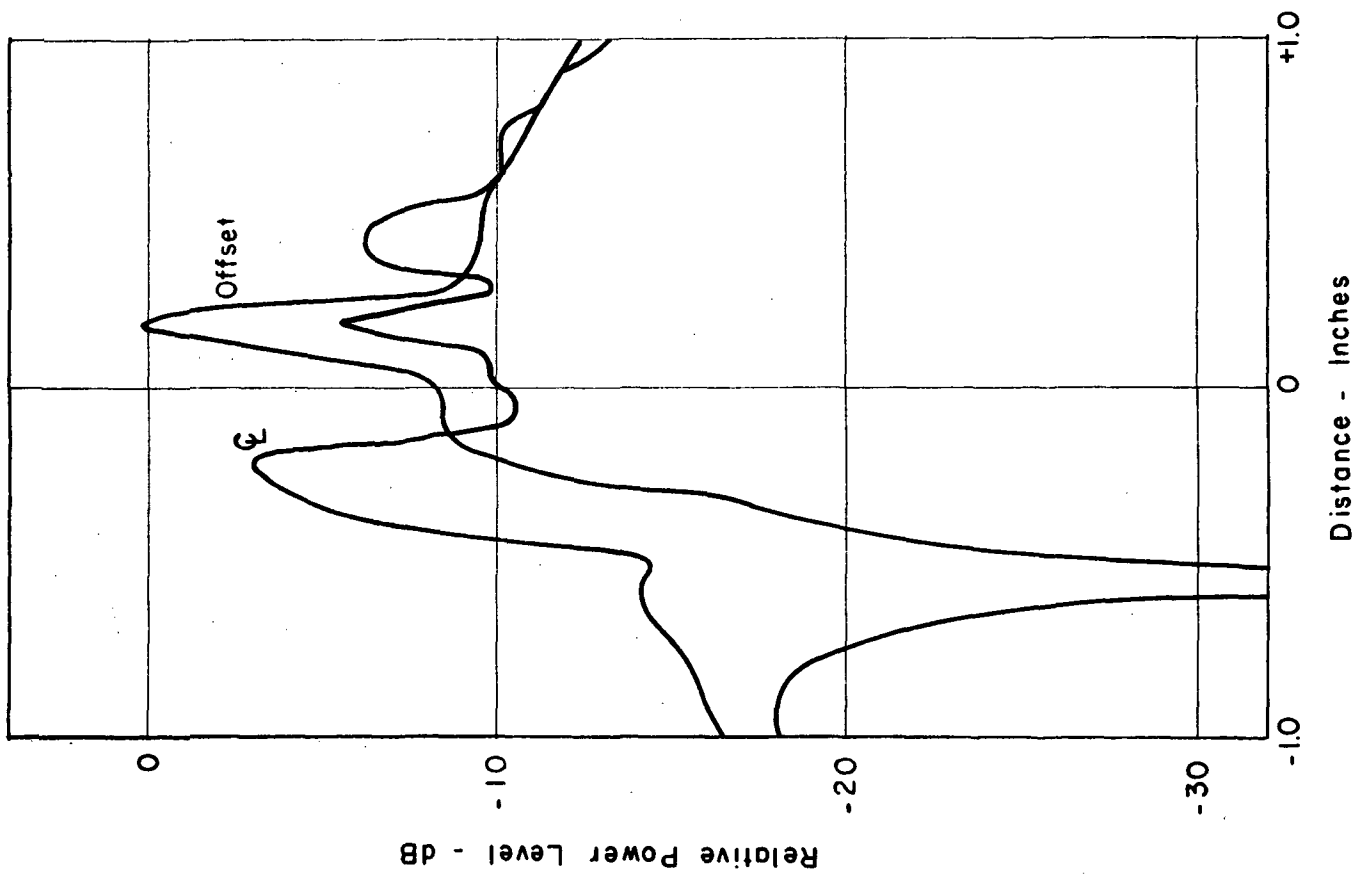
Fig. 33 a   FIELD DISTRIBUTIONS IN JUNCTION   Y-I , FREQ. = 8.5 GHz

73
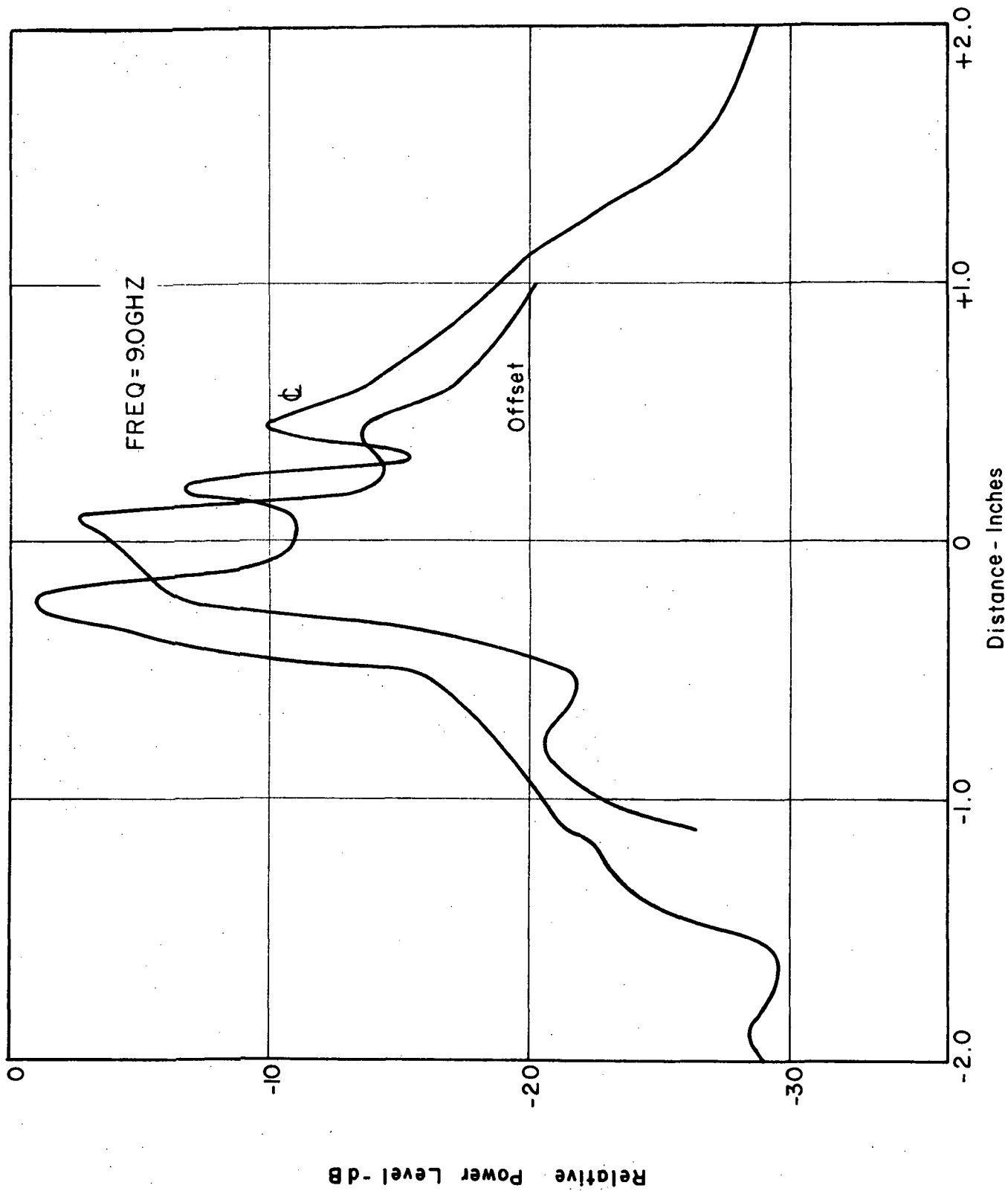
Fig. 33b FIELD DISTRIBUTION IN JUNCTION Y-I, FREQ. = 9.0 GHz

74

75
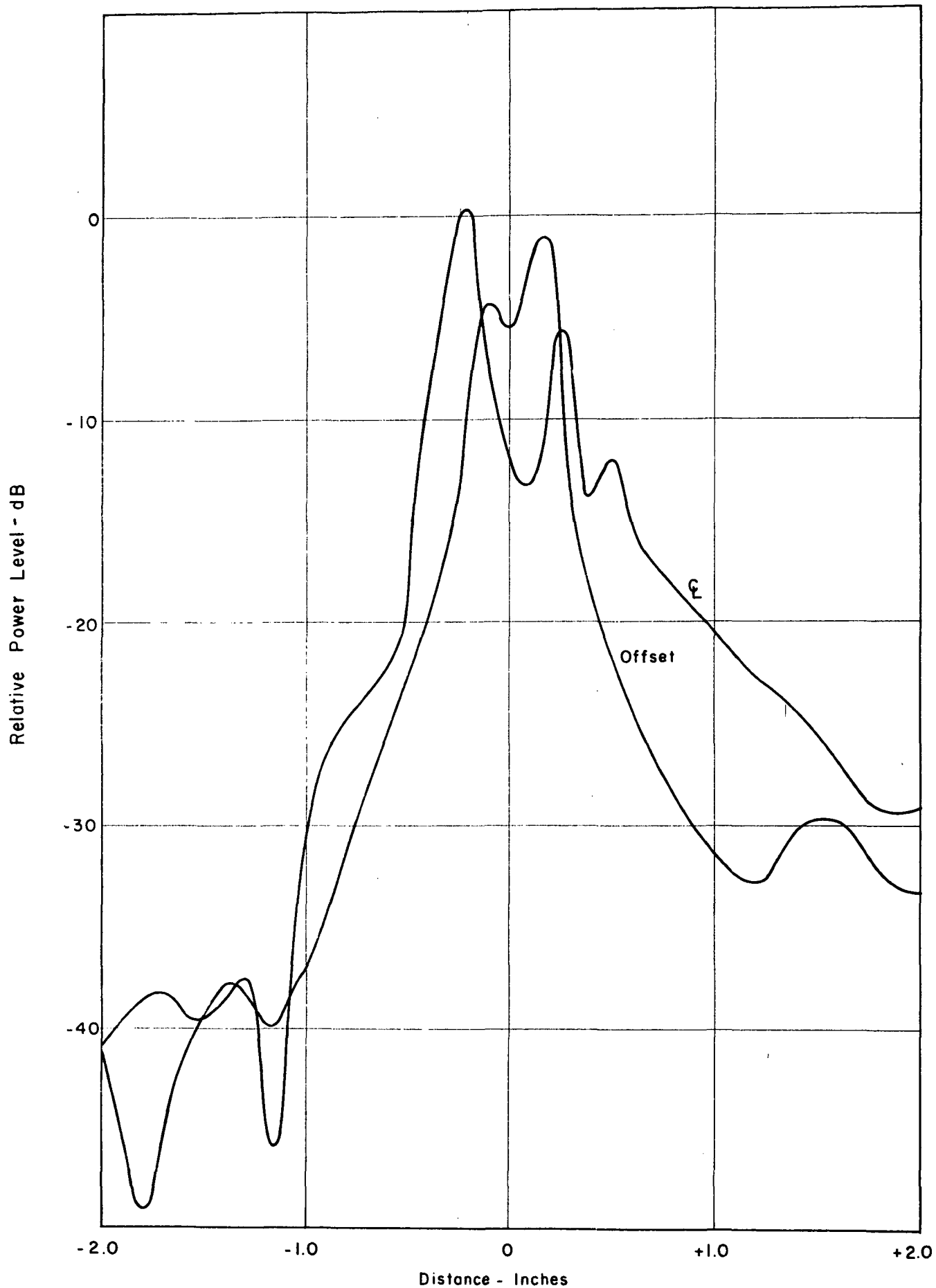
Fig. 33c FIELD DISTRIBUTION IN JUNCTION Y-I, FREQ = 10.0 GHz
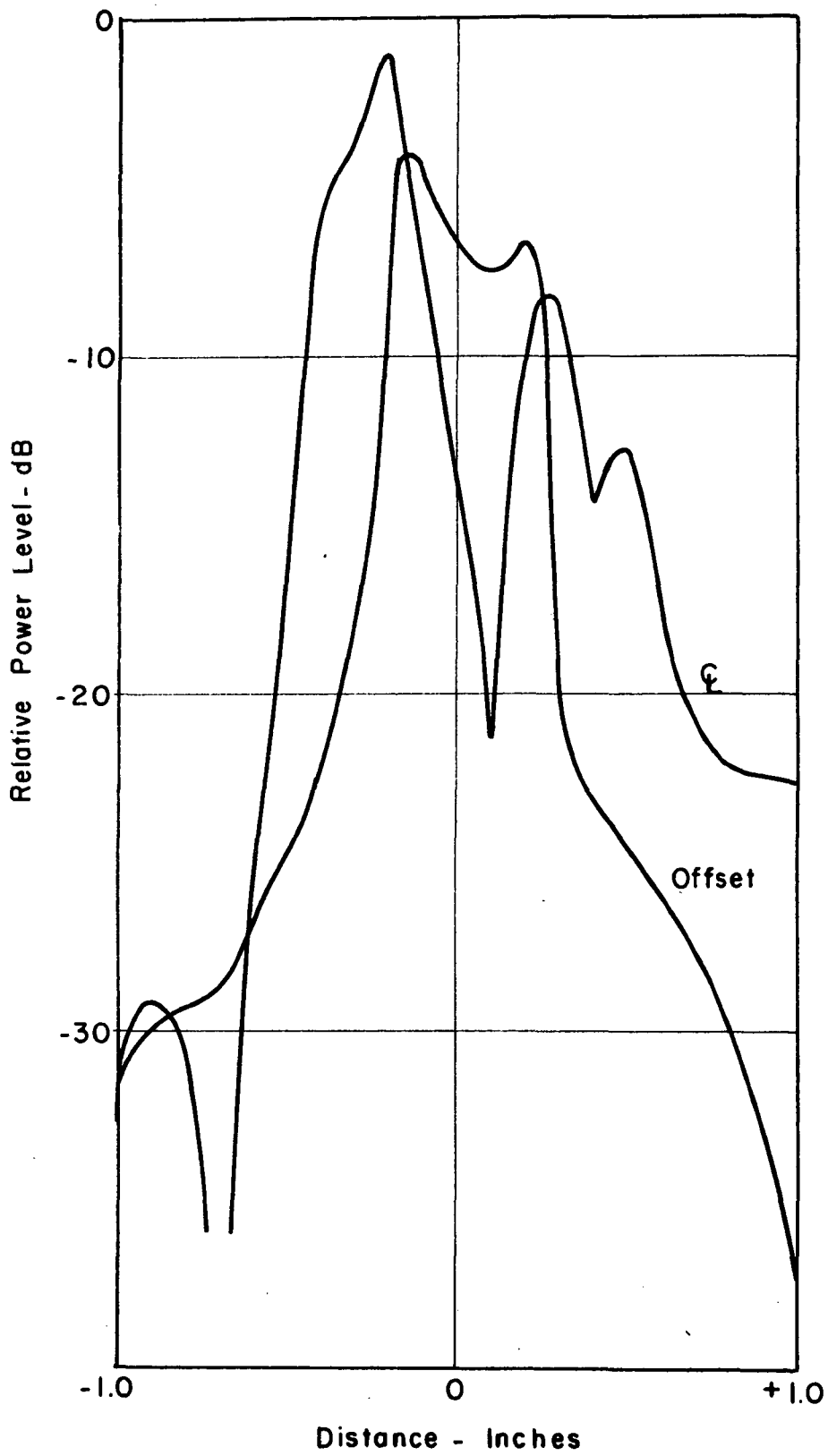
Fig. 33d FIELD DISTRIBUTION IN JUNCTION Y-I, FREQ.≈II.O GHz
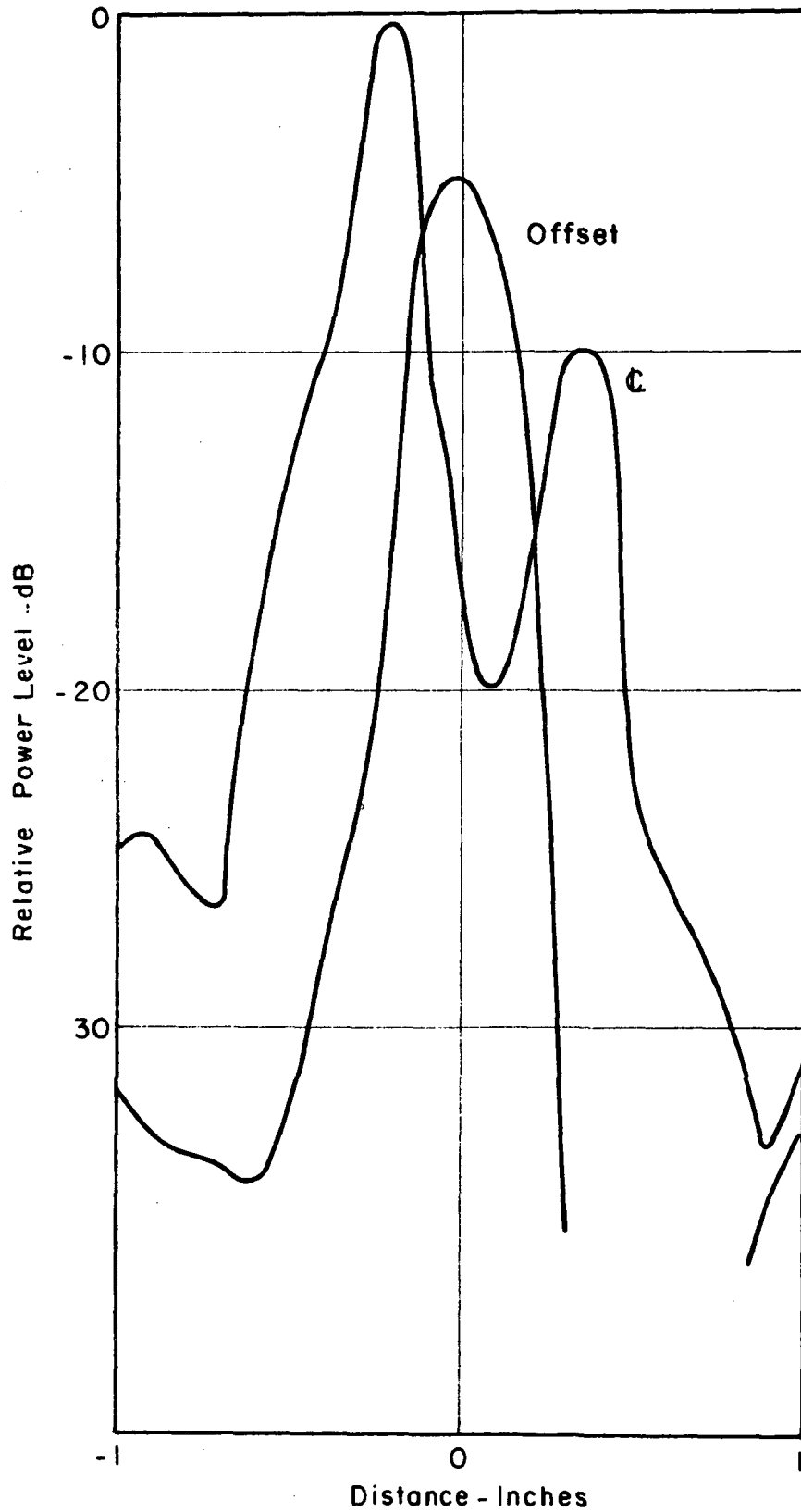
Fig. 33e FIELD DISTRIBUTION IN JUNCTION Y-I, FREQ.=12.0 GHz

77

with the outer radius* of branch 1. This indicates poor guidability because the fields are shifted away from the center of the waveguide. The poor guidability of the divided field modes in branches 1 and 2 accounts for the poor null at the 0 distance and for the double peak occurring at +0.2 in. and +0.4 in. As frequency was increased, the double peak became a single peak at a distance +0.35 in., which is the approximate center of branch 3. A deep null developed at a distance +0.1 in. which is close to the center of the junction. The first peak remained at -0.2 in. for all frequencies which indicates somewhat of a guidability deficiency even at 12 GHz. This observation could account for excess losses that were measured in this junction (see Figure 43).

The field distribution along the offset line showed a single dominant peak at a distance +0.2 in. at lower frequencies. As frequency was increased, a second peak developed at -0.15 in. which is the center of branch 1. This change represents the improvement of guidability in branch 1 between 8.5 and 11 GHz. At 12 GHz the two peaks became one broad peak indicating that the modes in branches 1 and 3 were closely coupled together.

The transmission characteristics for junction Y-1, given in Figure 43, showed that despite some excess radiation and loss, the behavior of the junction was about as expected--between 10 and 12 GHz. This same observation can be made about the two sets

_____

* Outer radius refers to the edge of the waveguide closest to the center of the junction.

of field distribution measurements described above. The conclusion drawn from these results is that no circuit component which involves curved waveguides can perform as desired at frequencies where radiation from the curved waveguides is significant.

3.5 Radius of Curvature Effects

3.5.1 Introduction

During the course of the program, both theoretical and experimental investigations were conducted in an attempt to determine quantitatively the amount of energy radiated from curved dielectric image guides. Two curved waveguide configurations were used in the experimental work: (1) the "U" shaped guide and (2) the "C" shaped guide. As shown below, the correlation between theory and experiment was good with differences resulting primarily from gaps under the image waveguide which were not taken into account in the theoretical model.

3.5.2 Theoretical Analysis

Two different methods of analysis were employed to determine energy loss by radiation from curved dielectric guides. The first method viewed the guide configuration as a boundary-value problem. Employing Maxwell's equations and applying appropriate boundary conditions at the interfaces of the image guide, a set of two characteristic equations were obtained as shown in Appendix A. Solving for the eigenvalues of this system of equations yields two important pieces of information, i.e., the guide wavelength in a curved waveguide section and also the attenuation constant

(dB/radian) due to radiation. However, as explained in Appendix A, numerical difficulties were encountered in the process of searching for complex eigenvalues which represent the order of the various Bessel functions involved. The computer program yielded numerical results which were accurate for the guide wavelength of a curved waveguide but entirely erroneous results for the radiation constant (see Appendix A for details).

To circumvent this difficulty, another method was used to obtain only the radiation from curved guides. This analysis is presented in Appendix B where numerical results are included.

3.5.3 Experimental Results

The experimental measurements were conducted at X-band using "U" and "C" shaped image line configurations with a/b = 1 and ε_r = 9. The results are presented in Figure 34 where the attenuation constant (in dB/radian) is plotted versus frequency. The radiation effects are clearly seen at the lower end of the X-band. In addition to the experimental results, Figure 34 includes the theoretical results obtained on the basis of the approximate analysis presented in Appendix B.

The fact that the general shape and slope of the theoretical and two experimental curves are approximately the same is considered verification of the validity of the approximate theoretical model. The lateral displacement (in B) of the three curves is attributed to gaps between the dielectric waveguide and the image plane (see Section 3.6 below). The theoretical calculation, since it does not consider the existence of a gap, predicts lower

80
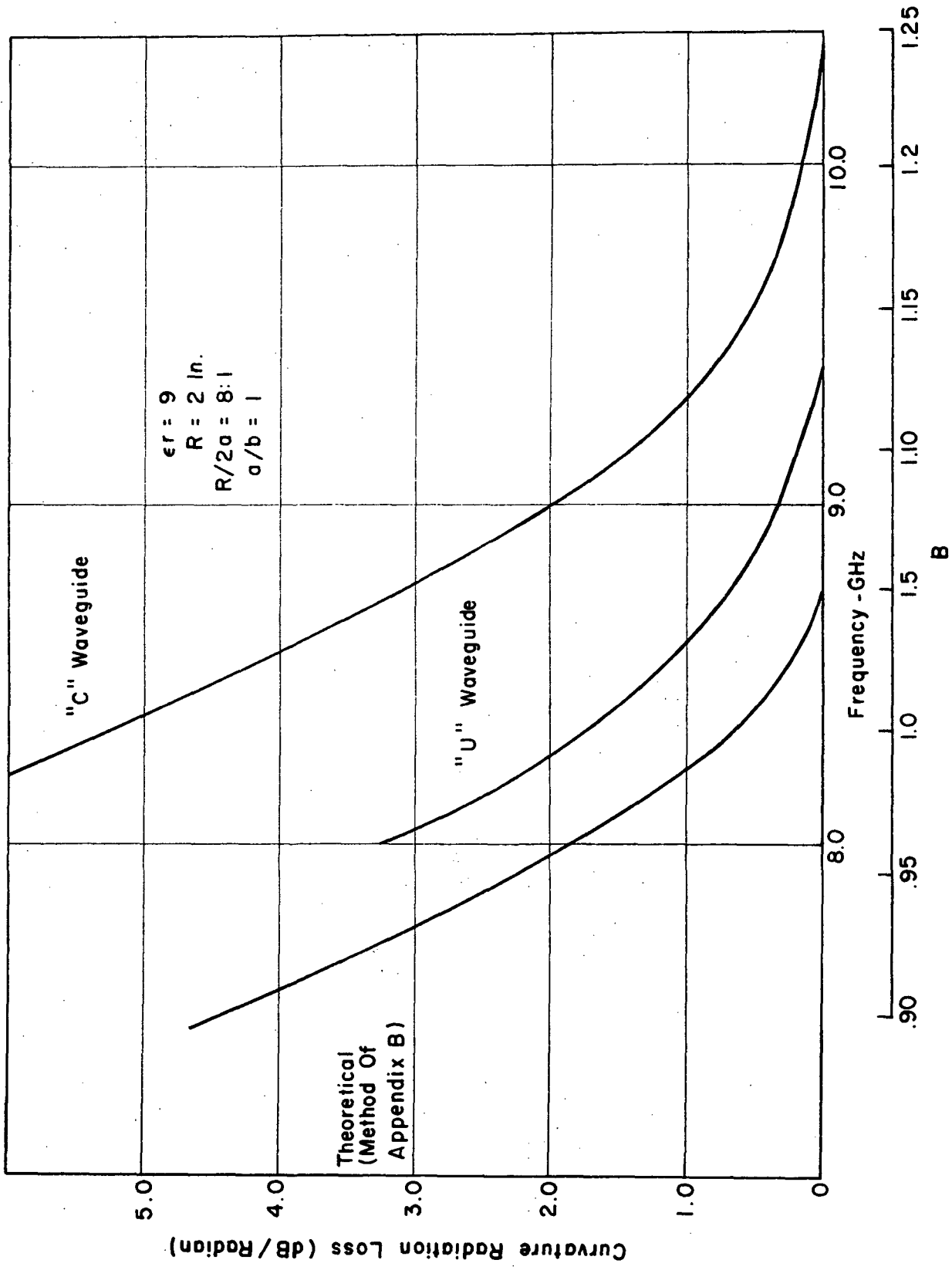
Fig. 34 CURVATURE RADIATION LOSS FOR THE "U" AND "C" WAVEGUIDES

81

attenuation due to radiation. The existence of the gap in the
"U" and "C" waveguides increases the wave velocity and causes
greater radiation from curves.

3.6 Gap Effects

In the process of realizing dielectric image waveguides
during the course of this program, the presence of a small but
finite gap, either air or dielectric filled, between the dielec-
tric waveguide and the conducting image plane was unavoidable.
Figure 35 shows two different techniques that were employed to
fasten the image guide to its ground plane. In Figure 35(a) a
thin film of adhesive was used to minimize the gap size. Theo-
retical calculations have been performed and, as expected, have
shown that even very small gaps can increase propagation velocity
or guide wavelength substantially because the guided energy experi-
ences, in effect, a smaller overall dielectric constant if the gap
material has a dielectric constant lower than that of the image
waveguide. The result of this gap effect is that the waveguide is
less capable of guiding energy around bends, or that its guida-
bility is poorer than that of the corresponding no-gap guide.
Experimental measurements confirm this conclusion as shown in
Figure 34.

The thin film conducting coating, shown in Figure 35(b),
was introduced for the purpose of reducing any excessive dielectric
losses in the gap glue. Measurements, however, showed a substan-
tial increase in insertion loss due to radiation from a curved
image guide (see Figure 29). A qualitative analysis of this
particular configuration substantiates the measured excessive
loss, since the guide configuration of Figure 30 can be viewed
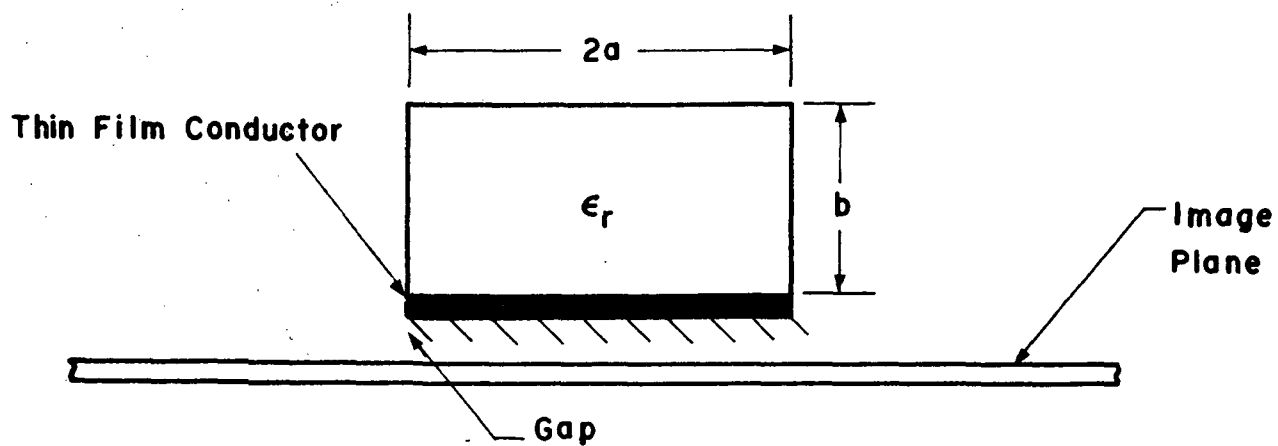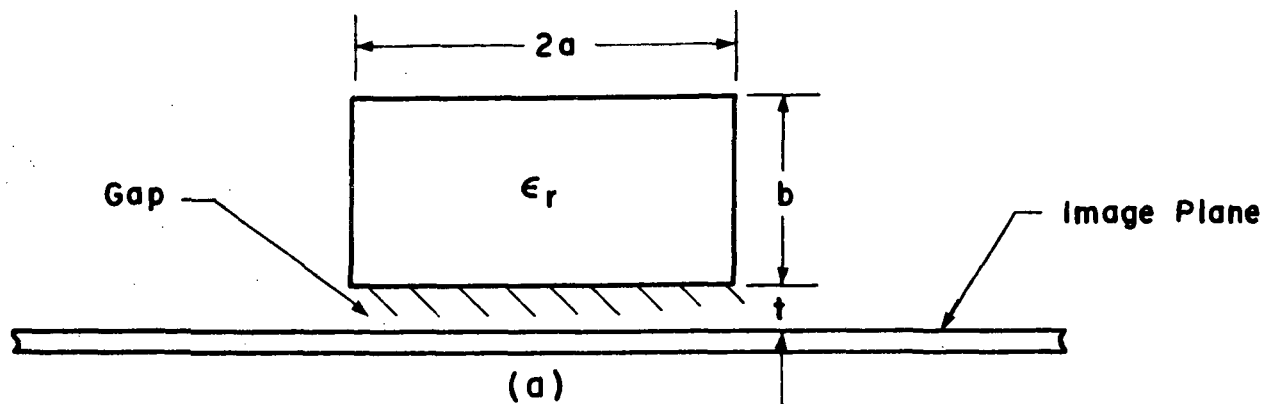
Fig.35 IMAGE LINE CONFIGURATIONS : a) WITH GAP AND
b) WITH PLATING AND GAP

as two parallel transmission lines, one corresponding to the rod and the other consisting of the thin conducting film and ground plane. The later, being a two-conductor line, can support a TEM type mode and can guide a substantial amount of energy if excited efficiently. Considering the launcher configurations used in the experimental work, it is possible that some energy was coupled into the TEM mode of the two-conductor transmission line. Thus the glue losses could conceivably still be present despite the presence of the film and could increase the insertion loss of the guide, the amount of increase depending on the loss tangent of the glue. Furthermore, additional loss due to radiation would also be possible from the two-conductor equivalent transmission line when the image guide is curved.

4. PASSIVE COMPONENTS

4.1 Introduction

A family of passive distributed components will be required in order that various integrated modules may be designed and fabricated to provide necessary system signal processing functions. This family should include three-terminal junctions, couplers, attenuators, four-terminal hybrids, and various filter functions. The nature of these various components for image line integrated circuits will generally be somewhat different than the corresponding component when fabricated in metal waveguide, microstrip, or coaxial line. The two factors which contribute to these differences are:

(1) the fact that the image line is not enclosed by metal, and

(2) the need to observe minimum radius of curvature requirements.

The subsections below will describe the specific nature of these components and illustrate the differences brought about by these two image line properties.

4.2 Attenuators

Two approaches were used to the introduction of absorbing devices in the vicinity of the image waveguide for the purpose of achieving signal attenuation. Both devices employed were made from machinable microwave absorbing material,* such as typically used in waveguide attenuators or terminations.

---

* Eccosorb MF124, Manufactured by Emerson and Cuming, Canton, MA.

The configuration of the first attenuator is shown in Figure 36. This device was intended to serve as a variable coupler where the absorbing block would be moved laterally on the ground plane with variable spacing S between the absorbing block and the image waveguide. Attenuation and VSWR measurements were made at the three spacings S = ∞, S = 0.125 in., and S = 0.062 in., as shown in Figure 37. These results show that the coupling into the absorber is very frequency dependent as is the resulting signal attenuation. This is not an unexpected result in view of the frequency dependence of parallel-coupled image waveguides (described in reference 17). When the spacing between coupled image lines is uniform, the coupling factor was shown (Figure 17 of Ref. 17) to vary with frequency in such a way that, as frequency is decreased, the coupling increases to a maximum value and then oscillates between maxima and minima.

In Figure 37 the coupling is very small at 12 GHz but increases rapidly as the frequency is decreased. The attenuation increased to about 8 dB for a spacing S = 0.125 in. and to about 22 dB for a spacing of S = 0.062 in. at 10 GHz. The input VSWR was improved by the presence of the attenuator because the reflections from the output launcher were somewhat absorbed and did not fully contribute to the measured VSWR.

Uniform attenuation with frequency requires uniform coupling between the image waveguide and the absorbing block. One possible approach to achieving uniform transverse coupling is to use nonuniform spacing between the coupled image waveguides.
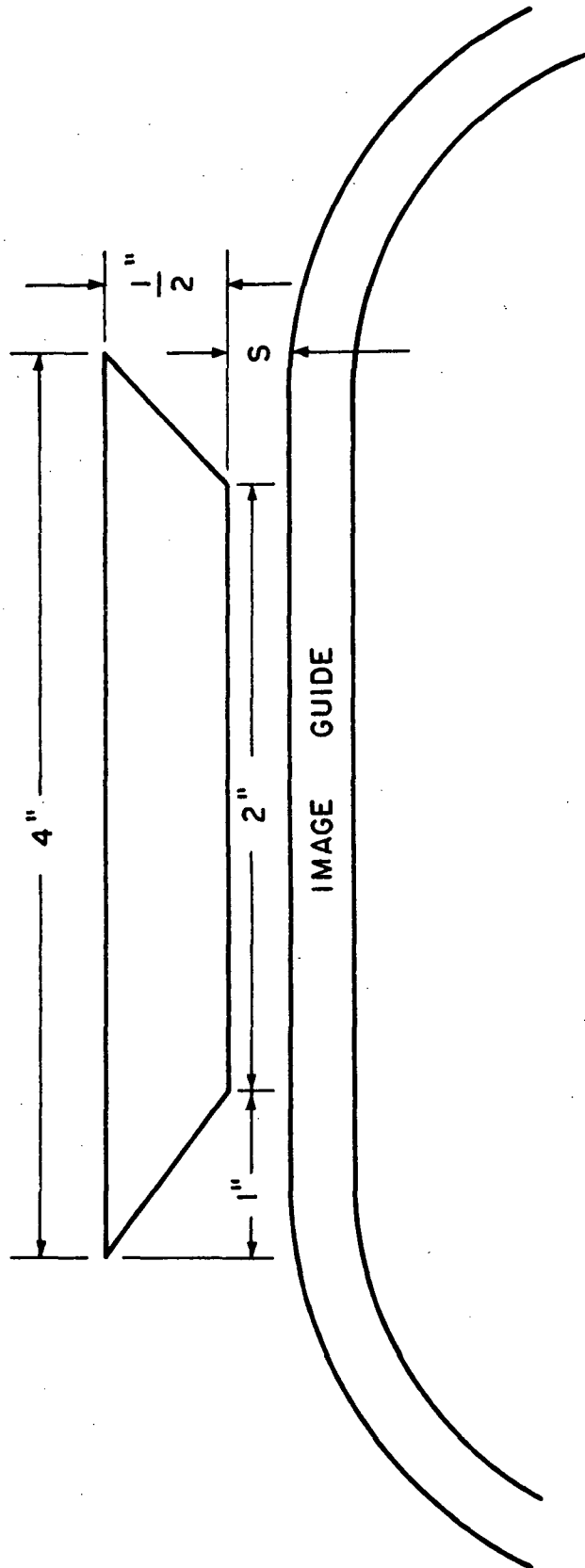
Fig. 36 CONFIGURATION ATTENUATOR NO I.
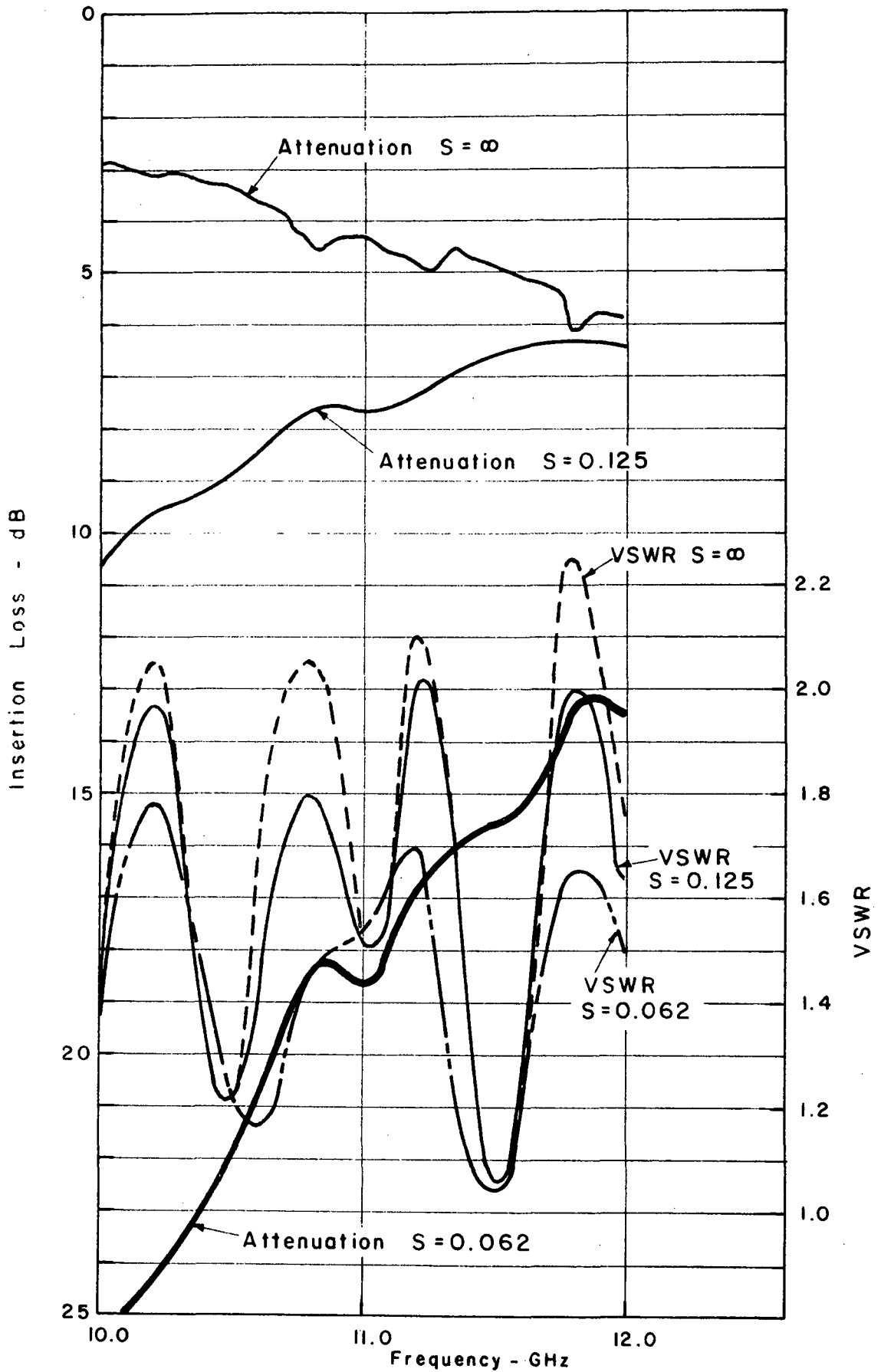
Fig. 37 MEASUREMENT OF ATTENUATION AND VSWR FOR
ATTENUATOR NO. I

Theoretical modeling for such couplers has not as yet been carried out. There is, however, reason to assume this will be an effective method by analogy with various microwave directional couplers in which coupling is allowed to vary along a distributed coupling region.

Results with a second absorber indicate that uniform coupling can be obtained by placing the absorber in contact with the top surface of the image waveguide. A diamond-shaped absorber was placed on the image waveguide as shown in Figure 38. The attenuation properties of this absorber are shown in Figure 39. The attenuation, due to the absorber, was reasonably constant at 10 dB from 9 to 12 GHz. The attenuator also helped remove nonuniformities in the transmission due to the launchers.*

Considerably more investigation would be required to relate physical dimensions to attenuation properties. However, these results encourage the conclusion that frequency independent absorbers for attenuators and terminations can be realized conveniently with the image waveguide.

4.3 Y Junction

A device of fundamental importance in several passive transmission line components is the three-terminal junction. Power dividers and various types of hybrids are examples of such components. The three-terminal junction usually takes the form of

---

* The launchers used for these measurements were not well matched and efficient throughout the frequency range as is clearly shown by the excessive ripple on the attenuation curves in Figures 37 and 39.
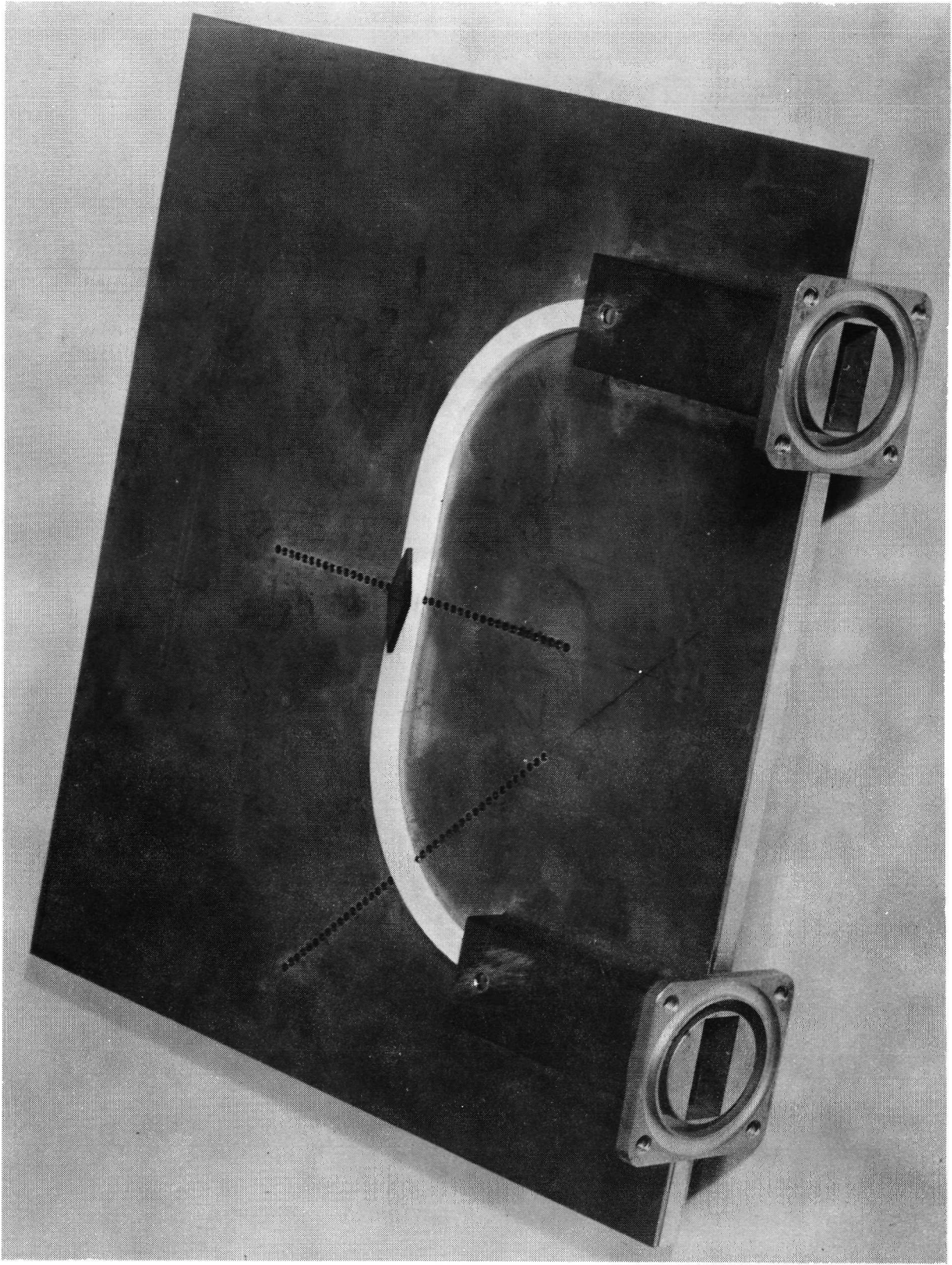
Fig. 38   ATTENUATOR NO.2 PLACED ON THE IMAGE WAVEGUIDE

90
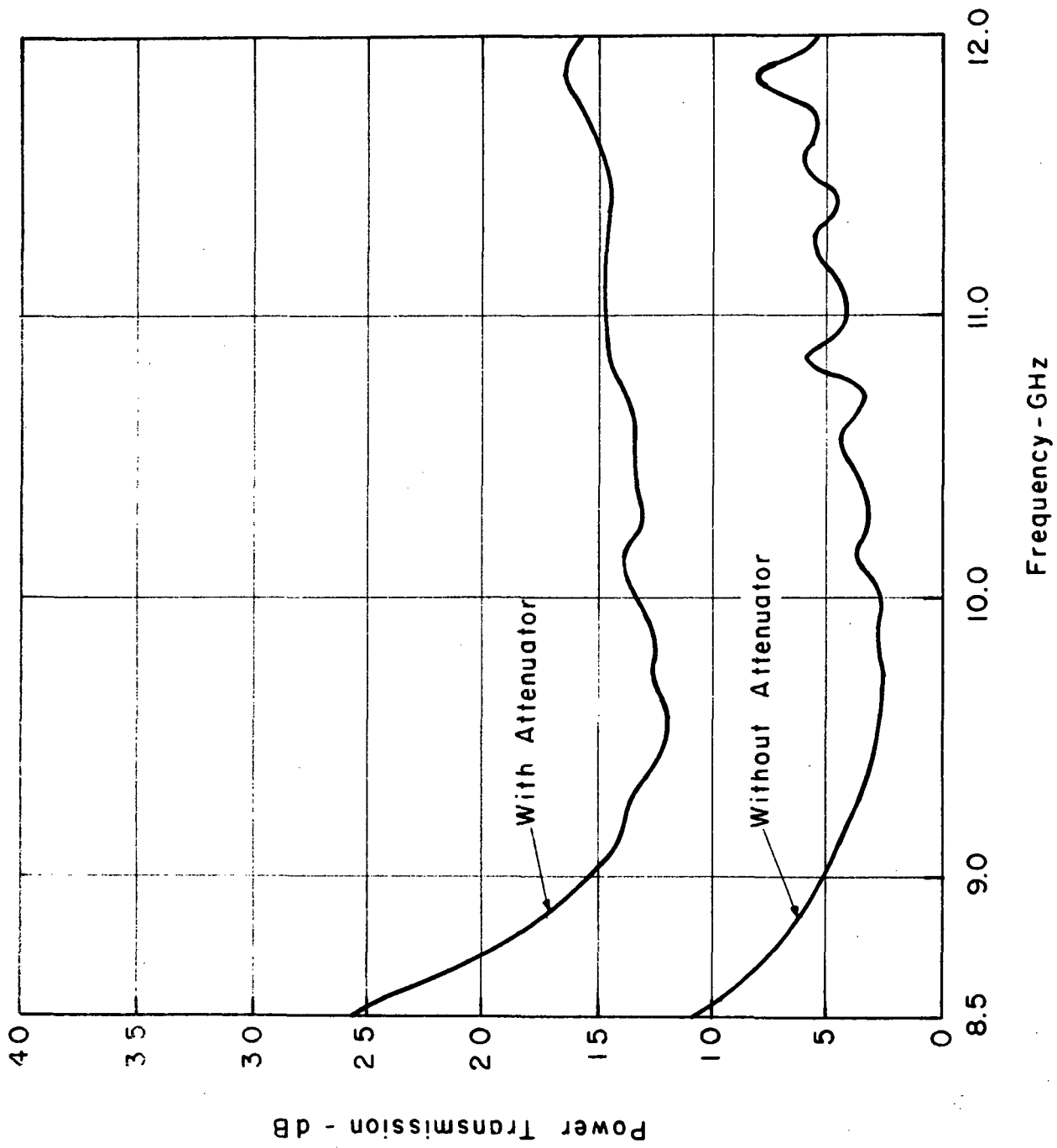
Fig. 39   ATTENUATION PROPERTIES OF ATTENUATOR NO.2

a "T" or "Y" in rectangular metal waveguides, the latter used when electrical and/or physical symmetry is required at all three terminals.

The discussion of radius of curvature limitations in Section 3.5 has shown that the image waveguide cannot tolerate an abrupt change in the direction of propagation without introducing undesirable radiation losses. Therefore, a three-terminal junction which requires abrupt changes in direction cannot be used. The "T" junction and even the abrupt "Y" junction are not suitable configurations for the dielectric image waveguide.

A curvalinear "Y" junction in which minimum radius of curvature limitations are observed has been investigated. The configuration of this junction is shown in Figure 40. The principal component application for which this "Y" junction has been considered is the ring hybrid. A four-terminal ring hybrid in which the curvalinear "Y" is employed is shown in Figure 41. This component will be considered in more detail in Section 4.4.

Each terminal of the "Y" junction is characterized by its waveguide width w and a transition region from single-width to double-width waveguide. The junction region consists of three curved arms of single-width waveguide. The radius of the waveguides in the junction region must exceed the minimum allowable for the dielectric constant, dimensions, and frequency range applicable to the circuit.

Fig. 40   THE   CURVILINEAR   "Y"   JUNCTION

Diagram Showing Length
Of Mean Circumference
Of Ring
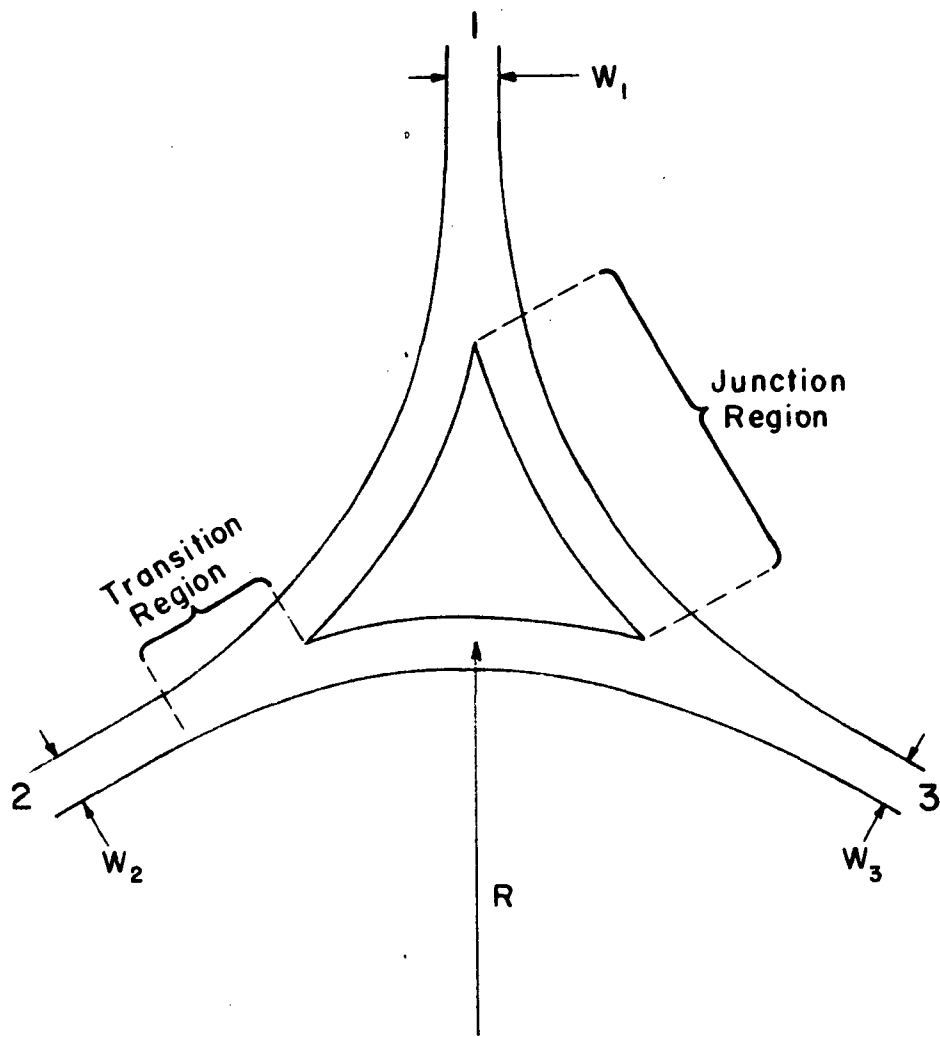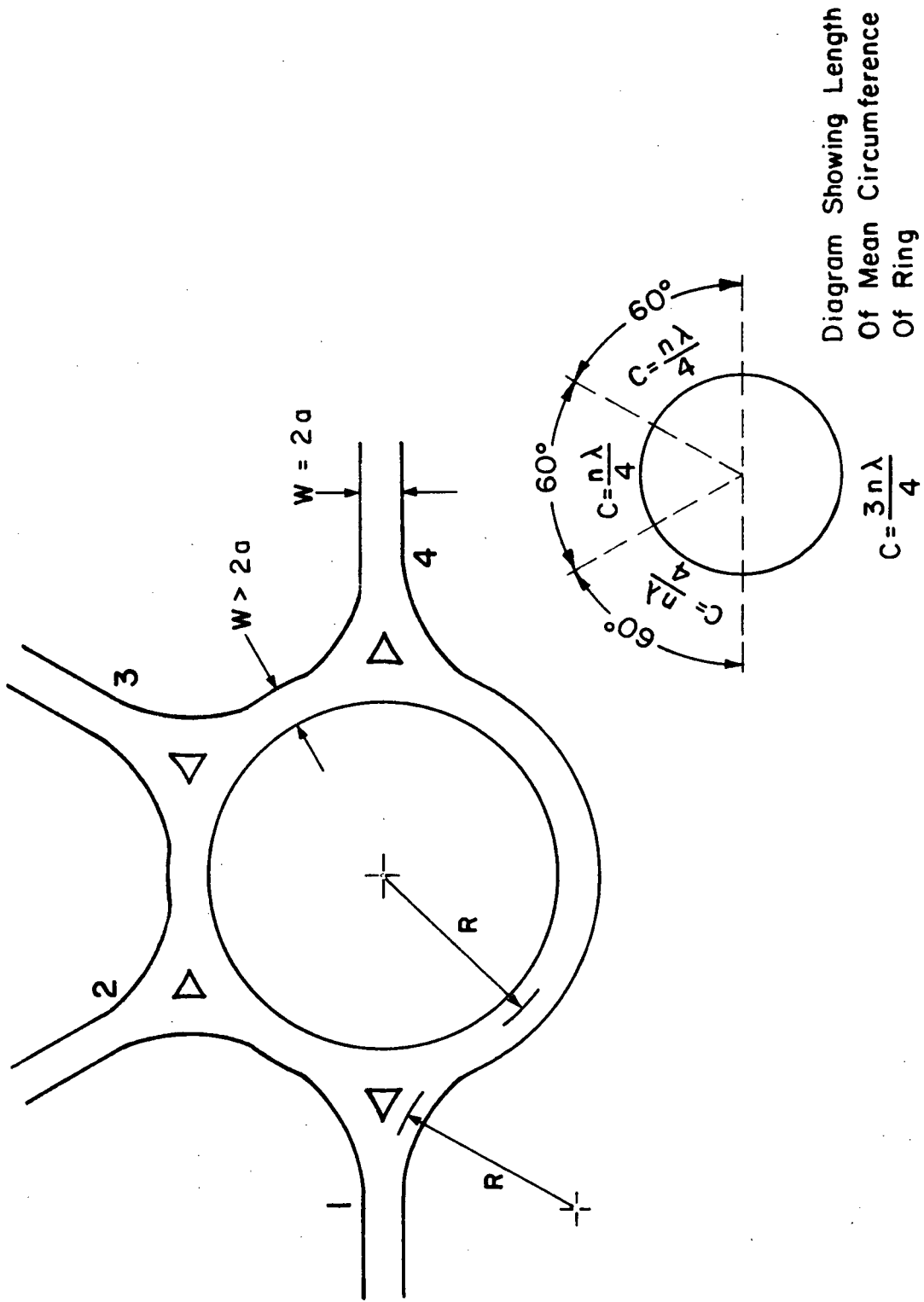
Fig. 41   A RING HYBRID USING THE CURVILINEAR "Y" JUNCTION

Two "Y" junctions were fabricated and evaluated in X-band (8 to 12 GHz). The waveguide in each case was a commercial ceramic-filled plastic.* Cross-sectional dimensions were 0.125 in. by 0.250 in. The adhesive used was a quick-setting contact cement.** The launchers were the type A (see Section 3.2). The evaluation of the "Y" junctions was carried out prior to the time in the program when a greater appreciation developed for the importance of the gap, the adhesive, the conductor, and the launchers in contributing to excess transmission line loss (see Sections 3.2 and 3.3). Therefore, the total losses observed in the various "Y" junctions include contributions from these factors as well as those associated with the properties of the junction.

Junction Y-1 is shown in Figure 42. The mean radius of the curved guides was 1.66 in., and the transition region was rather short, approximately 0.6 in. The power transmission loss from the input terminal (No. 1) to the two output terminals (Nos. 2 and 3) is shown in Figure 43. The output power transmission curves are labelled P_2 and P_3. The minimum loss was about 6 dB with typical loss ranging from 6 to 11 dB. There was considerable variation in output with frequency, and differences in output from terminals 2 and 3 were as high as 4 dB. The in-

---

* Custom Materials Inc. material No. 707L, $\epsilon_r = 9.2$, tan δ < 0.001 at 10 GHz.

** Eastman 910.
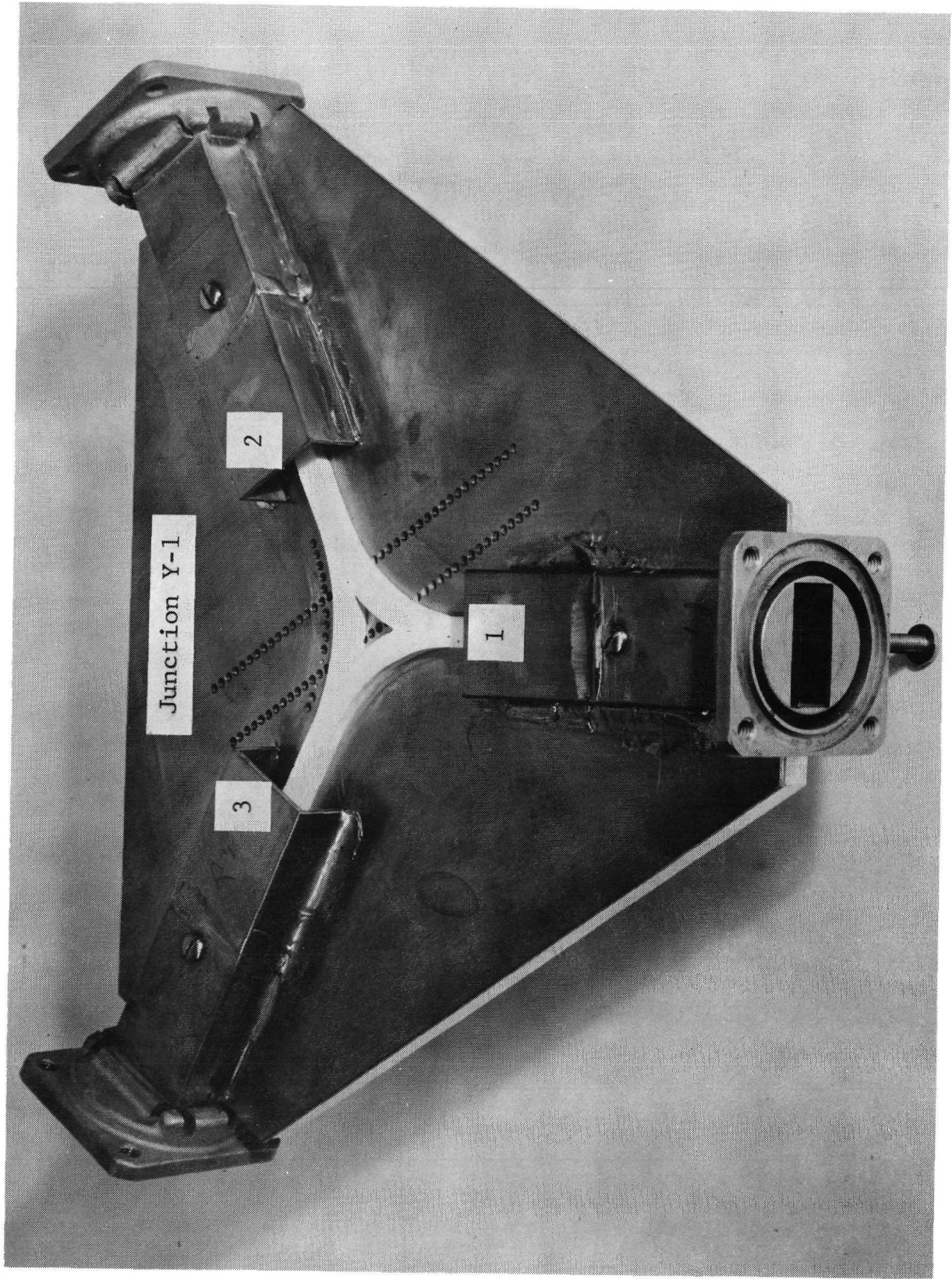
Fig. 42   THREE TERMINAL JUNCTION NO. Y-1

Junction Y-1

1

2

3
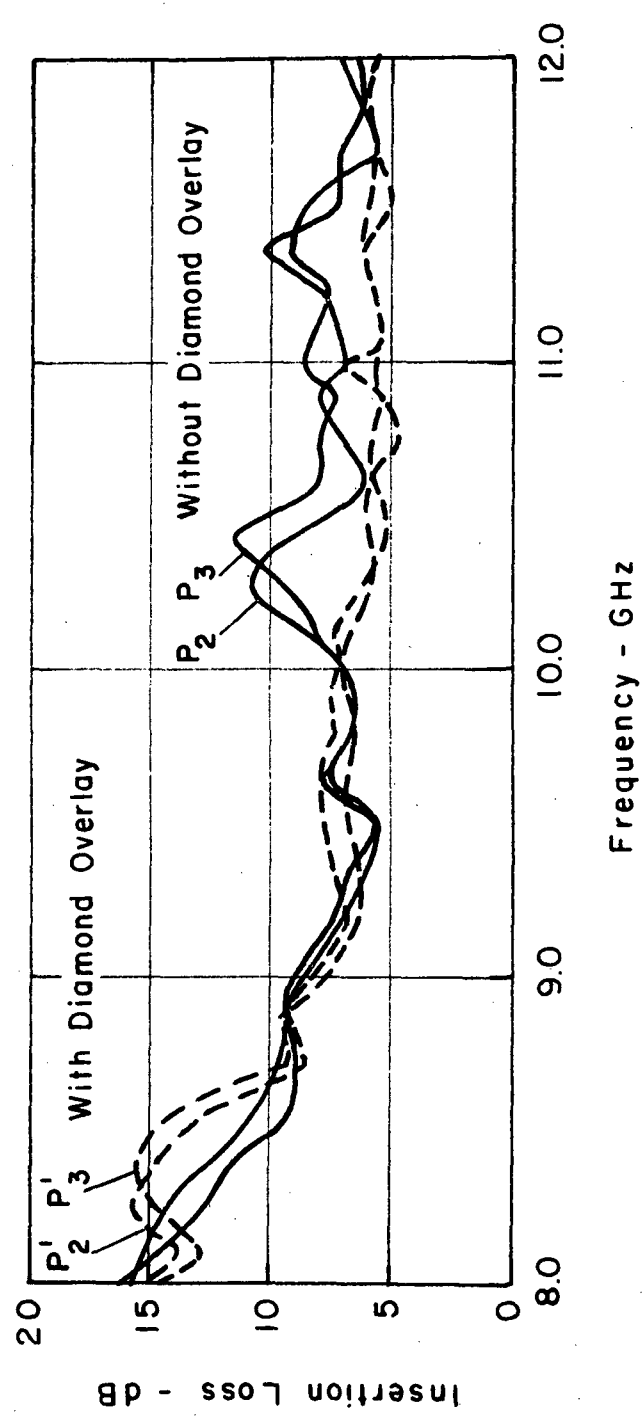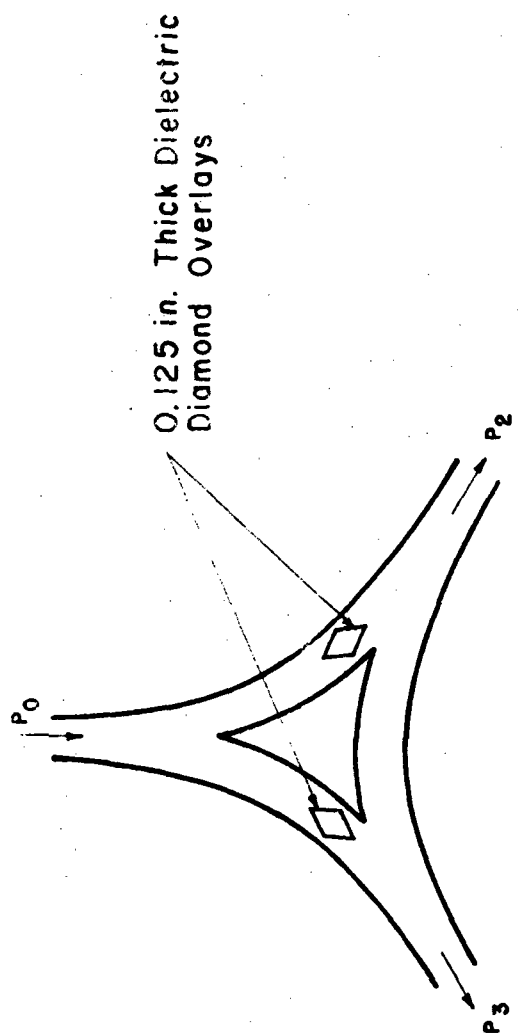
Fig. 43   TRANSMISSION CHARACTERISTICS FOR JUNCTION Y-I

crease in loss at frequencies below 9.5 GHz was due to radiation from the curved waveguides. The input VSWR was less than 1.9:1 over the band with typical values 1.4:1 or less.

Initially it was concluded that the excess loss (above 10 GHz) resulted from junction mismatch and radiation. Later insight into the excess loss contributed by the launchers and by gap effects led to the conclusion that about 1.5 to 2 dB of this excess loss was attributable to factors not involving the junction design.

The junction was, however, radiating excessively at frequencies above 10 GHz for reasons not attributable merely to the curvature of the guides. Two locations for impedance mismatch are apparent. One is where the input waveguide divides, and the second where the waveguides recouple at the two output terminals. A number of attempts was made to reduce junction radiation by placing dielectric and metal overlays at the point of division. These attempts were relatively fruitless, leading to the conclusion that significant radiation was not resulting from mismatch at that point.

Considerable improvement in transmission characteristics was obtained by suppressing radiation at the point of recoupling. Diamond-shaped overlays, placed as shown in the insert of Figure 43, caused a change in the power transmission as indicated by curves P_2' and P_3' in this figure. The improvement above 10 GHz was typically 2 dB or more. The overlay, which was 0.125 in. thick and made of the same dielectric material

98

as the waveguide, increased the impedance of the waveguide locally and provided a better match at the region of recoupling.

It was shown in an earlier section that, with the type A launchers, an insertion loss of 1.5 to 1.75 dB can be expected. The use of the type 910 adhesive apparently added about 0.25 dB additional loss. Thus, if only the junction properties are considered, the curves of Figure 43 can be adjusted to show approximately 2 dB less insertion loss. Therefore, with the use of improved matching, as shown by curves P_2' and P_3', the Y junction was typically within 1 dB of desired performance over much of the frequency range above 10 GHz.

In order to provide a match, the impedance of the junction region waveguides should be higher than that of the input-output lines. The impedance match of the Y junction will also depend on the terminal impedances. If the Y was intended for use in a ring hybrid, then impedance matching requires that the impedance of the ring waveguides be less than the input-waveguides by a factor $1/\sqrt{2}$.* Suppose the input (terminal 1) impedance is Z_o. The terminating impedances for the Y junction at terminals 2 and 3 would be $Z_o/\sqrt{2}$. Impedance matching at the coupling point would require that the transition region impedances be $2(Z_o/\sqrt{2})$ or $Z_o\sqrt{2}$.

---

* The input terminal is loaded on the ring by two output terminals with impedance Z_o. The arms of the ring having impedance $Z_0/\sqrt{2}$ act as impedance matching sections.

Locally, the input (terminal 1) would see a lower impedance equal to $1/2(Z_O\sqrt{2})$. This mismatch could be accommodated by gradually lowering the impedance as the dividing junction is encountered.

Field distribution in junction Y-1 was measured at several frequencies. These measurements will be found in Section 3.4.3.

In a second version of this junction, more gradual transition regions were introduced. This junction, designated Y-2, also had a mean radius of curvature of 1.66 in., but the transition regions were given a gradual taper from a line width W to a width 2W. The dimension W was 0.250 in. as in junction Y-1, but the transition region length was 1.5 in. This junction is shown in Figure 44. The type 910 adhesive was once again used to attach the dielectric waveguide to the ground plane and the launchers were again type A.

The power transmission P_2 and P_3 at terminals 2 and 3, respectively, is shown in Figure 45. Clearly, this junction had greater attenuation than junction Y-1. The VSWR was 1.85 or less and typically 1.45 or less over the band. Radiation from the junction was apparent, as in junction Y-1. The first attempt to suppress this radiation was with dielectric overlays in the coupling region as was done with junction Y-1. The transmission was improved, as shown in Figure 46, by the overlays which were diamond-shaped, 0.125 in. thick and 1.0 in. long.

A second approach to reducing the radiation was to cut long slots down the center of the impedance tapers in the transition
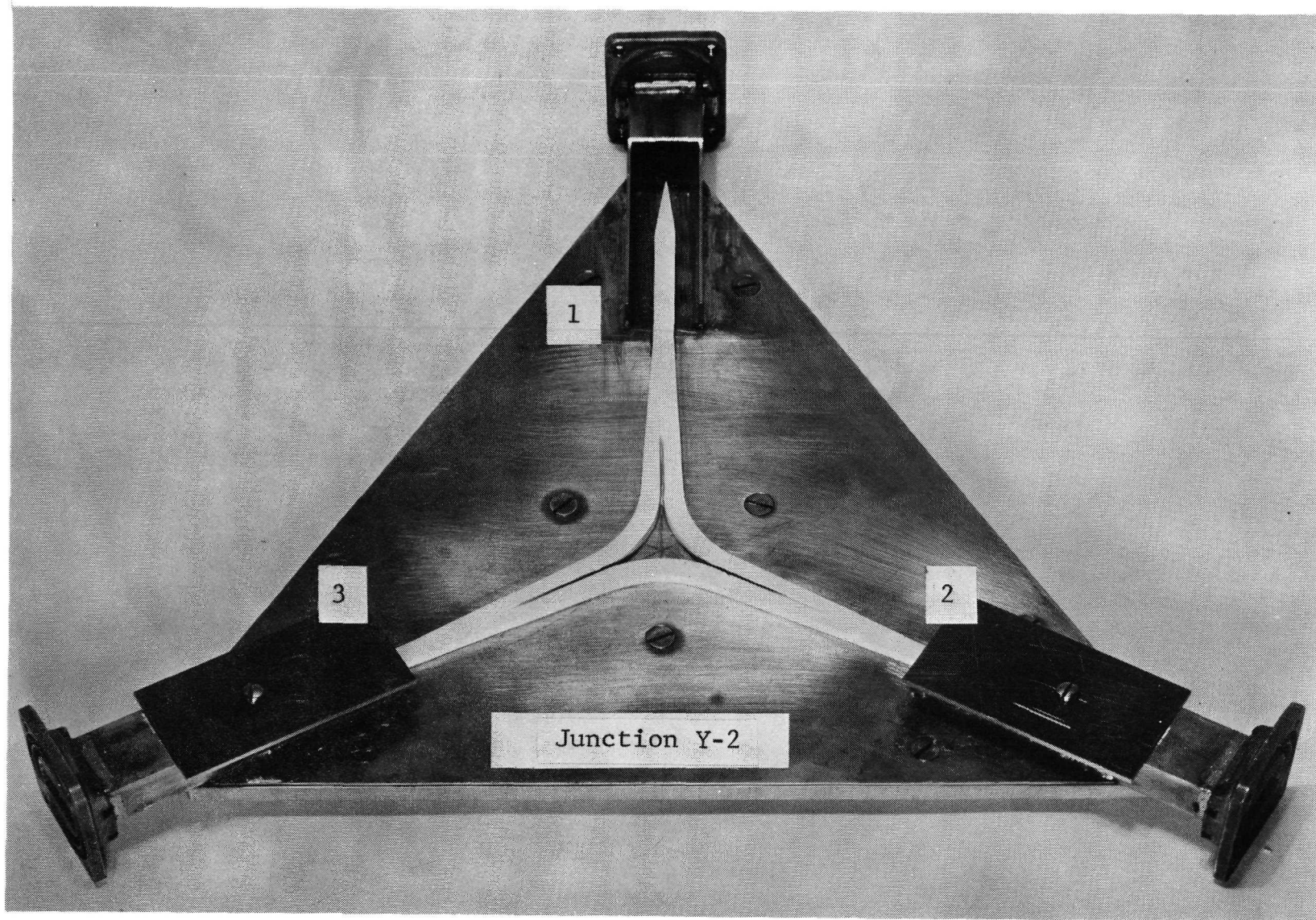
Fig. 44   THREE TERMINAL JUNCTION Y-2 WITH ELONGATED TRANSITION REGIONS
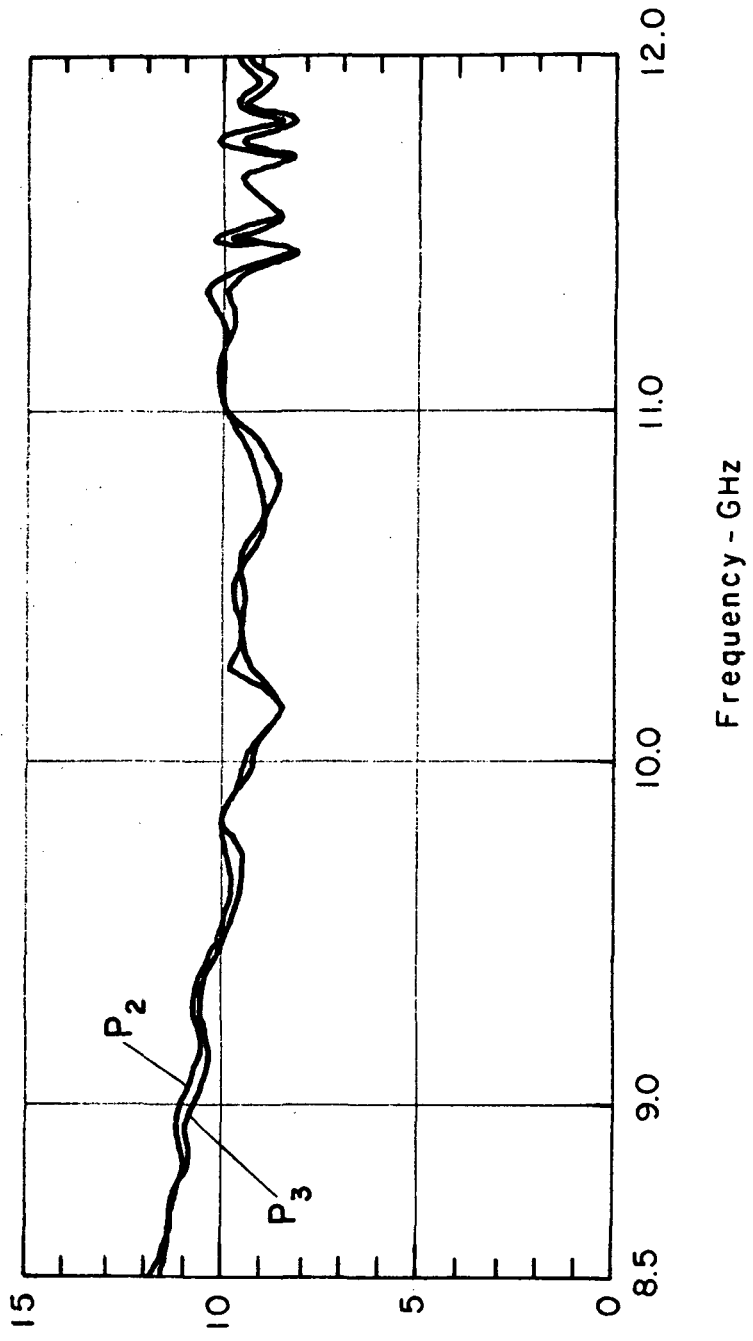
Fig. 45   TRANSMISSION CHARACTERISTICS FOR JUNCTION Y-2
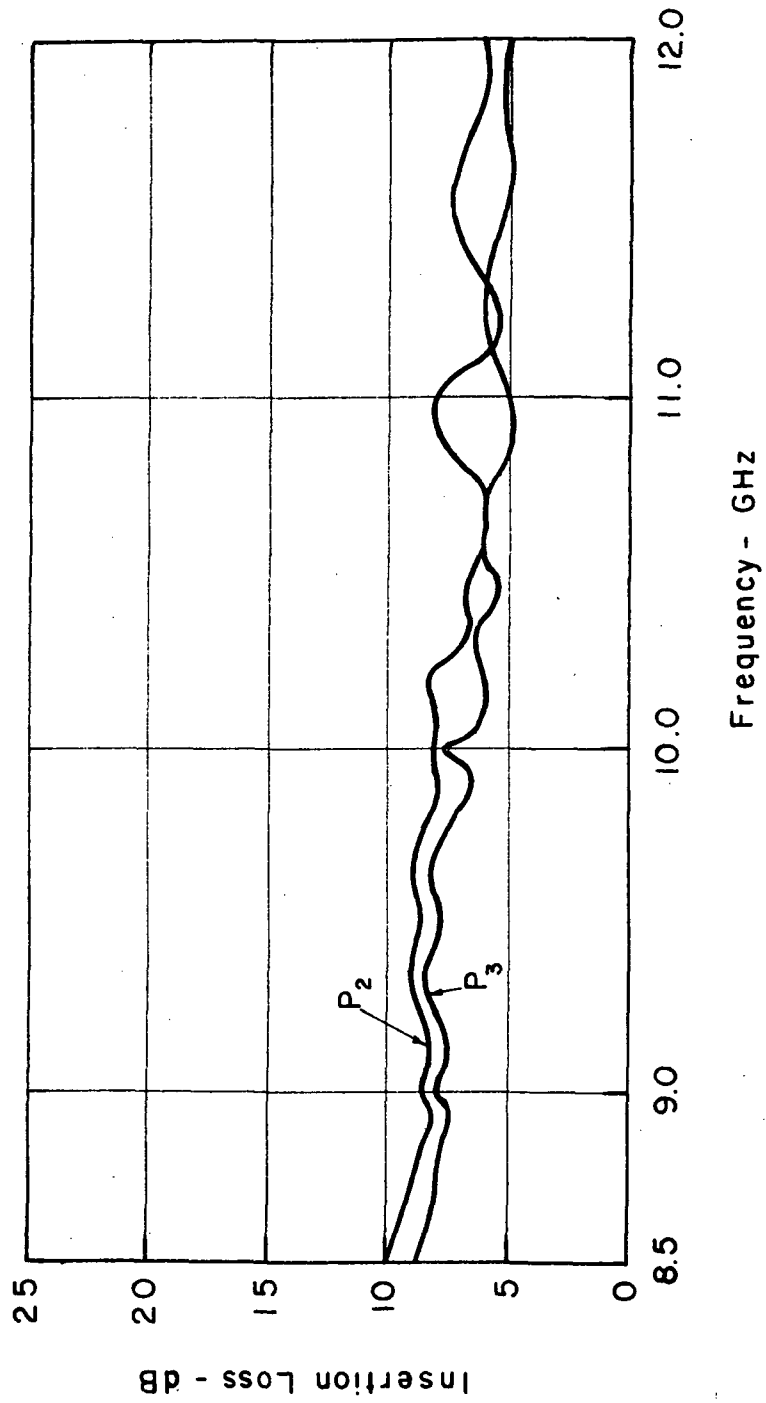
Fig. 46 TRANSMISSION CHARACTERISTICS FOR JUNCTION Y-2 WITH THE ADDITION OF DIELECTRIC OVERLAYS IN THE JUNCTION REGION

103

region to cause the waveguides to recouple more gradually. The results are shown in Figure 47, and it is clear that this method did not produce the desired reduction in excess radiation loss.

In summary, the most favorable results with both junctions were obtained when the impedance in the junction region was increased using dielectric overlays. Excess losses were present due to the launcers and the adhesive used. Obtaining satisfactory performance from this device will require modeling of the impedance properties of the junction and transition regions in order to avoid excess radiation losses which occur where the waveguides recouple.

4.4 Ring Hybrid

A limited investigation of a ring hybrid was conducted in which the three-terminal junction Y-1, described in Section 4.3 above, was used. The mean radius of curvature R_m = 1.66 in., which was used in junction Y-1, was also used in the design of the ring hybrid. The waveguides were of uniform cross section* everywhere, with the same a and b dimensions as were used in the Y-1 junction. The design of the four-terminal ring hybrid is shown in Figure 48.

---

* The cross-sectional dimensions were a = b = 0.125 in. The impedance of the ring, for proper impedance matching, should have been lower by a factor $1/\sqrt{2}$. Therefore, the terminals of this ring hybrid were not matched.
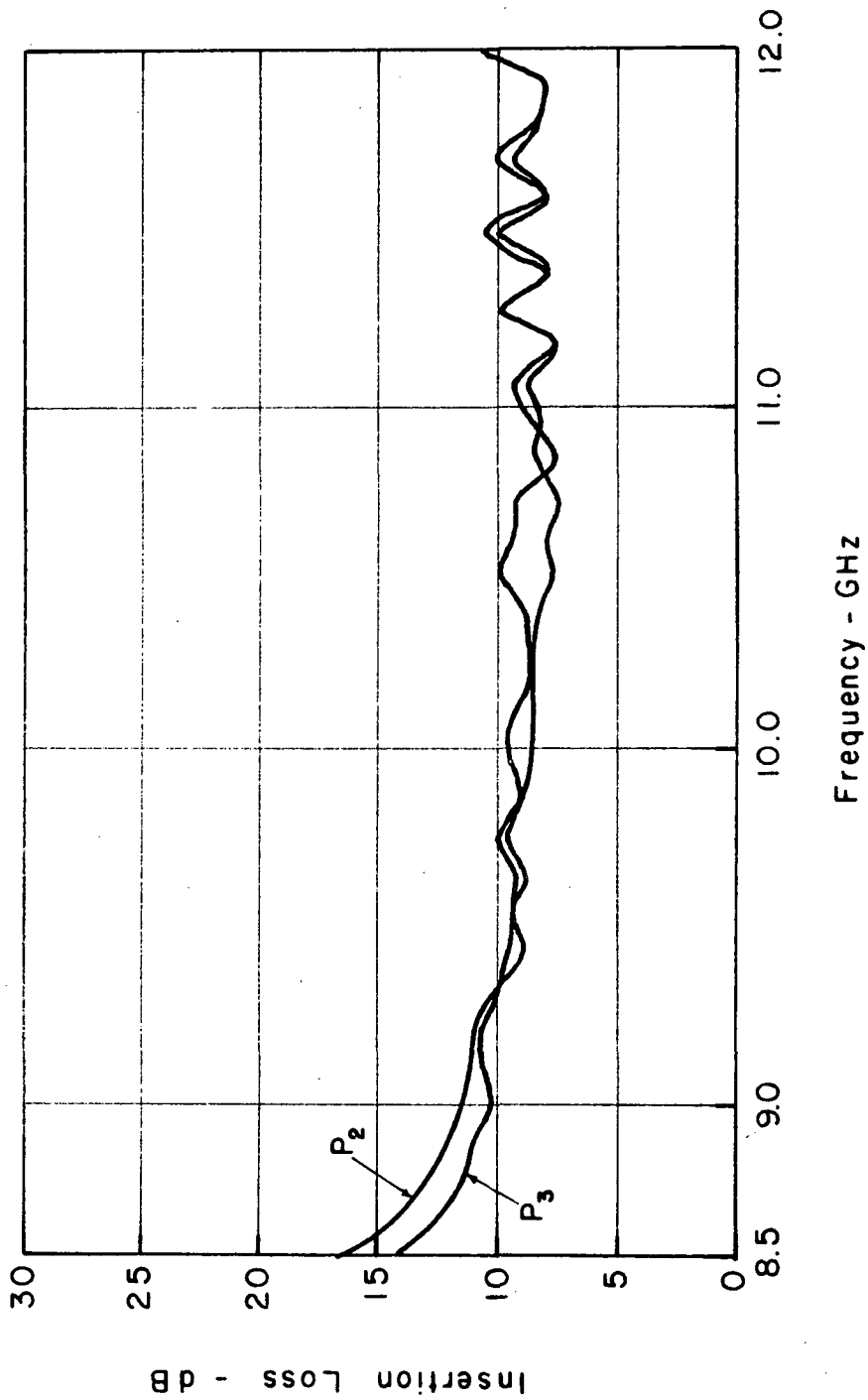
Fig. 47 TRANSMISSION CHARACTERISTICS FOR JUNCTION Y-2 WITH 1.0 in SLOTS CUT IN THE TRANSITION REGION

105
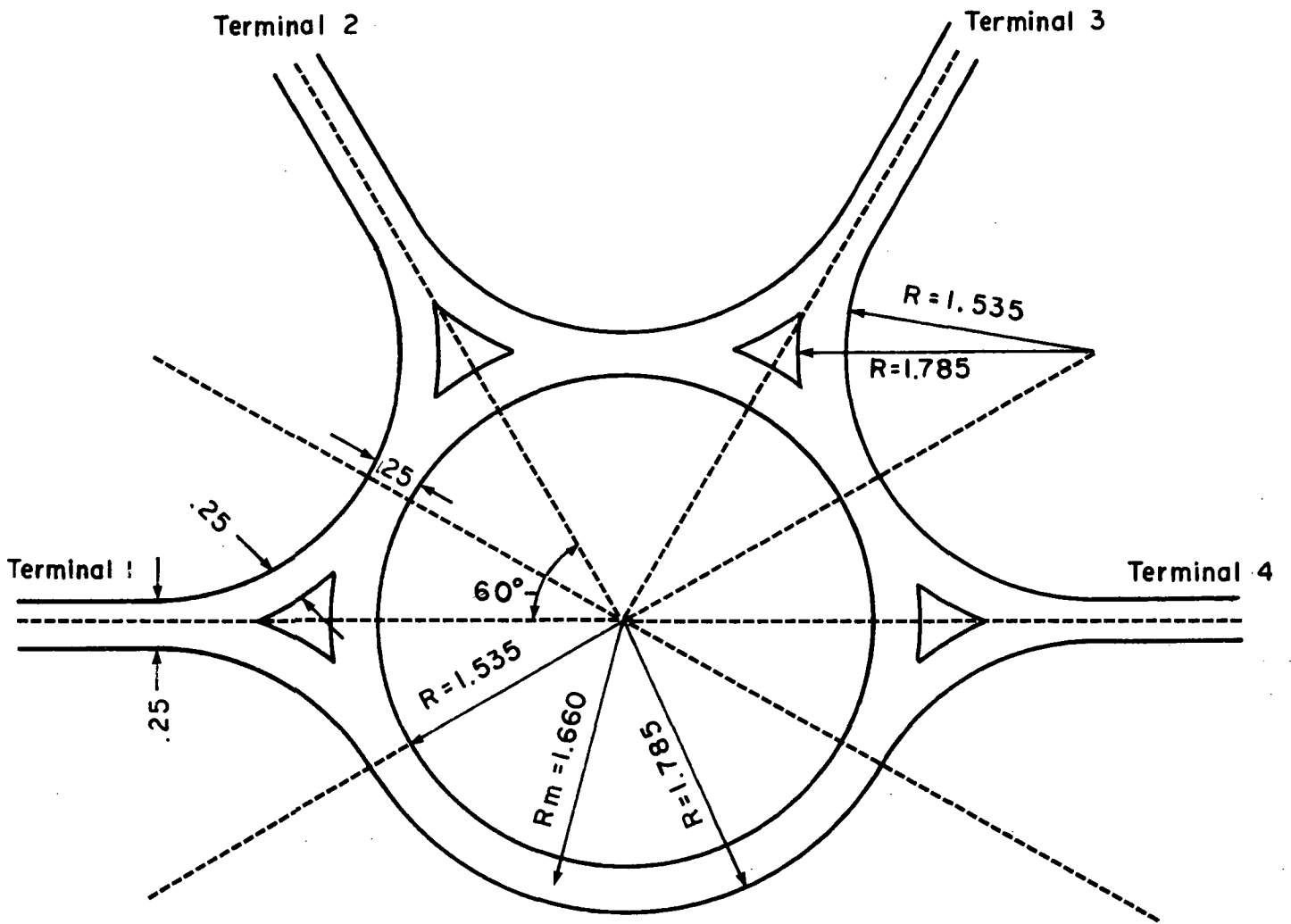
Fig. 48 DESIGN OF THE RING HYBRID

The following general aspects are applicable to any ring hybrid. The circumference for proper phase isolation must always be an odd multiple of 3/2 λ_g, where λ_g is the actual guide wavelength at the design frequency.

Thus

$$C = \frac{n\, 3\, \lambda_g}{2} \qquad n = 1,3,5\, ---$$

The circumference is also related to the mean radius of curvature, thus

$$C = \pi\, 2\, R_m$$

Equating the above expressions gives

$$\lambda_g = \frac{4\pi\, R_m}{3n}$$

This relationship gives the guide wavelength, for a given ring radius, at which will occur the nth multiple of the fundamental phase relationship. The guide wavelength is related to the frequency by the dispersion curves given in Figure 2. The theoretical frequencies at which isolation should occur in the ring are tabulated below.

n	Frequency of Isolation (GHz)	
	Theoretical	Experimental
7	8.9	9.0
9	9.7	9.86
11	10.6	10.6
13	11.4	11.7

The ring hybrid is shown in Figure 49. The power transmission characteristics, which give the output powers P_1, P_2, P_4 at terminals 1, 2 and 4, respectively, are given in Figure 50. The frequencies of isolation predicted theoretically were confirmed by the experimental measurements.* The input signal at terminal 3 should have divided equally between terminals 2 and 4. The excess attenuation in the output was typically 8 to 15 dB. This result is consistent with earlier measurements of the single Y junction, shown in Figure 43, in which excess attenuation of 4 to 8 dB was measured. This ring hybrid was subject to all of the excess attenuation mechanisms described in Section 3.3.

While the performance of the hybrid was rather poor due to excess attenuation and mismatch in the Y junctions, some encouragement is taken in the fact that isolation ratios as high as 20 dB were achieved at two frequencies.

4.5 Band Stop Filter in V-Band

A ring-resonator type band-stop filter was fabricated for V-band operation. The same ring resonator was measured in two different waveguide circuits and with different methods of attachment to the base plate. The ring was made with a diameter

---

* The apparent isolation at 11.7 GHz may not be that expected due to the phase cancellation in the ring. This drop in the output at terminal 1 could have been caused by junction mismatch. Reflections could also have prevented the isolation expected at 11.4 GHz from occurring.
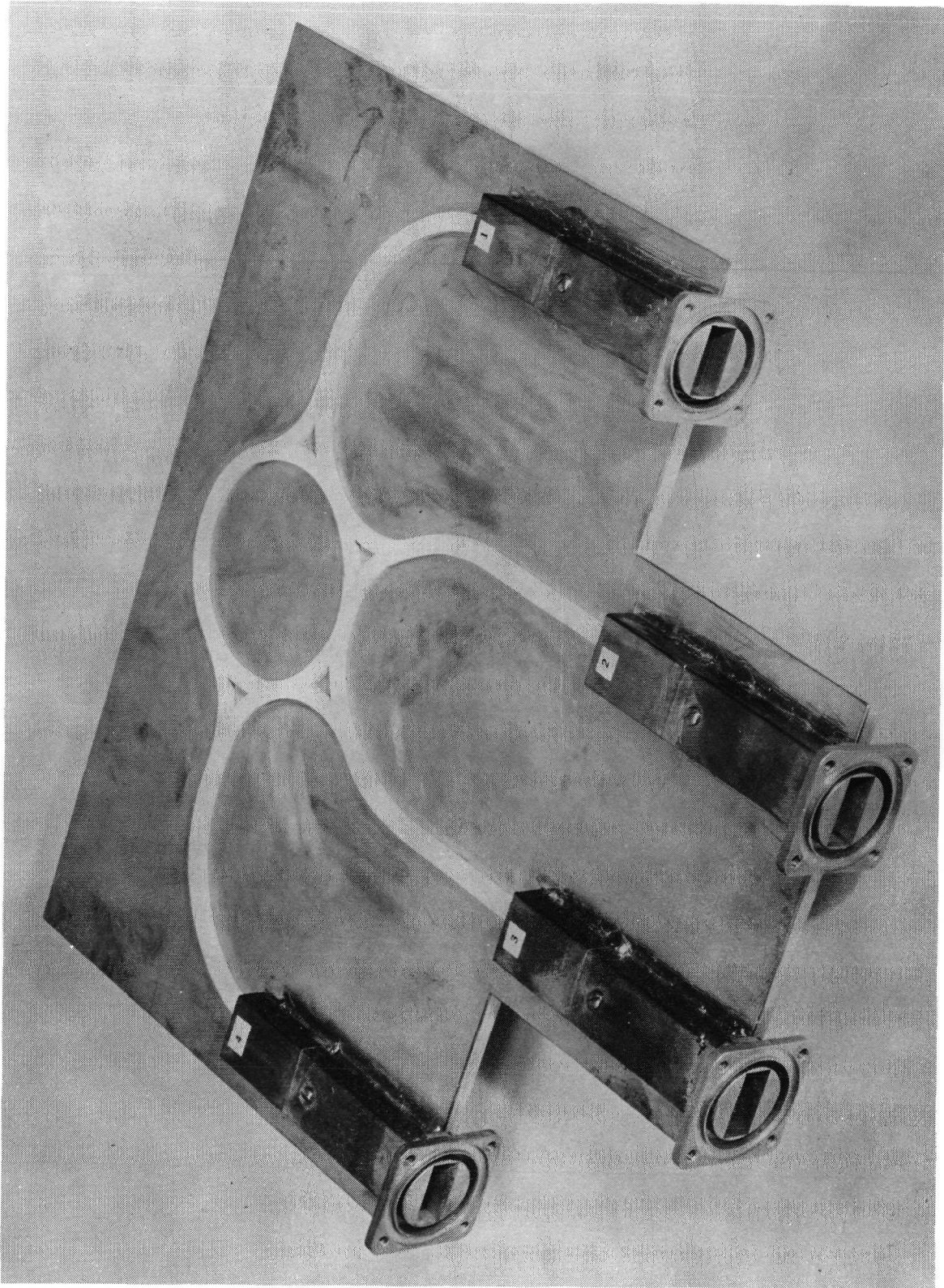
Fig. 49   X-BAND RING HYBRID
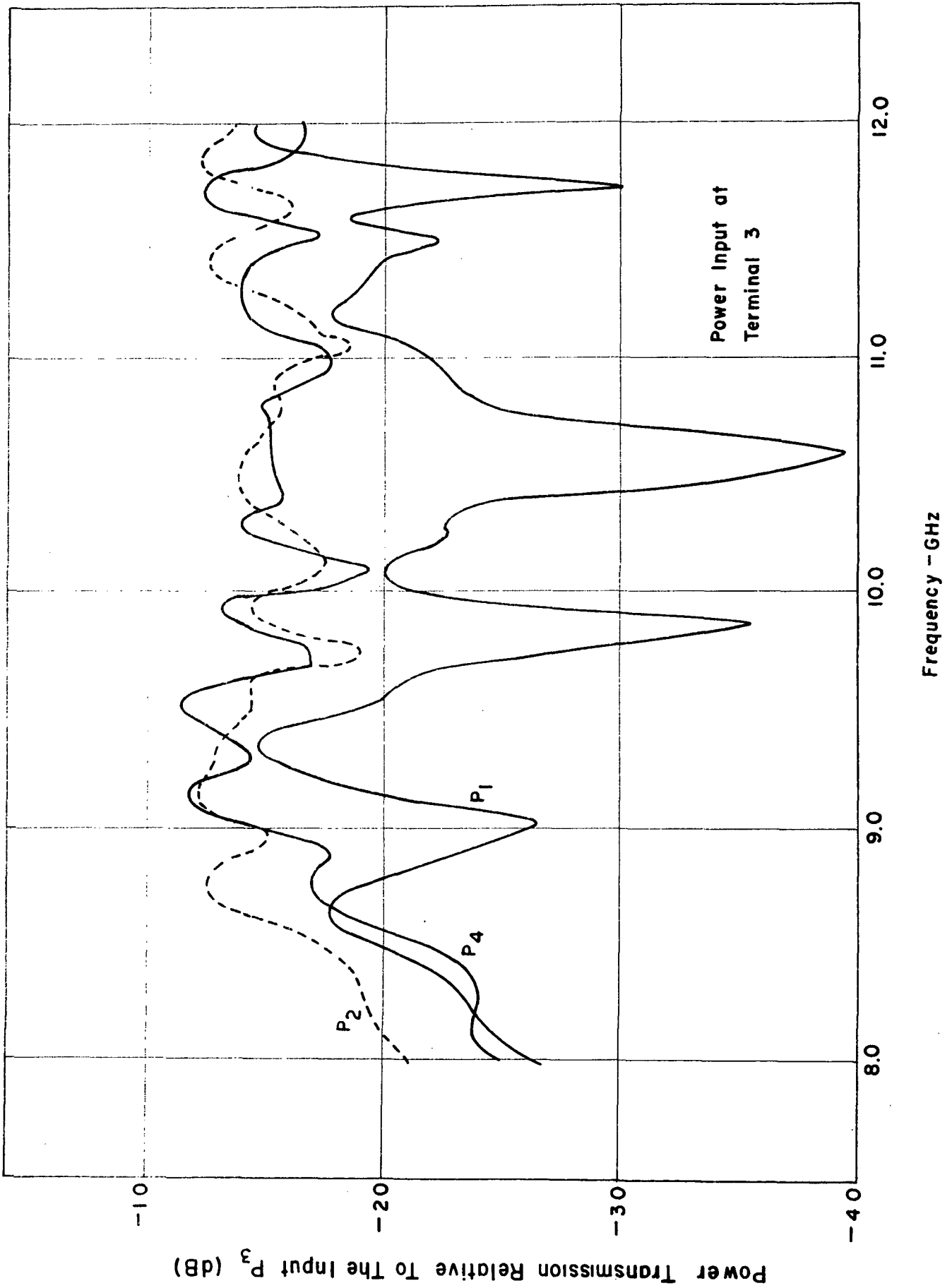
Fig. 50 POWER TRANSMISSON CHARACTERISTICS FOR THE X-BAND RING HYBRID

110

of 0.5 in., which is rather large in V-band. Since a typical guide wavelength is about 0.1 in., the circumference of the ring would be as many as 15 wavelengths. The ring was made rather large in order to avoid any possibility of significant radiation from the ring due to curvature. The large diameter results in rather closely spaced stop bands, giving a response which is frequently termed a comb-filter.

The first version of the band-stop filter is shown in Figure 51. Both the main waveguide and ring were fabricated of alumina using the abrasive machining method described in Section 6. Templates were made for use with the pantograph which guided the machining tool. The edges of these waveguides were quite irregular and the cross section was trapezoidal rather than rectangular.* Measurements of the insertion loss of the waveguide without the ring gave typical values of 5 to 7 dB. When attempts were made to measure the filter characteristics with the ring positioned approximately as shown, the loaded Q of the ring was rather low because the ring coupled to the main waveguide over an extended length and the high attenuation per unit length of the guide essentially appeared as additional attenuation in the ring.

The ring was subsequently placed adjacent to the straight section of waveguide, and the measured filter characteristics are shown in Figure 52. In these measurements the ring was

---

* The width at the top was typically 0.040 in. and at the bottom 0.060 in.
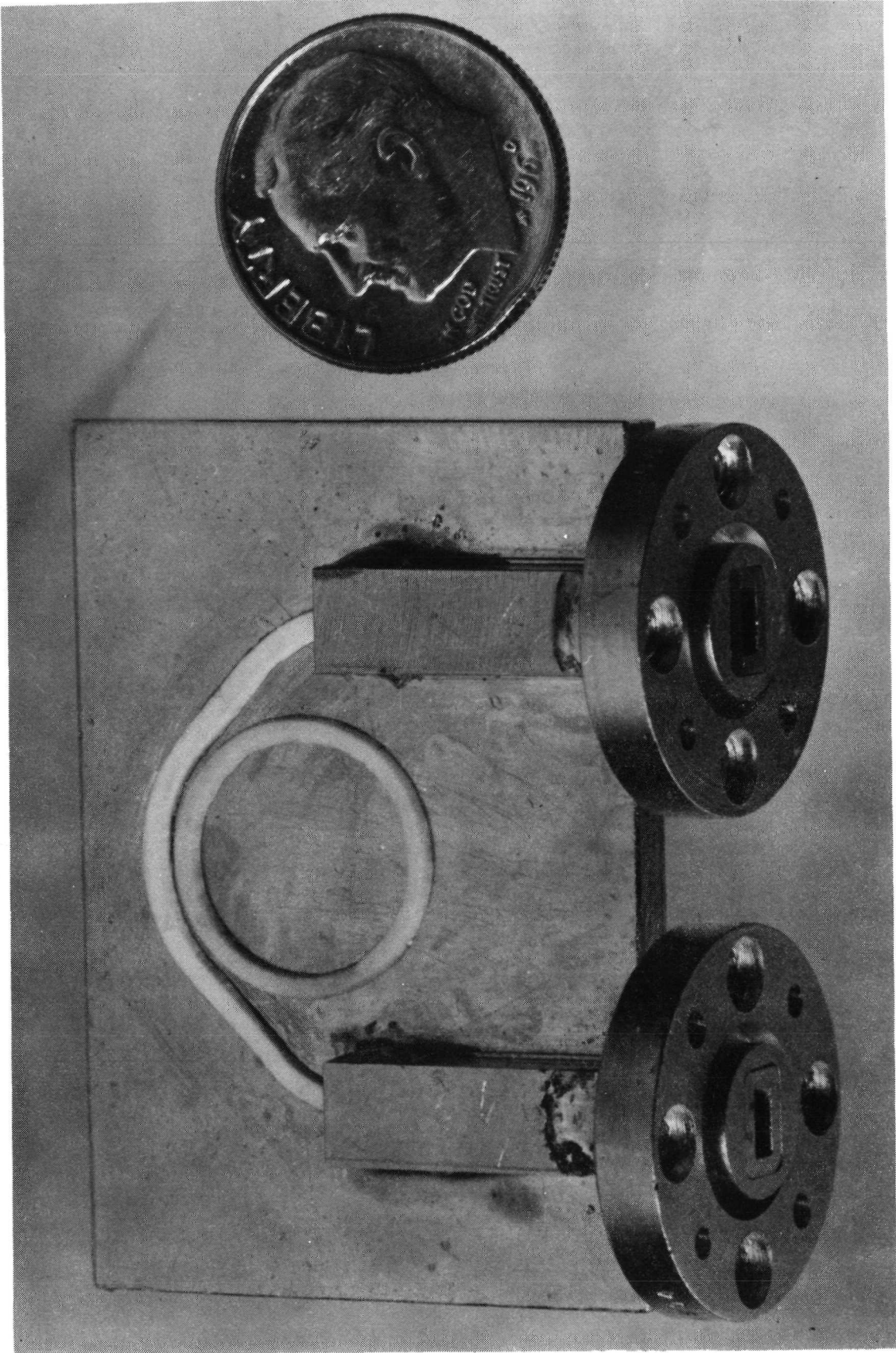
Fig. 51   V-BAND COMB-TYPE BAND REJECT FILTER FABRICATED ON A
GOLD PLATED BRASS BASEPLATE
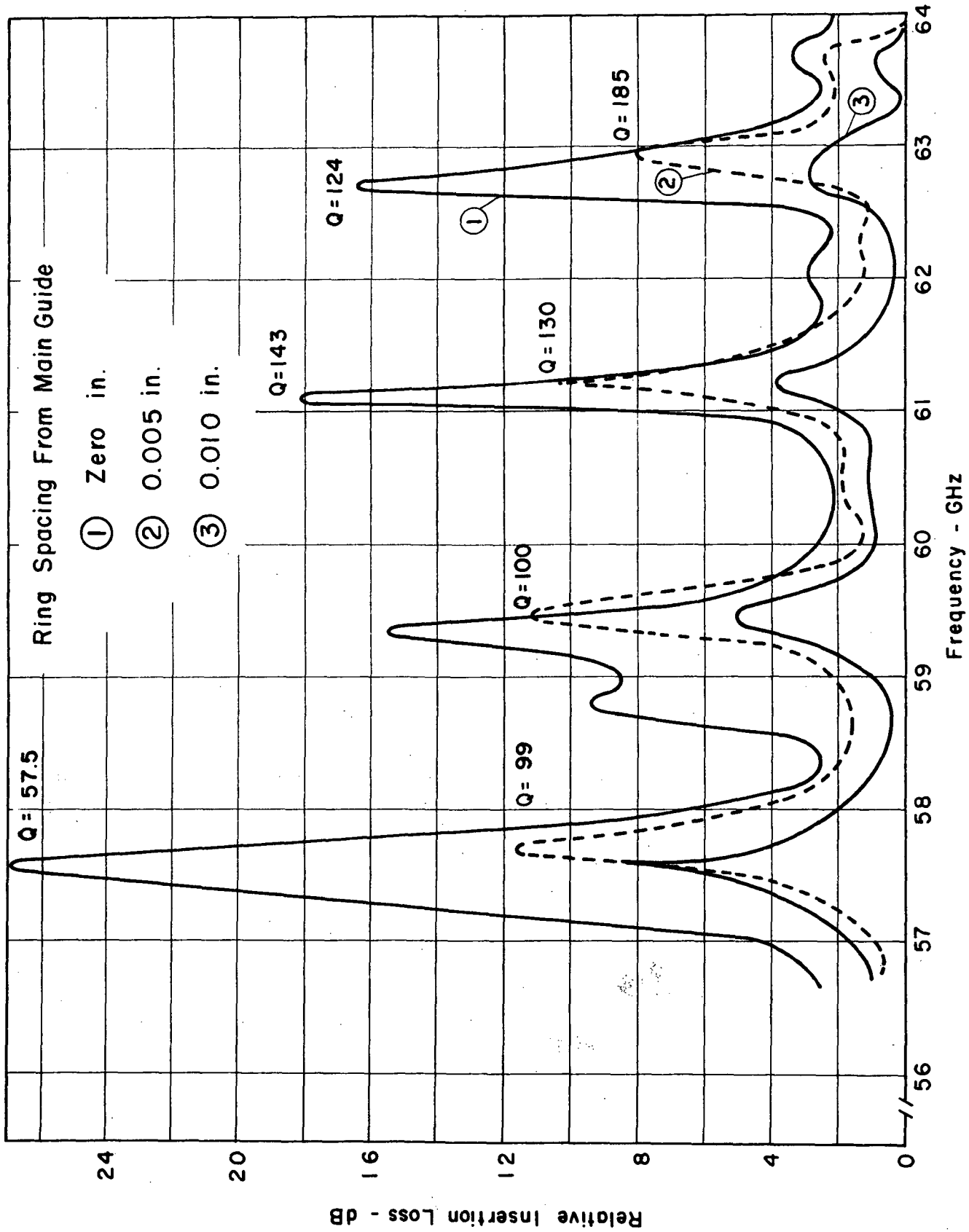
Fig. 52 RING FILTER CHARACTERISTICS—RING PLATED WITH ALUMINUM AND MEASURED ON THE GOLD/BRASS BASEPLATE

113

plated on the underside with an aluminum film* and not attached with any adhesive. Three curves for different spacings between the ring and the line are shown in the figure. The three spacings (at the lower edge) were (1) contact, (2) 0.005 in., and (3) 0.010 in. The response labelled (1) in Figure 52 gave loaded-Q values ranging from 57 to 143. The Q values for increased spacing (curve 2) were 98 to 185. This increase in measured Q results from reduced coupling to the input waveguide. Coupling for curve 3, however, was too light to make a Q determination.

The same ring resonator was measured as a band-stop filter on the polished aluminum base plate shown in Figure 53. Three measurements were made of the filter characteristics. In each case the ring was contacting the main waveguide (this was the "U" waveguide designated No. 1 in Section 3.3.4) shown in Figure 53. Figure 54 shows the first filter response in which the ring was plated with an aluminum film* and no adhesive was used. The loaded Q measured in this case ranged from 99 to 135, about the same as the gold plated base plate for tight coupling. The filter response, when the aluminum film was removed, is shown in Figure 55. In the measurements shown in Figures 54 and 55 the ring was merely resting on the aluminum base plate.** The loaded Q increased to the range 184 to 304 without the aluminum film. Clearly, the film was not accomplishing its intended

---

* Approximately 0.00016 in. thick.

** The main waveguide was attached with type 509 adhesive with 25% coverage.
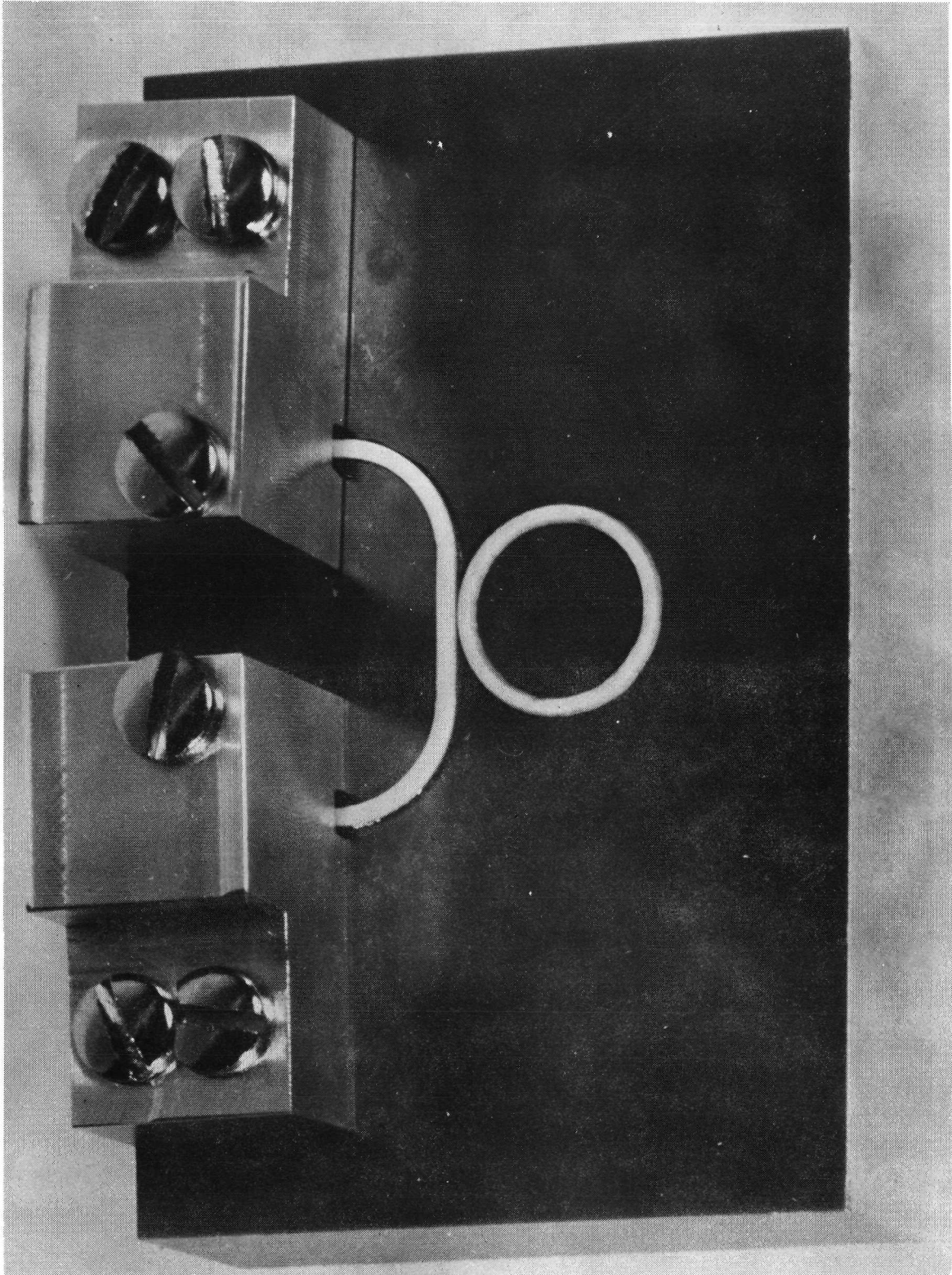
Fig. 53   V-BAND COMB-TYPE BAND-STOP FILTER FABRICATED ON AN ALUMINUM BASE PLATE

115
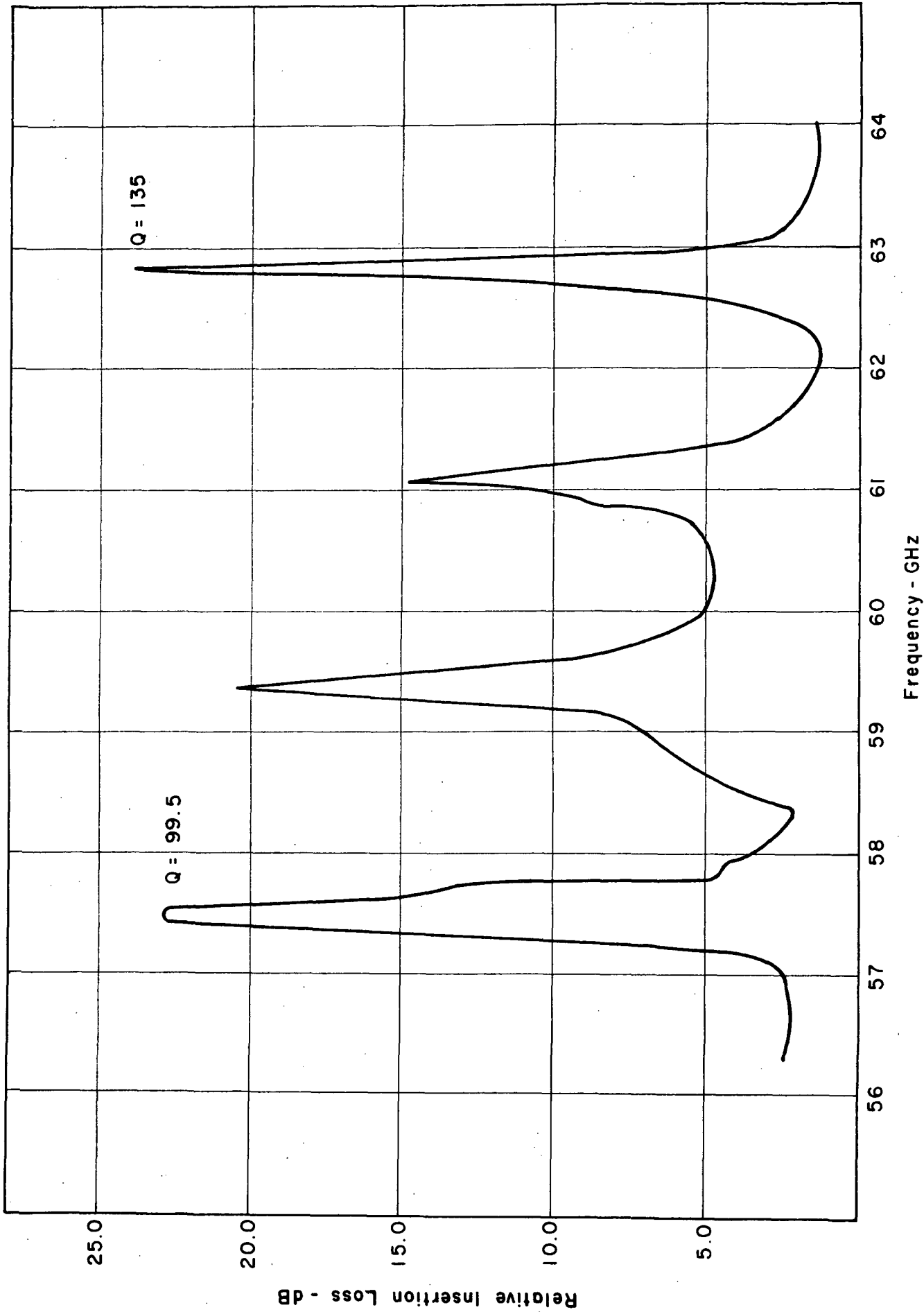
Fig. 54 V-BAND RING FILTER RESPONSE — RING PLATED WITH ALUMINUM AND MEASURED ON A POLISHED ALUMINUM BASE PLATE

116

purpose of reducing conductor losses. A third measurement of the filter characteristics was made with the ring attached with about 25% coverage of the type 509 adhesive shown in Figure 56. The measured Q decreased to the range 132 to 195. This is due to the losses added by the adhesive.

The highest Q achieved with this resonator was 304. The theoretical unloaded Q, based on calculations given in Section 3.3.4, should be 825. There is a discrepancy between theory and experiment of approximately 2:1. This can be explained in terms of excess radiation loss caused by the nonuniform side surfaces of the ring waveguide. Because the ring was fabricated by the abrasive machining technique, the edges were not straight and smooth as they should be. This could lead to degredation in guidability, particularly in a curved waveguide.
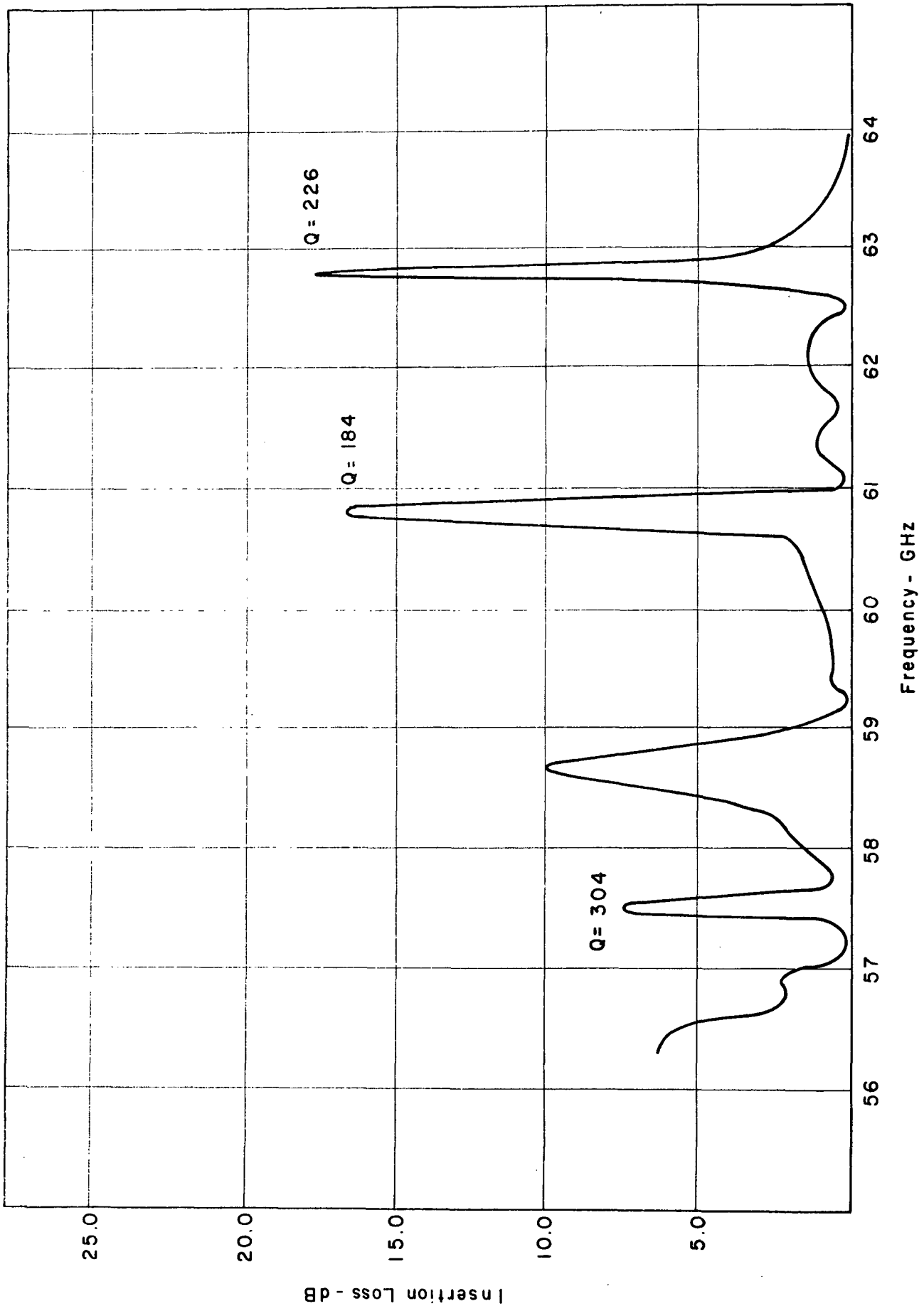
Fig. 55   V-BAND RING FILTER RESPONSE WITHOUT
ALUMINUM FILM
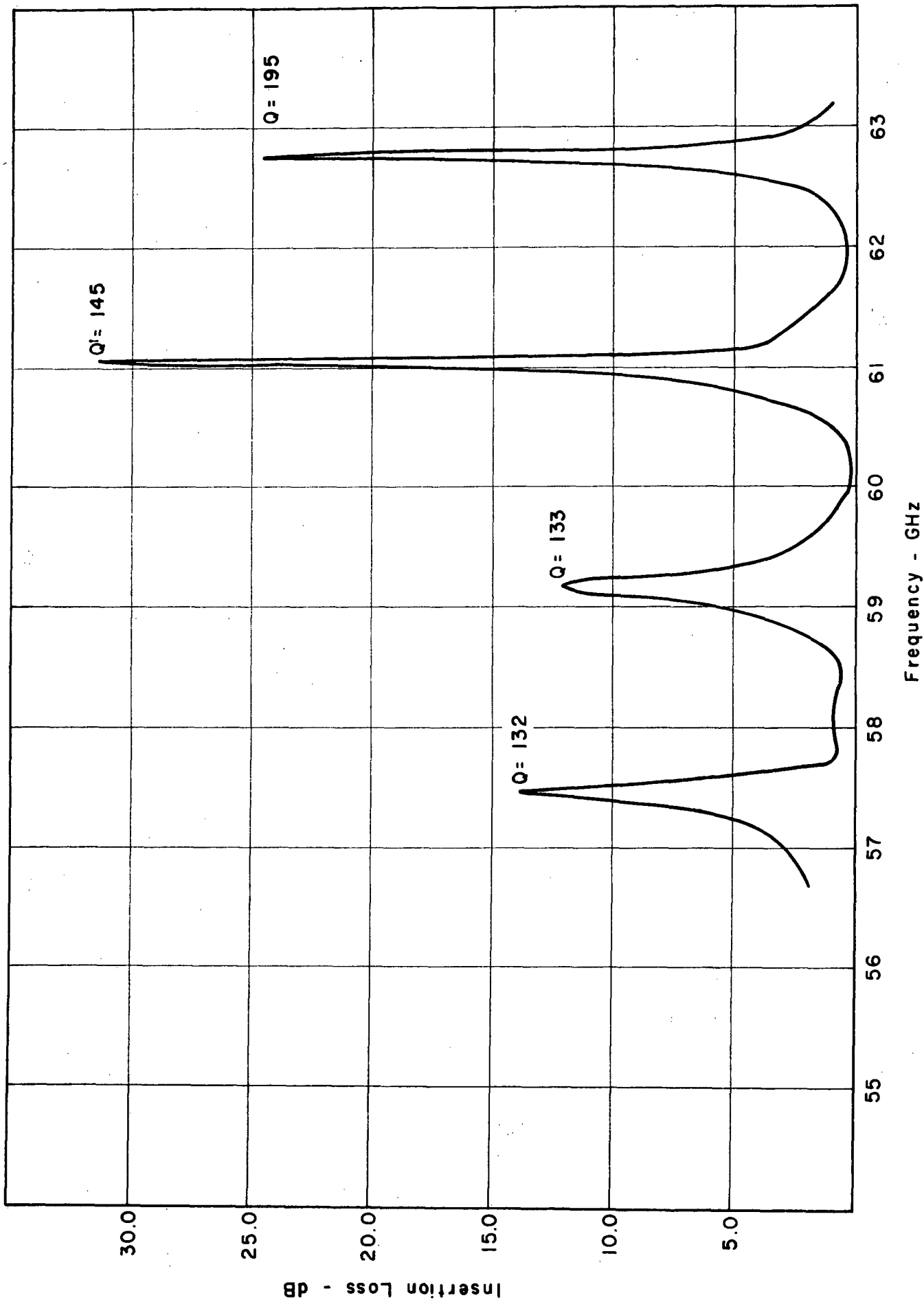
Fig. 56 V-BAND RING FILTER RESPONSE - RING ATTACHED WITH
TYPE 509 ADHESIVE

5. ACTIVE DEVICES

5.1 Introduction

Hybrid microwave- or millimeter-wave integrated circuits require the use of active semiconductor devices for circuit functions such as amplification, oscillation, multiplication, limiting, switching, frequency conversion, phase shifting, and modulation. Methods for mounting such devices which consider the specific nature of the circuit function, the geometry of the device package, and the image line configuration are required. The next subsection will consider mounting techniques in general. The following subsection will describe an experiment for mounting a mixer/detector diode in image waveguide.

5.2 Mounting of Active Semiconductor Devices

Incorporation of a semiconductor device into a microwave hybrid integrated circuit requires both physical compatibility and electric match over a desired bandwidth. In the range of frequencies from 8 to 40 GHz, the most suitable choice is a pill-type package. In this range the cross-sectional dimensions of the image line are large enough to be suitable for mounting a commercial pill package which typically ranges in diameter from 0.050 to 0.125 in. At frequencies higher than 40 GHz parasitic reactances of a pill package will usually prevent its use. In this range of frequencies a chip device becomes the appropriate choice. Some chip devices have only metalized contacts; others have "beam" leads for making electrical contact.

Figure 57 shows a typical pill package. This style has the
stud base and is used with oscillator diodes requiring a very
effective heat sink. Other devices have only a base plate for
contact with the image plane. Either package style is compatible
with the image line as shown in part b of Figure 57. The met-
alization has the purpose of suppressing higher-order modes and
preventing radiation. The dimensions of the image waveguide may
be tapered or varied in some fashion to help achieve good elec-
trical impedance match to the particular semiconductor device.
If the semiconductor is a mixer, detector, switch or other device
requiring a dc, video or IF contact, this may be made through a
flying or printed wire, suitably choked to prevent microwave
leakage. If the IF frequency is also a microwave frequency, the
use of a microstrip output line may be appropriate, as shown
in Figure 58. A low-pass filter prevents the incoming microwave-
or millimeter-wave frequency from following the microstrip
output line.

Impedance matching of the incoming microwave signal to the
active semiconductor device will usually be required in order
to achieve optimum device performance. A tuning device is shown
in Figure 59 in which three metal or dielectric screws are used
to introduce reactive loading on the dielectric image waveguide.

The mounting of a chip semiconductor device in an image
waveguide for millimeter wavelength operation is shown in Fig-
ure 60. Wire bonding is used to make electrical contact between
the chip and the millimeter-wave signal induced on the metaliza-
tion. The chip is connected to a post ground terminal directly

D.C. Terminal

Metalization

Top Plate

High ϵ_r Ceramic
Body

Metal - Ceramic
Seal

Semiconductor Device

Metal Stud
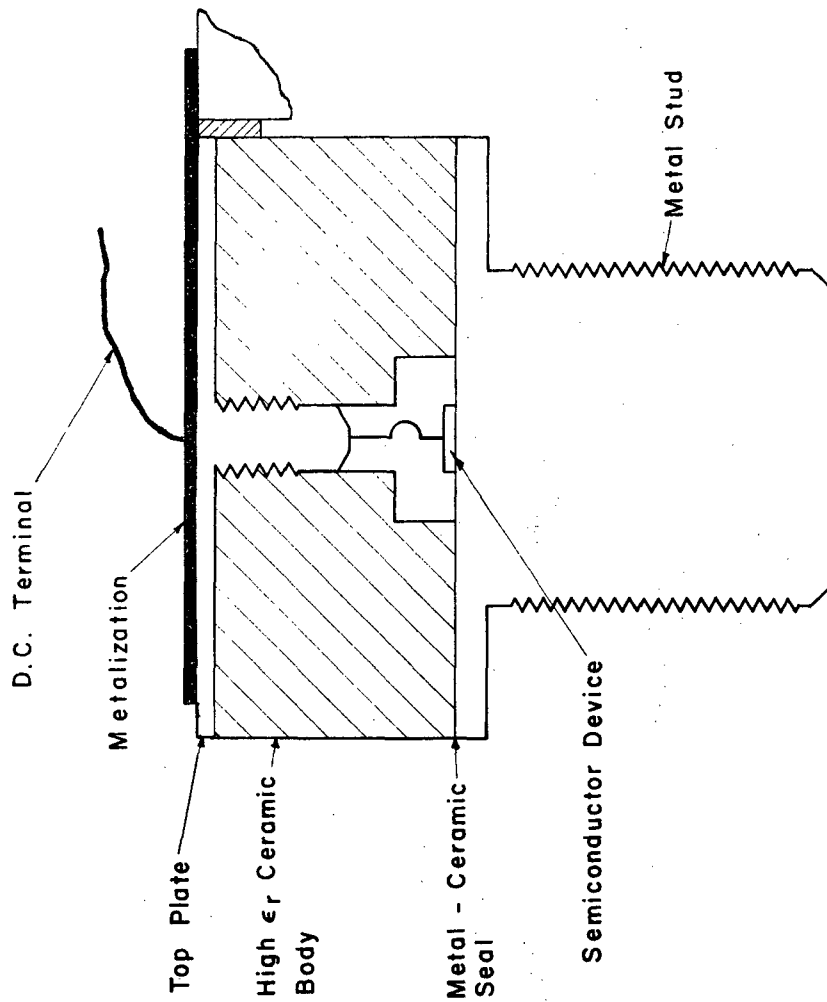
a) Section View Of Package

DC - Video
Terminal

Ceramic Body

Metalization

High ϵ_r Ceramic
Guide

Image Plane
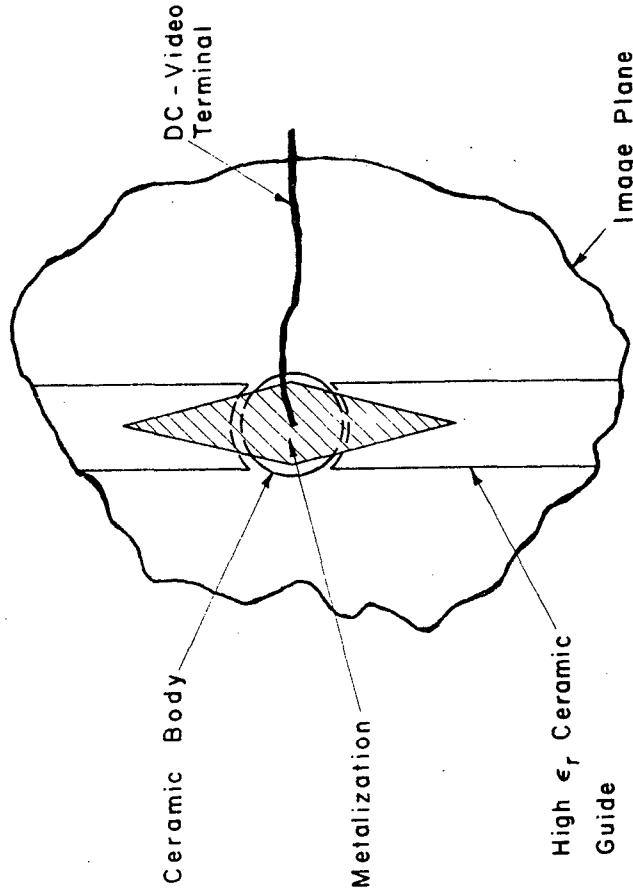
b) Top View Of a Package Installed in an Image
Line

Fig. 57 ACTIVE SEMICONDUCTOR DEVICE
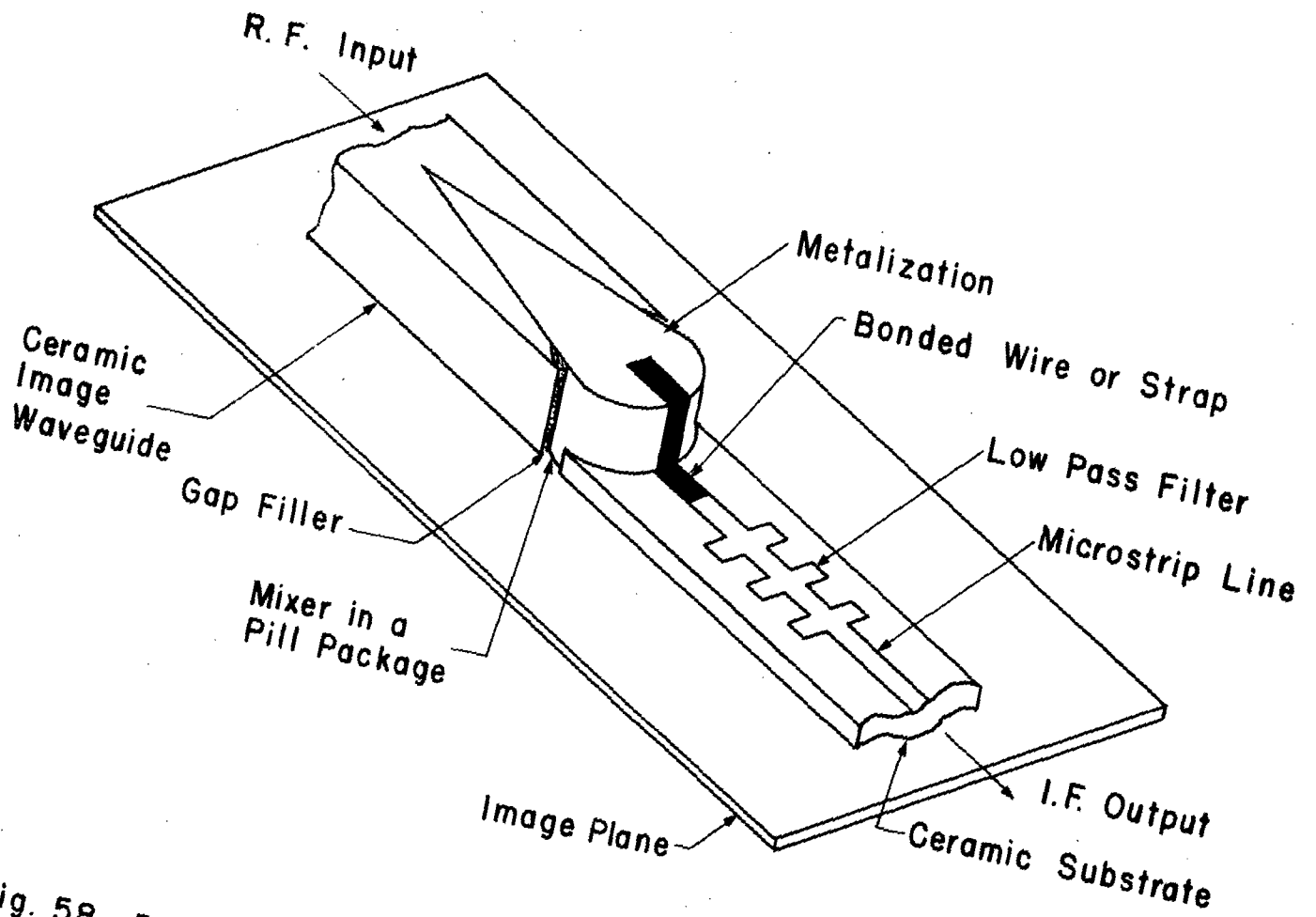
Fig. 58 PILL DIODE MIXER MOUNTING FOR A MICROWAVE I.F.
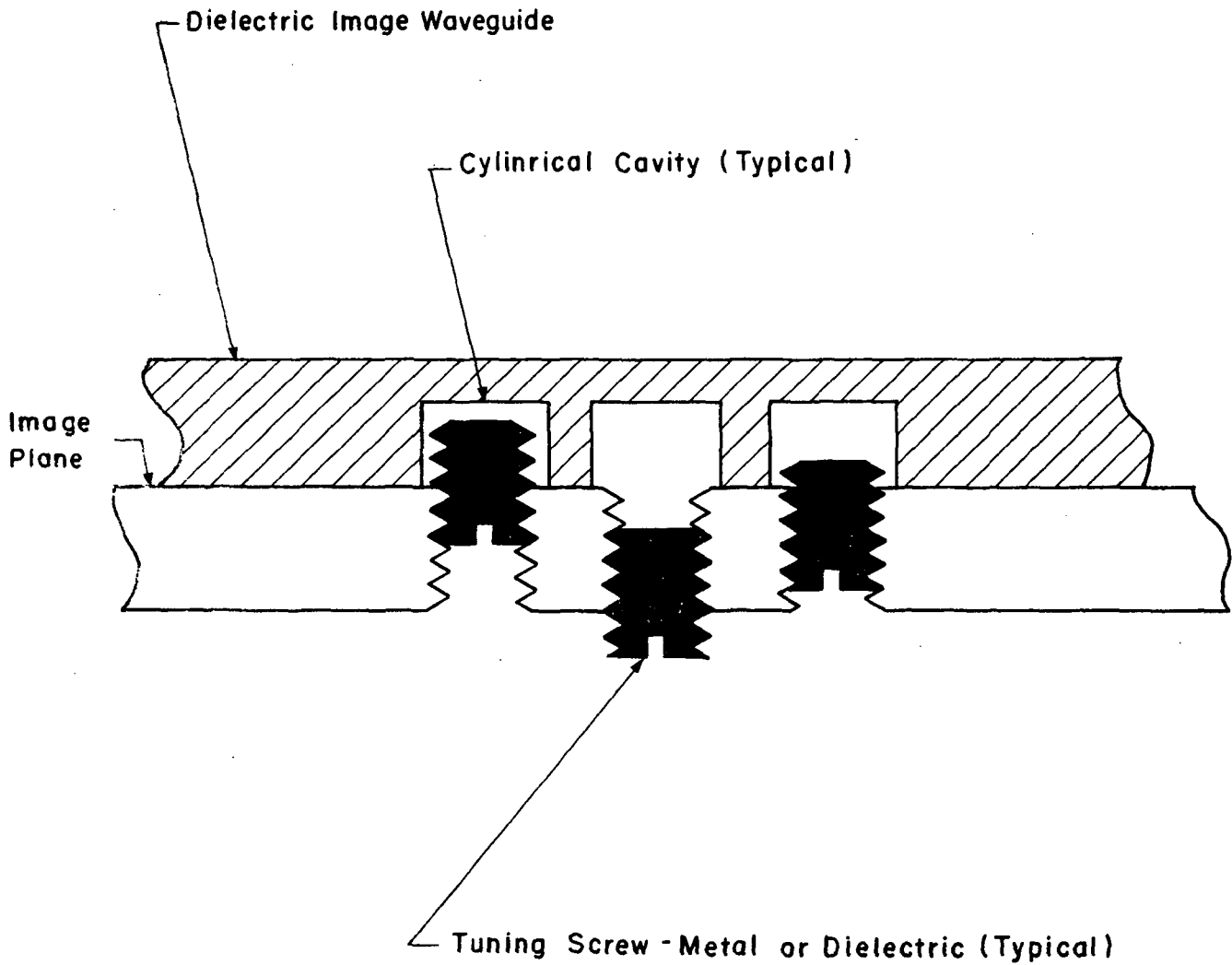
Fig. 59 THREE SCREW TUNER
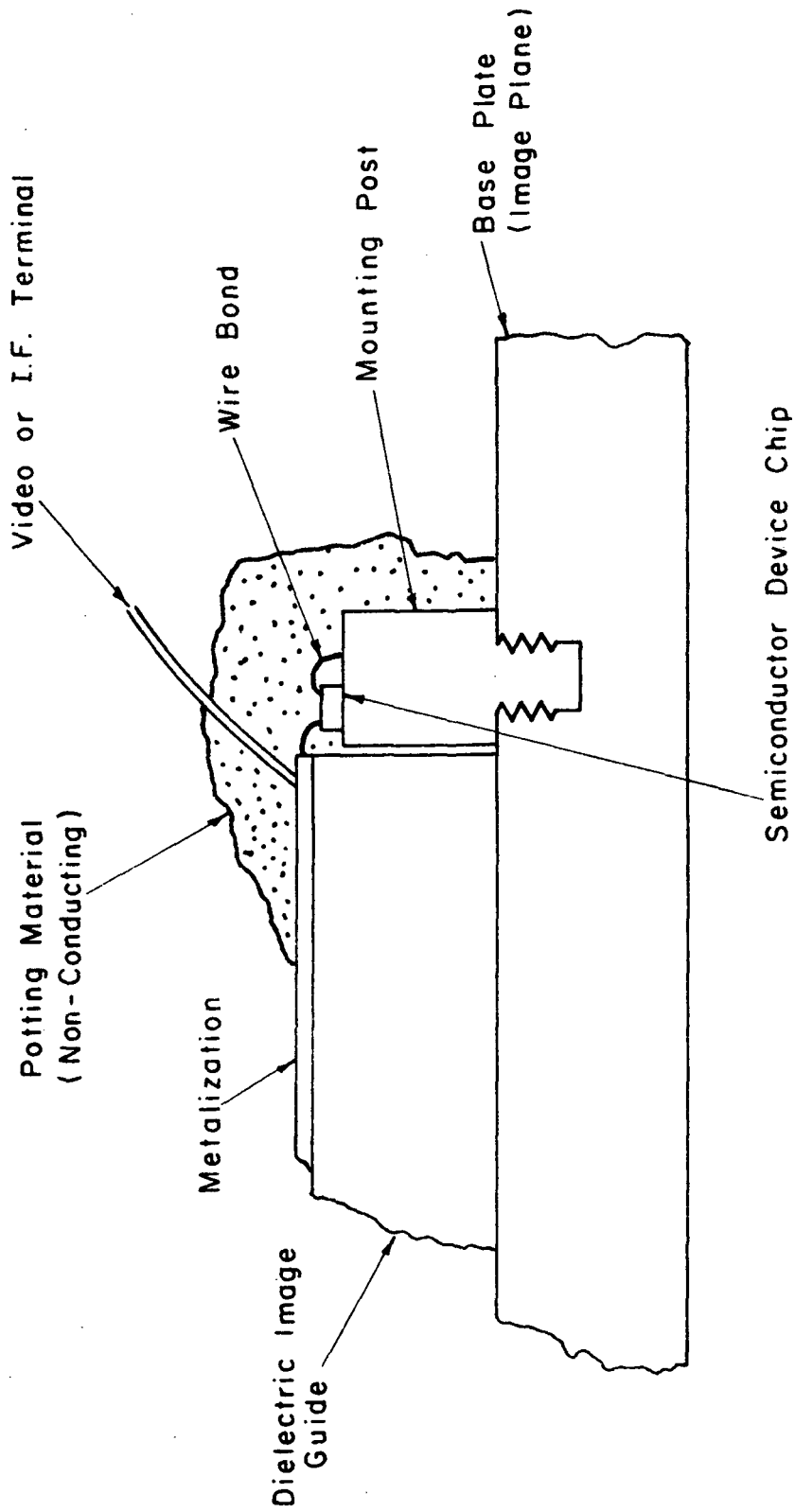
Fig. 60   POSSIBLE CONFIGURATION FOR MOUNTING A CHIP SEMICONDUCTOR DEVICE IN IMAGE LINE

through its own metalized contact or with a wire bond as shown. If the device has beam leads, these replace the wire bonds. Again the video/IF terminal can be a flying lead, printed-wire, or microstrip line as the frequency may necessitate.

The above package mounting techniques have not been demonstrated experimentally and therefore remain conceptual. During the present program an approach to mounting a mixer/detector diode was investigated which represented a compromise because no chip (or pill) devices were available for 60 GHz at the time the experiment was conceived. The results of this investigation are described in the following subsection.

5.3 A 60-GHz Mixer/Detector Mount

This experiment involved converting a conventional waveguide cartridge-type mixer mount to one in which the signal was carried on an image line up to the semiconductor chip within the cartridge package. The plan was to measure the impedance and conversion loss properties of the diode with and without the image line to demonstrate that a signal could couple efficiently into a diode using an image line. Unfortunately, several factors combined to prevent the desired quantitative measurements from being made. The image line mount was indeed operated as both a mixer and detector, but the absolute and comparative data desired could not be obtained. The mount, along with the factors which prevented its effective operation, will next be described.

126

A modified standard mount is shown in Figure 61. The incoming

V-band signal was guided through standard V-band waveguide attached

to the flange at the left. A type B launcher coupled the waveguide

mode to the image guide mode. The alumina waveguide is partially

visible to the right of the launcher. The signal was then carried

on the image waveguide within the metal waveguide of the standard

mount.* The cartridge outline is shown in the insert of Figure 61

and in greater detail in Figure 62. Alumina inserts were fabri-

cated** so that the image line would be continuous up to the point

where the diode chip is mounted (see Section A-A in Figure 62).

Thus, the cartridge diode was intended to simulate as closely

as possible the mounting of a chip diode shown in Figure 60.

The instrumentation for mixer impedance measurements is

shown in Figure 63. The primary limitation of the instrumenta-

tion was that the local oscillator signal available through the

directional coupler was only 0.2 mw. Compounding this problem

was the fact that the attenuation through the image line was

about 16 dB.*** Thus, the local oscillator signal actually

---

* This was a Baytron type 1ES-15 mount. The diodes were 1ES-15/M
  mixer diodes in a cartridge package. A shorted diode was also
  obtained to facilitate making impedance measurements.

** These are the small parts visible in Figure 67.

*** This attenuation was determined by comparative measurement of
    the diode as a detector with and without the image line. The
    excess attenuation was due to warpage in the base plate which
    caused a gap between the alumina and the base plate. Time
    limitations on the program did not allow for refabrication of
    this base plate.
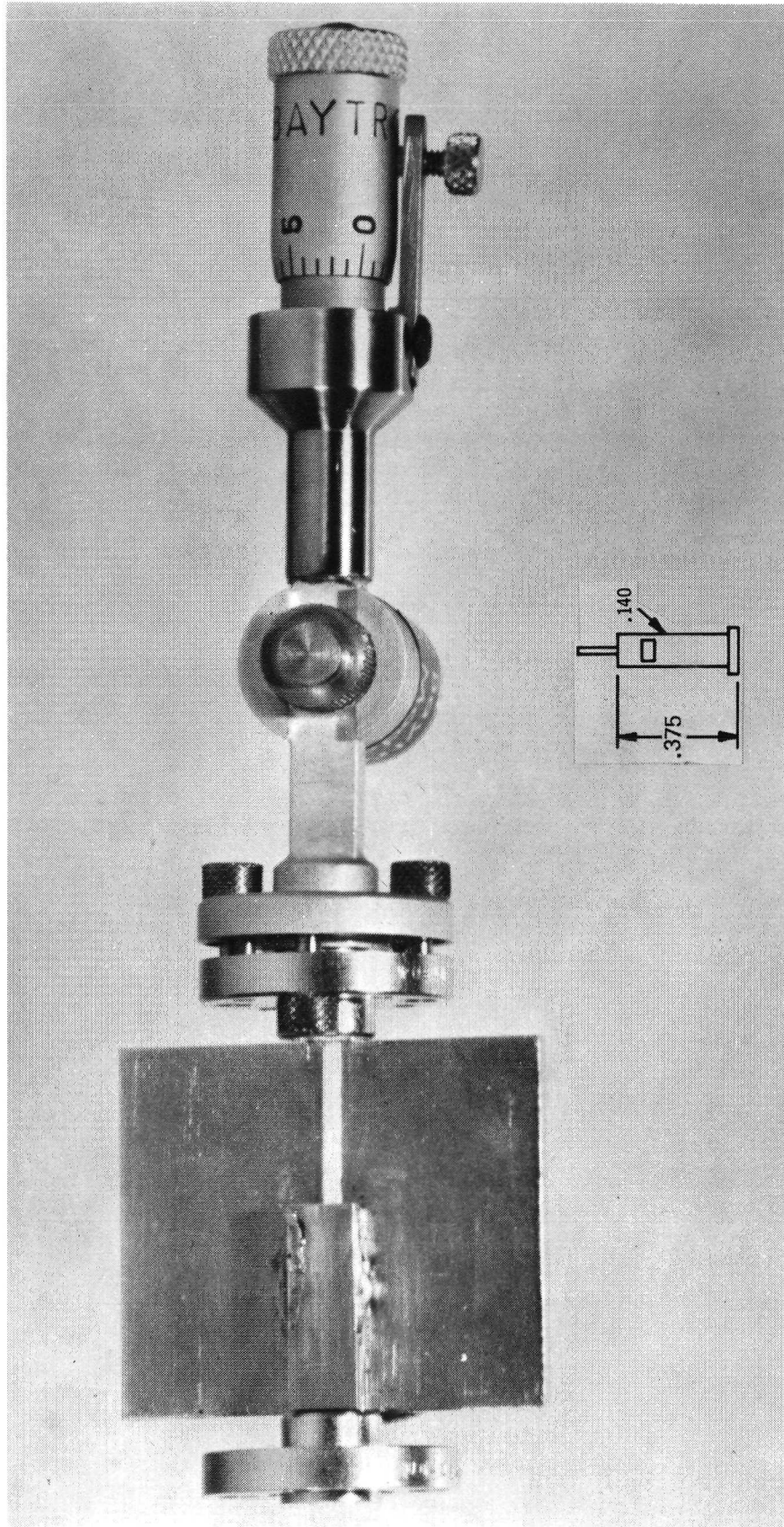
Fig. 61   MODIFIED WAVEGUIDE MOUNT DESIGNED FOR OPERATION
WITH CERAMIC IMAGE WAVEGUIDE

Alumina
Insert

0.0135 R

Diode Chip
Mounting Post

Alumina
Image Line

0.070

0.050

SECTION A-A
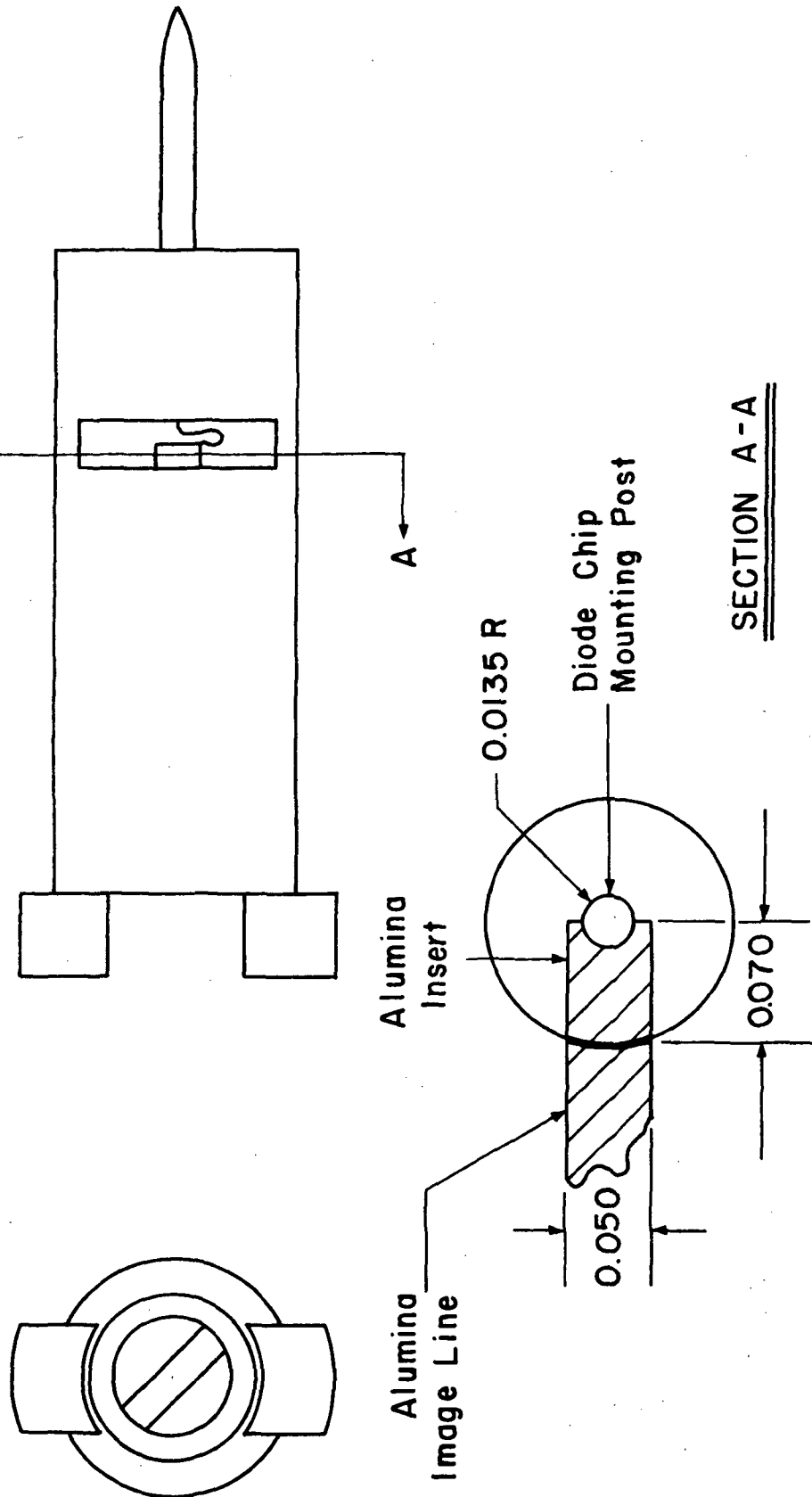
Fig. 62 V-BAND IMAGE LINE CARTRIDGE DETAIL
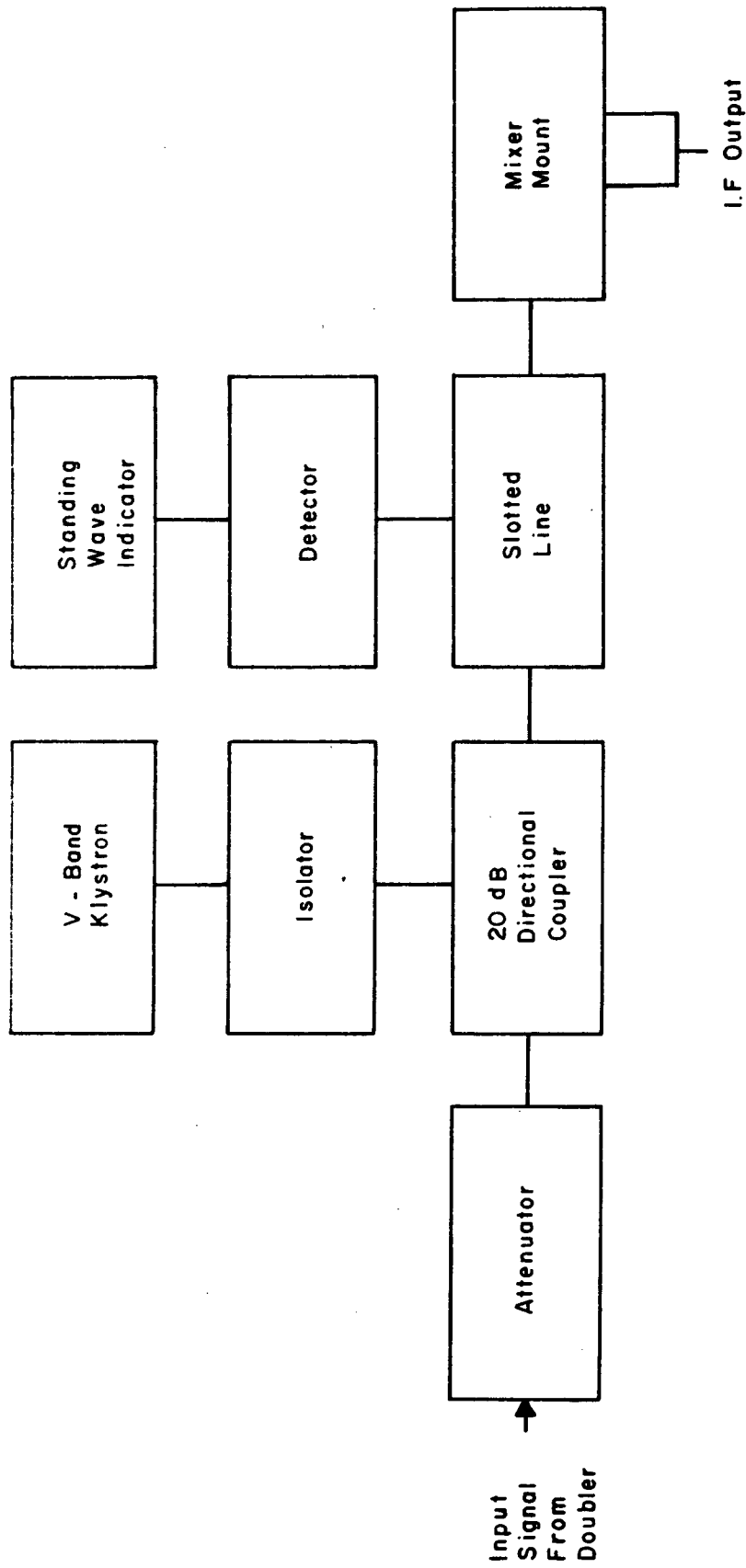
Fig. 63 INSTRUMENTATION FOR V-BAND MIXER MEASUREMENTS

reaching the diode was about 0.005 mw, far too low for mixing. The rather high attenuation in the image line also prevented impedance measurements.

Despite the very low level of the local oscillator, the image line mount was used to generate an IF frequency of 1 GHz at a signal frequency of 61.7 GHz. The sensitivity was rather poor, making it impossible to determine the efficiency with which the image line signal was coupled into the mixer diode.

6. THE FABRICATION OF CERAMIC WAVEGUIDE COMPONENTS

6.1 Introduction

The purpose of this section is to examine in detail the possible methods of fabricating ceramic waveguide components. It is necessary to establish that the ceramic components for image line technology can be fabricated in a practical manner. The fabrication process must yield components with good electrical quality, reproducibility, and dimensional accuracy.

The state-of-the-art methods of ceramic processing were surveyed and analyzed in terms of the requirements for waveguide components. Ceramic manufacturing personnel were contacted for information and advice. As a result of this analysis, certain processing methods were judged to be closely suited for present needs. Some experimental work on fabrication was initiated to study the feasibility of producing waveguide components. The results of the survey, analysis, and experimental work are presented in this section.

6.2 Ceramic Processing Methods

6.2.1 Solids Processing of Ceramics

Most electroceramics are fabricated by solid processing techniques. Solids processing involves the use of solid particulates, which are consolidated into a shape by some type of forming method and densified at high temperature.

There are a number of methods for consolidating particulates into specific shapes, or "green bodies." The selection of method

depends on many factors, such as body shape and size, economic considerations as to number of bodies required, the cost of processing, and the quality of green body as it affects the fired product. Each method must be considered individually to determine its applicability for a specific product. The more common forming operations are:

(1) Dry Pressing

(2) Isostatic Pressing

(3) Extrusion

(4) Slip Casting

(5) Plastic Molding

(6) Tape Casting

These operations will be briefly described in the next subsections.

6.2.2 Forming Methods

6.2.2.1 Dry Pressing

The pressing of powder in a steel or carbide die is one of the most important processes because of the economy afforded in rapidly producing simple shapes with a high degree of uniformity. In this process, the ceramic powder must be granulated to produce a free flowing material which is necessary for high speed automatic pressing. For this reason the granular mass contains an organic binder and lubricant. The die cavity formed by the die wall and upper and lower punch surfaces determines the shape of the pressed part. After ejection from the die, the compact is fired to high density.

6.2.2.2 Isostatic Pressing

Isostatic pressing differs from dry pressing in that pressure is applied as nearly as possible over all outside surfaces of the part, rather than from the ends only. Rubber molds or containers are used to transmit a uniform isostatic pressure from pressurized, liquid surroundings.

6.2.2.3 Extrusion

The ceramic powder is mixed with water and organic plasticizers to produce a plastic mass. The mass is extruded through a die to form a long body having the cross-section of the die. Extrusion pressures of a few thousand psi are typical.

6.2.2.4 Slip Casting

Ceramic powder is suspended in water to a high concentration by use of deflocculants. The slurry or slip is poured into a plaster mold of two or more pieces. The mold is porous and absorbs water from the slip, building up a solid coating on the inner surfaces. When the coating reaches a desired thickness, the mold is inverted and excess slip is allowed to drain out. The cast shell is allowed to further dry in the mold until it gains strength and shrinks away from the mold. Then the mold is opened, and the part removed.

6.2.2.5 Plastic Molding

This process, often referred to as injection molding, utilizes a mixture of ceramic powder and a hot thermoplastic liquid. This mixture can be processed by the usual injection molding

method for forming thermoplastic articles. The hot mixture is injected under pressure into a mold. The mold is cooled to solidify the thermoplastic resin, and the article is removed. Since the green bodies contain 15 to 25% organic resin, a slow bakeout schedule is needed to remove the organics before the ceramic can be sintered.

6.2.2.6 Tape Casting

Thin sheets of green ceramic are formed by doctor blading a powder-liquid-binder slurry onto flat plastic sheet and allowing the liquid to evaporate. These green sheets, or tapes, are generally around 40 mil or less, and are easily handled because of flexibility imparted by the organic binder and plasticizer.

6.3 Waveguide Processing Approaches

6.3.1 Applicability of Forming Methods for Waveguide Components

Slip casting is generally used for large shapes. The problem with slip casting is that the particulates are not compacted with high pressure and therefore do not generally form dense fired bodies. Furthermore, these bodies undergo large shrinkage during firing, making it difficult to obtain precision parts. Slip casting is usually used only for large, intricate bodies that would normally require massive presses and/or a great deal of secondary machining. Thus, for flat, waveguide components slip casting is not considered applicable.

Isostatic pressing is used for pressing ceramic shapes that cannot be carried out by dry pressing. The alumina insulator in spark plugs is a well known example. It is also used for pressing large shapes, since they would otherwise require massive presses. This process is not useful for making flat, substrate-like sheets or components, since there is little control afforded in obtaining parallel top and bottom surfaces.

Extrusion would be useful if the extruded green bar can be sliced to form the thin, flat component. However, several problems are evident. First, sufficiently accurate slicing is difficult, particularly for thin parts. Secondly, there is less compaction of the ceramic powder than in dry pressing, so poor densification and large shrinkage during firing often result. These problems are not insurmountable, but the development required to optimize the process would be rather extensive and is justified only if a very large number of components are to be processed. For waveguide components, these justifications are not present.

Injection molding produces the poorest quality parts of those processes discussed. The reason for its usefulness is for lower quality, high production item parts having intricate shape. The problem with green bodies is the low green density and high organic content that has certain destructive influences during burnout.

Tape casting and dry pressing are the two most promising methods for forming waveguide components. They are basically

planar processes in that parts with parallel top and bottom surfaces are formed. Complex planar components with various branches and loops can be fabricated by combining either process with special green body machining. The general approaches for manufacturing waveguide components by these processes will be described in detail in the next sections.

6.3.2 Waveguides by Tape Processing

6.3.2.1 Preparation of Green Tapes

Green ceramic tapes are made by the doctor blade tape cast process. The first step of the process is preparing a slurry containing the ceramic powder, the organic binder, plasticizers, an organic solvent, and a deflocculant. Generally, the ceramic powder is extremely fine grain, with diameters between 0.1 to 10 μm. The mixture of ingredients is ball milled for effective mixing and breakdown of agglomerates. After milling, the mixture becomes a dispersion having the consistency of paint. The paint, or slip, is de-aired by vacuum and filtered to remove agglomerates and undissolved binder.

The casting machine has the general features described below. A plastic strip, usually polyethylene or cellulose acetate, is pulled from a storage roll between a metal plate support and a doctor blade unit. This unit has a chamber that holds the slip and a doctor blade at the exit side of the chamber. This blade can be adjusted to produce different thickness deposits. As the plastic tape is pulled, a thin layer of slip is formed. This layer dries slowly while it is being carried downstream

through the machine. Generally the tape travels about 25 feet
before it is fully cured. The drying process is controlled
by heating and by adjusting the vapor pressure of the solvent.
The composite layer of plastic and cast alumina is wrapped
on a large drum for easy handling and storage. When used,
the plastic backing tape is peeled away from the ceramic tape.

The green tape is quite flexible because of the organic
binders and plasticizers. It feels like leather and can be
cut into various shapes as desired. Once cut, the parts are
loaded on a carrier plate (setter) and passed through a kiln
(furnace) where the organics are burned out and the ceramic
powder is sintered to form a dense ceramic material.

The green tapes range in thickness from about 0.005 in. up
to about 0.040 in. Green thicknesses between 0.028 and 0.033 in.
are most common, since they shrink to around 0.025 in. in the
fired condition, which is commonly desired for electronic substrates.
For example, microstrip hybrid integrated circuits are frequently
fabricated on 0.025 in. alumina substrates.

6.3.2.2 Machining of Green Tapes

For large scale production items, green tapes are cut into
desired configurations with a punch press. The parts are punched
oversize to allow for shrinkage during firing. The punches
employed are similar to those used for sheet metal work. For
cutting small quantities, hand punches resembling cookie cutters
are often utilized. If rather intricate work is required, par-
ticularly if it involves thin strips and loops, careful cutting

138

by sharp hand tools is required. Since the green tape is some-
what abrasive, carbide cutting dies are employed for large
scale production runs.

6.3.2.3 Sintering of Machined Parts

The sintering heat treatment schedule depends largely on
the type of ceramic being processed. Most ceramics require
sintering temperatures from 1000°C up to 1800°C. Alumina, for
example, must be fired somewhere between 1450 to 1700°C,
depending upon the reactivity of the raw material.

Machined green parts are placed on a ceramic setter, which
usually is in the form of a top-open-end box. The floor of the
box must be very smooth, since the fired tape tends to replicate
the surface on which it is sitting. When loaded with parts, the
setter is covered, either with a lid of the same material or
by another box setter on top. The complete enclosure of the
parts by setter material is essential for obtaining uniform tem-
perature during firing. Nonuniformity in temperature usually
causes warpage of the parts.

In large scale commercial practice, the setters containing
the parts are stacked on kiln cars that can be pushed through
a tunnel kiln. The temperature of kiln is highest at the center
and decreases gradually to room temperature at the entrance and
exit ends. By slowly moving the kiln car through the tunnel,
the parts are heated and cooled gradually. Slow heating is also
needed so that the organics can be burned out without disrupting
the body. Slow cooling helps prevent thermal shocking not only
of the parts but also the setter and car furniture.

A periodic kiln, or batch furnace, is useful when single batches of small numbers are involved. The setters are loaded into a cool furnace, and then the temperature is gradually increased to the peak value, held at this value for the desired time, and gradually cooled back to room temperature.

The sintered part is considerably smaller than the green part because of the densification that takes place. Shrinkage values for the tape must be measured in all three directions (thickness, length, and width directions) to judge what green dimensions for parts are needed to produce specific fired dimensions. Linear shrinkage values can range from 10 to 20%, depending on the specific material.

6.3.2.4 Thickness Limitations

Doctor blading of green tapes thicker than about 0.040 in. is not yet state-of-the-art, although research activities by various companies are apparently about to overcome some of the difficulties. The major problem is the changes that take place in the cast tape as the solvent evaporates during drying. The thicker the tape, the greater the tendency for the tape to crack or warp during drying. This problem exists because of differential shrinkages that take place from nonuniform drying through the thickness of the tape.

Because of the particular advantages of utilizing tapes, some ceramic producers have adopted the practice of piling together layers of tape to form thicker sheets. It is claimed

that the layers fuse together during sintering with no evidence of the original layer structure. If successful, this technique should be particularly valuable for making waveguide components having thicknesses in the 0.030-to-0.100-in. range. Thicker samples, as discussed in the next section, can be made by dry pressing techniques.

6.3.3 Waveguides by Dry Pressing

6.3.3.1 Preparation of Green Bodies

Dry pressing appears as the most promising method for forming thick waveguide components, particularly for thicknesses greater than 0.100 in. The die is machined to have the shape desired. Top and bottom plungers compact the granular feed material in the die, using pressures of 5000 psi or higher.

The first important step of processing, after the selection of appropriate reactive raw material, is to prepare a pressable batch material. This involves the mixing of the powder with an organic binder, plasticizer, and solvent. This mixture is processed by one of a variety of techniques for making granules (agglomerates). The granules are essentially dry and consist of ceramic particles bonded together by the organic binder. The purpose of the granules is to convert the fluffy raw material to a flowable form so that die cavities can be efficiently filled. The granules, if prepared properly, also aid in the compaction of the material.

The organic binder not only makes possible the formation of granules, but it also provides strength to the pressed compacts.

Without this green strength, the compact would be weak and fragile and could not be removed from the die and handled without damage. After green parts are formed, they are loaded on setters and undergo a similar sintering process as described for machined tape parts.

6.3.3.2 Laboratory Techniques

The use of shaped dies is necessary for large-volume production. However, it is justifiable only for this case, since die machining for complicated configurations is extremely expensive. For experimental purposes, where a variety of waveguide configurations are to be studied, the use of machined dies is impractical strictly from economics.

A satisfactory alternative, and one particularly suited for experimental purposes, is to press flat sheets or extrude (doctor blade) green tapes and then machine cut, or punch the green sheet or tape to the configuration desired. The reason for this is that it is much easier and far less costly to machine a soft, chalk-like material than a steel or carbide die.

Machining of sintered ceramic plates into desired configurations may also find limited applications in preparation of laboratory devices. Total or partial fabrication of a ceramic waveguide component by diamond or wire sawing, drilling, grinding, or abrasive machining is possible for limited quantities of parts. These techniques, while minimizing the time required to modify a device, are also limited in the types of operations which can be performed.

142

During the course of this program an investigation of abrasive machining was conducted. An industrial abrasive unit* was operated using silicon carbide powder for machining sintered alumina substrates having an 0.025-in. thickness. The hardness of the ceramic necessitates the use of a very hard powder. Unfortunately, very hard powders operating at high pressures (about 90 psi) result in limited lifetime of the nozzle tip which controls the powder flow. Small diameter orifices (0.008 in.) gave faster, more precise cutting, but the tip lifetime was rather short. Carbide tips lasted only minutes, sapphire tips lasted about one hour. Larger orifices (0.018 in.) lasted three to four hours but cut at a considerably slower rate. Despite the use of hard powder and high pressure, the maximum cutting rate was found to be rather slow. The waveguide described earlier and pictured in **Figure 51 required about 1.5** hours cutting time. The estimated cutting rate for an alumina substrate 0.025-in. thick is three to four inches per hour.

A pantograph was fabricated so that waveguide devices could be cut using a template guide. A photo of this pantograph, which has a 2:1 motion reduction factor, is shown in Figure 64. The template in place under the guide is that used to machine the waveguide in Figure 51. A template was machined, and is shown also in Figure 64, that would serve as a guide for the pantograph to yield the "U" waveguide of Figure 22. This template was not required as explained in Section 3.3.4. The abrasion

---

* S.S. White Model D
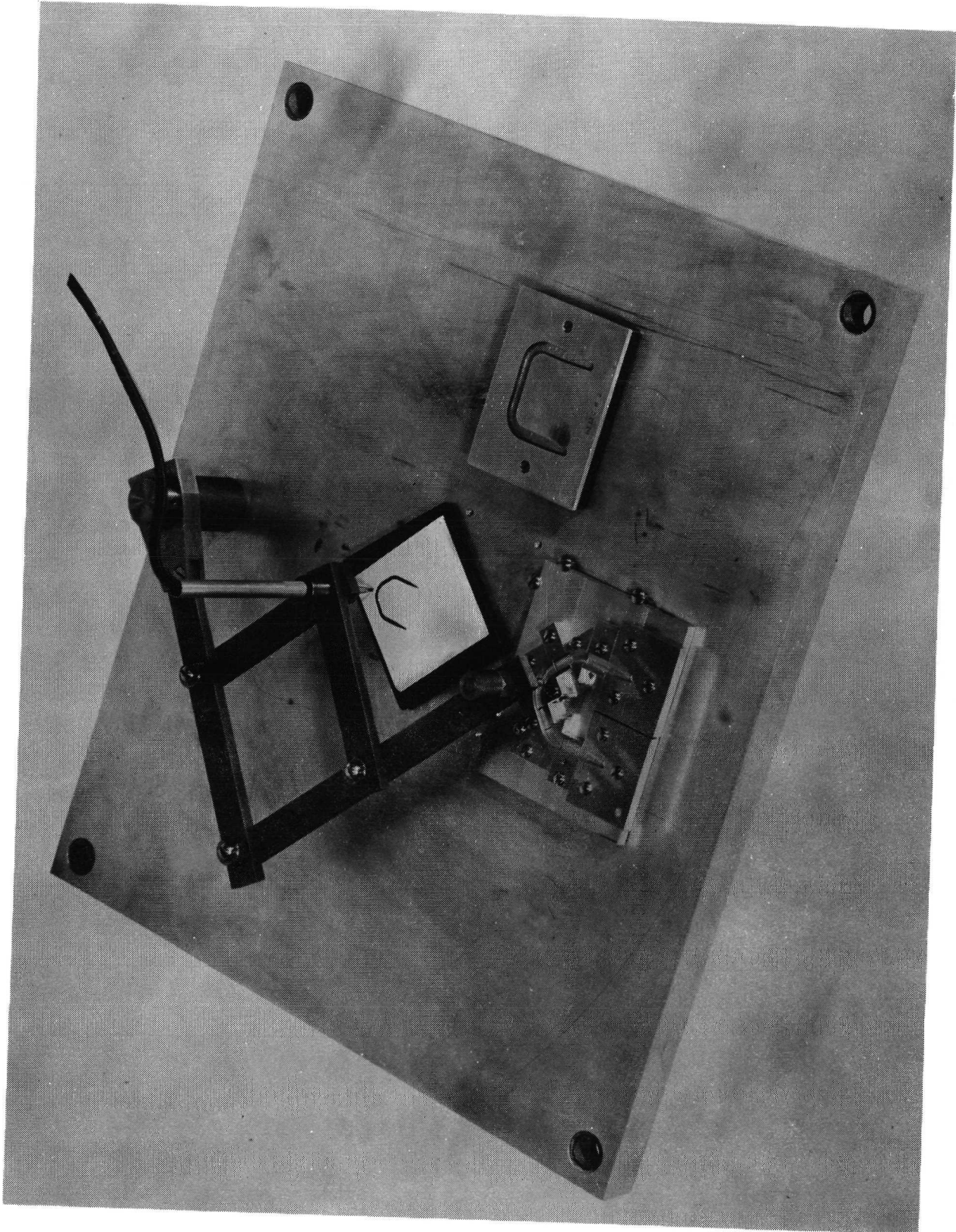
Fig. 64. A PANTOGRAPH FOR FABRICATION OF WAVEGUIDES USING ABRASIVE MACHINING

144

technique does not give a verticle side wall. The waveguide

of Figure 51 had a trapezoidal cross-section in which the width

at the top surface was typically 0.040 in., and the width at

the lower surface was typically 0.060 in. The width of the

waveguide varies because the cutting width depends on time

of exposure to the stream of particles.

Clearly, this method of fabrication is somewhat impractical

for general fabrication, but could find usefulness in limited

situations where other techniques for machining sintered ceramics

might be difficult to employ. An example might be the removal

of stabilizing bars from finished parts in which poor accessibility

prevents the use of other machining techniques.

6.3.4 Adherence of Waveguide Component to Metal Base Plate

The ceramic waveguide component must be joined in intimate

contact with the metal base plate if predictable performance

and lowest losses are to be achieved. The ceramic must also

be extremely smooth (less than 10-μin. finish).

The ceramic can be bonded with the metal by a variety of

adhesives. Organic adhesives provide strong bonds, but they also

create a nonducting interlayer with higher loss and, therefore,

may prove to be unsatisfactory (see Section 3.3.4). More ideally,

a direct contact of metal to the ceramic would be preferred.

This suggests that a metal solder or braze would be the best

approach.

To apply a solder to a ceramic, the ceramic must be treated

by a metallizing process. Metal solders do not adhere to ceramics

unless the surface is modified. The present state-of-the-art in metallizing ceramics is to apply a thin coating of silver or alloys of silver, palladium, gold and platinum. This silver or alloy is applied in the form of a paint, having an organic solvent and binder. Once applied and dried, the coating is fired on at temperatures between 1000 to 1800°F, depending on the specific material.

Soft solders with alloys that melt below 700°F should be sufficient for present purposes. Many types of common soft solders are available, but the ones generally used on ceramic components approximate the tin-lead eutectic composition (63% tin, 37% lead). The solder often contains some silver (2%) so as to prevent leaching of the metallized layer of silver.

Forming a dense, well bonded interface between the ceramic and metal base plate is an art, requiring considerable practice, but there appears to be no reason why a satisfactory bond cannot be accomplished. The principal advantage of metallizing and soldering is the fact that the ceramic is intimately in contact with the metal conductor removing any possibility of a gap between them. Experimental results, described in Section 3., have indicated the need for intimate contact between the ceramic and the image plane.

6.4 Experimental Feasibility Studies

During the present research period, attention was focused on the possibilities of forming alumina waveguide components having thicknesses around 0.025 in. For this purpose, preliminary

studies were undertaken to establish general feasibility of utilizing cast ceramic tapes.

A visit was made to the American Lava Corporation, a leading manufacturer of alumina ceramics and tapes. Discussions with engineering personnel at their tape producing facility were helpful in verifying that the tape approach for making waveguide components would be the best approach for thin components. It was also recognized that green tape manufacturing is a highly skilled and rather secretive art and that it would be impractical for IITRI to attempt developing a laboratory casting facility. Therefore, it was decided that the best approach was to buy the green tape from the manufacturer. With this tape, IITRI could machine the configurations needed and sinter the parts in a high-temperature batch kiln in IITRI's ceramics laboratory facility.

6.4.1 Ceramic Tape Specifications

A green ceramic tape was purchased from the American Lava Corporation. The tape is supplied as a roll, shown in Figure 65. According to the manufacturer, the tape had the following specifications:

(1) Ceramic Materials

    AlSiMag 772 - Alumina

(2) Amount

    Two 100-ft rolls, 6 in. wide
    Thickness is 0.029 in. $\pm$ 0.003 in.

(3) Firing Shrinkage

    When fired to Pyrometric Cone Equivalent 30
    with a 36-hour total kiln cycle, the shrink-
    age values were:

Fig. 65   A ROLL OF CERAMIC GREEN TAPE AND SAGGERS USED FOR SINTERING CERAMIC PARTS

	Length	Width	Thickness
Unfired dimension (in.)	3.508	2.345	0.029
Fired dimension (in.)	3.020	2.017	0.025
Fired shrinkage	16.2%	16.3%	16.0%

For calculating the shrinkage, the formula below was used:

$$\% \text{ Shrinkage} = 100 \left(\frac{\text{unfired dimension}}{\text{fired dimension}} - 1 \right)$$

6.4.2 Inspection of Tape Thickness Variations at IITRI

Approximately 11 ft of the tape was unrolled, and the thickness variations along the length and width were measured. Thickness values near the edges of the tape varied from 27.1 to 30.7 mils, which is within the stated specification. Similar variations were found across the width of the tape, with the center region generally being about 0.0005 in. thinner than the edges. With these variations, it was possibile to locate and cut out small sections that had the desired thickness and thickness uniformity throughout.

6.4.3 Sintering of Specimens

A periodic, gas-fired kiln was used to sinter the tape specimens. The kiln has a working space of around a 10-in. length, 8-in. width, and 6-in. height. The fuel can be a combination of natural gas-air or natural gas-oxygen. With natural gas-air, temperatures up to 2850°F can be obtained, while temperatures above 3100°F can be reached with natural gas-oxygen.

Various samples were cut from selected green tape. The samples were either cut by hand, using a straight edge to guide a blade, or machined by a sandwiching procedure. The sandwich method involved a three-layer sheet, the top and bottom being aluminum and the middle being the green tape. This sandwich was machined to the configuration desired. The advantage of the sandwich method is that the tape can be cut into intricate configurations without danger of damage that could result if simply handcut directly.

The first sintering studies were carried out at a temperature of 2850°F. In the first firing, one U-shaped sample was machined using the sandwiching procedure. The sample was placed in a refractory box with a lid, made by two porous alumina bricks separated by an alumina cement wall around the edges. The fired sample shrunk approximately 15.5%. Some warpage resulted and the two arms of the U were not parallel, but spread out somewhat so that the width of the U was greater at the tips than at the base.

A second and third firing at 2850°F was made with a shorter firing schedule and using flat alumina plates on which to set the tapes. The object was to determine if the samples remained as flat as the plates during firing. However, the sintered parts were again warped slightly. The shrinkage value was found to depend on where the part was located in the alumina box. Apparently, the temperature was not uniform and the hotter area caused more sintering than the cooler areas. Lowest shrinkage values were around 11%, the highest around 15.5%.

Following a suggestion by the American Lava Corporation, a method to overcome the warpage problem was tried. It was suggested that flat samples could be obtained if a flat alumina weight was placed on top of the specimen. This could not be done directly on a green tape because the large shrinkage that occurs would lead to distortions in shape by frictional restrictions. Therefore, the green parts must be fired first to affect sintering, and then a second firing should be used with the weight so as to flatten the warped specimen. The flattening occurs presumably because of a diffusional creep process at high temperatures. The warped samples obtained in the previous firings were refired with several alumina substrates as weights. The samples were definitely flattened and exhibited no evidence of warpage.

The above experiments clearly indicated that the samples were not undergoing as much shrinkage as specified by the tape manufacturer. However, this was not unexpected, since the peak sintering temperature was lower than the recommended level of Pyrometric Cone Equivalent 30, which is roughly comparable to 3002°F. To obtain this temperature, oxygen instead of air had to be used in combination with the natural gas fuel. It was necessary to go to the higher temperature because an incompletely sintered body cannot be easily controlled in shrinkage, while a fully fired body has a more reliable and reproducible shrinkage value. Furthermore, the denser alumina body has better strength and electrical properties.

Mullite saggers were purchased to hold the specimens during firing. These are used commercially for firing precision electronic ceramics requiring flatness and close dimensional tolerances. The saggers are pictured in Figure 65.

To evaluate shrinkage and flatness of the tape fired at 3000°F, 3.0 in. by 3.0 in. and 1.7 in. by 1.7 in. green samples were fired at 3000°F for six hours. Shrinkage values for these samples are given in Table 4. The samples did not appear warped. Apparently, the higher temperature of firing increased the ease of diffusional creep to the extent that the samples flattened by their own weight. The data show that the achieved shrinkage value of 16% was consistent with the values furnished by the manufacturer.

Based on the shrinkage data, green U-shaped and ∪-shaped samples were machined so as to give the desired fired dimensions. Machined U-shaped samples were used along with samples with a bar across (∪-shaped), the purpose of the bar being to help maintain dimensional control. Figure 66 is a photograph of the sagger containing U and ∪-shaped samples before firing. The metal piece in Figure 65 was used to assure that the green U-shaped parts (without the bar) were properly shaped when placed in the sagger. The intention was to remove the bar from the ∪-shaped parts after firing. The sagger was closed with another inverted sagger, and the samples were fired to Cone 30 (1650°C). The following firing schedule was observed.

Table 4

FIRING SHRINKAGE

Dimension Parallel to the roll in cm		Shrinkage	Dimension Perpendicular to the roll in cm		Shrinkage	Thickness in		Shrinkage
Unfired	Fired	%	Unfired	Fired	%	Unfired	Fired	%
7.560	6.505		7.300	6.295		0.0309	0.0266	
5.595	6.550		7.280	6.275		0.0302	0.0266	
7.620	6.555		7.260	6.230		0.0299	0.0271	
7.680	6.580		7.190	6.200		0.0300	0.0262	
7.640	6.550		7.155	6.120		0.0297	0.0260	
7.619	6.548	16.356	7.237	6.224	16.3	0.0297	0.0260	
						0.0295	0.0263	
						0.0300	0.0260	
						0.0301	0.0263	
						0.0299	0.0263	13.52
4.250	3.648		4.175	3.552		0.0296	0.0260	
4.260	3.654		4.170	3.590		0.0299	0.0252	
4.250	3.623		4.155	3.595		0.0303	0.0255	
4.250	3.667		4.140	3.600		0.0301	0.0260	
4.230	3.656		4.115	3.600		0.0296	0.0263	
4.248	3.649	16.396	4.151	3.587	15.7	0.0300	0.0266	
						0.0299	0.0265	
						0.0297	0.0263	
						0.0297	0.0261	14.0
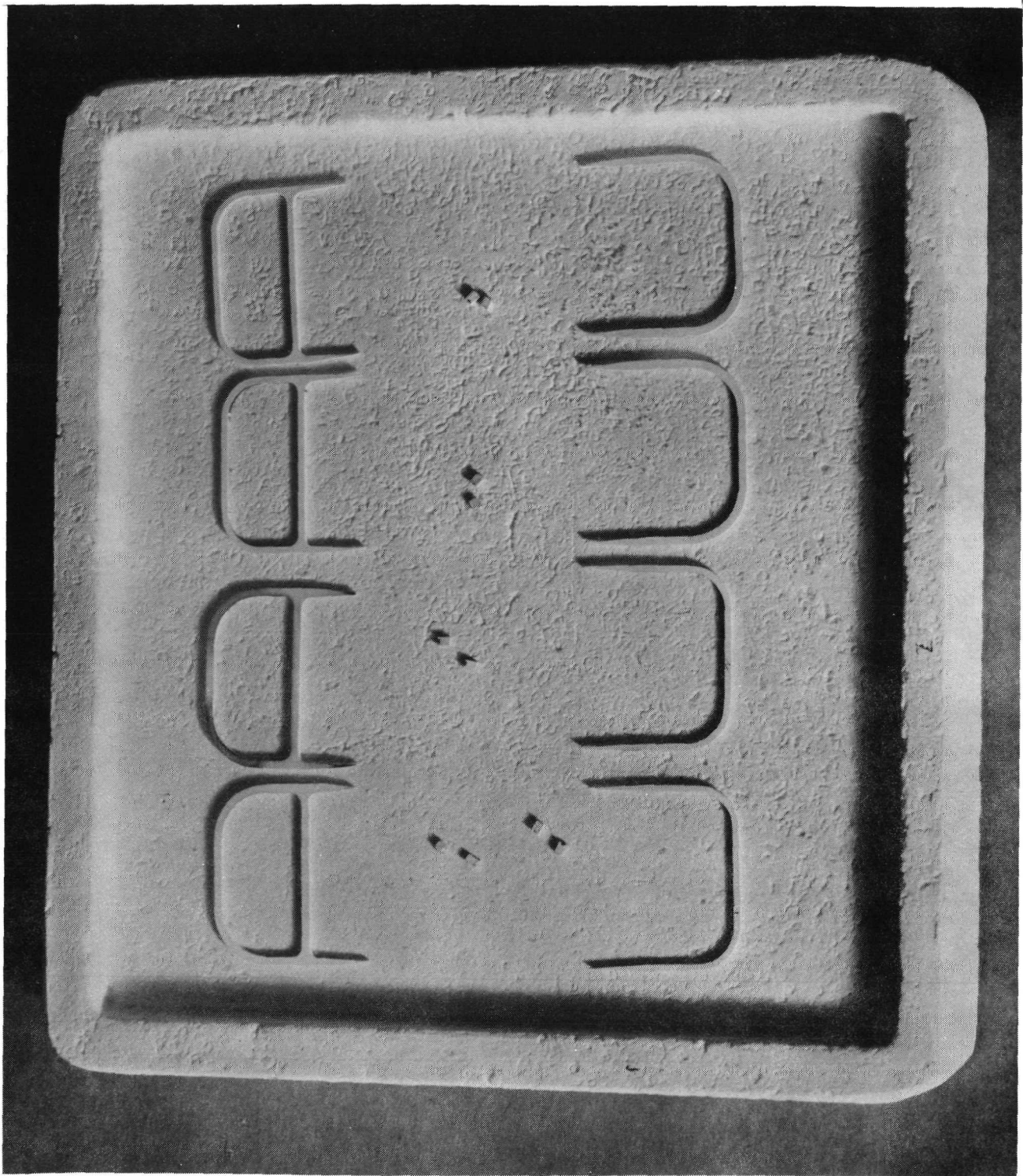
Fig. 66   MACHINED GREEN CERAMIC PARTS SITUATED IN THE
SAGGAR FOR SINTERING

154

1st Stage:	room temperature to 2400°F @ 100°F/hr
2nd Stage:	2400°F to 3000° @ 2000°F/hr.
3rd Stage:	soak @ 3000°F for 7 hours
4th Stage:	natural cooling ≈ 80°F/hr

During stage 2 oxygen-gas was used to reach and maintain the temperature of 3000°F. The samples were cooled by natural cooling. Figure 67 is a photograph of the fired samples. The U-shaped samples bowed considerably, while the Ʉ-shaped samples retained their shape very well. However, the tips of Ʉ-shaped samples were slightly warped. This warping presumably occurred because of the very small mass of the sample, which contributed little to flattening them.

The Ʉ-shaped samples were refired to 2950°F with a weight on top so as to flatten the warped tips. The weight used was an alumina disc. After firing, it was observed that the warped tips of two of the four samples flattened, but got fused to the alumina disc. The other two samples had a lighter weight alumina disc and did not fuse. It is probable that the relative weight difference was the factor responsible for the fusion of the tips.

This study proved the significance of having a bar across the Ʉ-shaped sample. Samples without the bar bowed and warped due to nonuniform shrinkage during firing. This was eliminated by firing Ʉ-shaped samples.

A last experiment consisted of sandwiching together several green tape layers to determine if the layers would fuse together during sintering. This technique may be particularly useful for
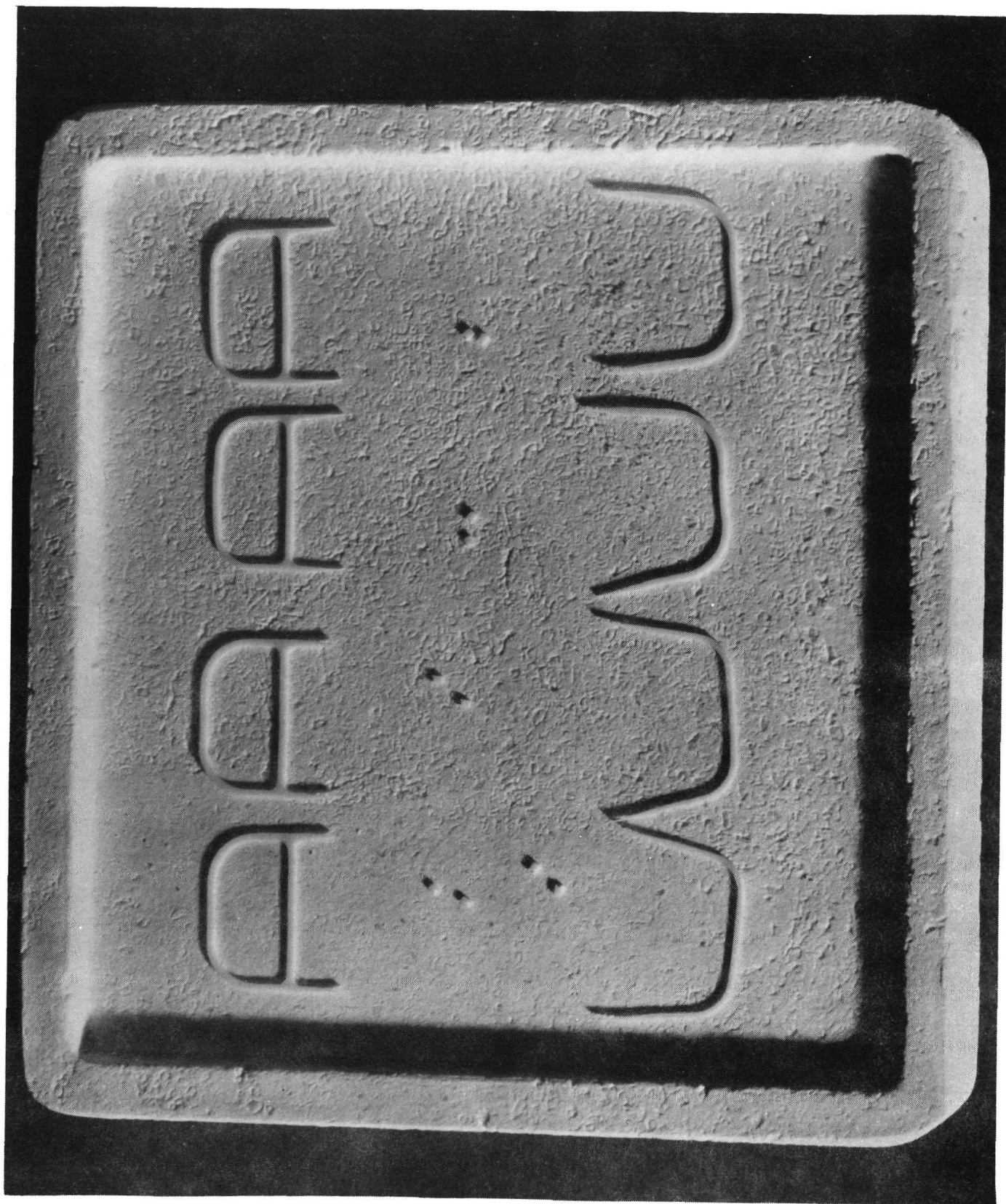
Fig. 67 CERAMIC PARTS AT THE CONCLUSION OF SINTERING

156

obtaining parts with thicknesses greater than what is normally obtainable in tape form (e.g., 25 to 100 mils). When fired at 3050°F, the layers bonded strongly together. When a cross-sectional cut was examined, the original boundary between layers was no longer evident over most of the region. Thus, this strongly suggests that the technique has merit and may be quite feasible for making thicker parts.

The bars which remained after firing were removed with a diamond saw. One surface of these parts was polished using a diamond-powder polishing compound. The polished surface was plated with a thin film of aluminum. Measurements of the properties of these waveguides were given in Section 3.

6.4.4 Conclusion

The processing studies have shown that waveguide components can be made by using green ceramic tape. Several problems were encountered in these feasibility studies, but none appear insurmountable. Warping problems were overcome by second firings with light weights on the sample. Predictable firing shrinkages resulted from high-temperature firing, which makes possible the prediction of green sizes which will form specific fired sizes. The most serious problem was with an open component (ᕒ-shaped). The bowing of the sample during firing is difficult to eliminate because even the slightest nonuniform shrinkage during firing contributes to bowing. The cutting of thin samples causes densification which contributes to nonuniform firing shrinkage.

157

The bowing problem was overcome, however, by adding a stabilizing bar that served to bridge the arms of the U. By proper design, using a stabilizing bar should introduce no dificulties because for production parts they can be made to snap-off after firing.

Although further processing studies are required to refine the techniques to a point where waveguide components can be made routinely, this should require only modest effort. Therefore, it can be concluded that the feasibility of tape processing for waveguides has been established. A principal area for further investigation is that of methods for achieving intimate contact between the finished ceramic part and the image plane.

7. CONCLUSIONS - FUTURE ACTIVITY

The objective of this program was to investigate the use of high permittivity rectangular dielectric image waveguide for microwave and millimeter-wave integrated circuits and to advance this technology towards its use in a 60-GHz switched Dicke-type radiometric receiver module. The specific areas of investigation included in this program encompassed the following: development of metal waveguide to image waveguide launchers; evaluation of the effect on waveguide attenuation of adhesives, films, radius-of-curvature, gaps, and surface finish; design of passive devices including a three-terminal Y junction, an attenuator, a ring hybrid, and a band-stop filter; incorporation of active devices such as mixers or detectors; and evaluation of ceramic waveguide fabrication techniques. The program activity in most areas fulfilled and, in some instances, surpassed original scope and objectives. However, additional effort is required to complete two of the tasks undertaken on the program: the more exact of two radius of curvature analyses performed and the mounting of mixer diodes in the image waveguide.

Therefore, in anticipating future program activity towards the realization of the radiometric receiver module, the early tasks would be to complete or expand upon present program activity. Other tasks represent new undertakings in the development of the image waveguide integrated circuit technology. The following list of tasks is therefore suggested:

(1) Proceed with the rigorous solution to the radius of curvature equations as presented in Appendix A. Obtain correlation with experimental results.

(2) Proceed with the mounting of a chip-type mixer diode in the image waveguide and characterize the diode in V-band.

(3) Perform a detailed evaluation of methods for attaching ceramic image waveguides to the metal base plate.

(4) Develop the required V-band passive devices including the preselector filter and hybrid.

(5) Develop the oscillator circuit using a Gunn or Avalanche diode.

(6) Develop the ferrite switch.

(7) Investigate packaging considerations, such as proximity effects of the top and side walls.

Completing these tasks would provide the necessary information and experience to proceed with the development of the integrated receiver module.

APPENDIX A

RADIUS OF CURVATURE EFFECTS
IN DIELECTRIC IMAGE GUIDES
OF RECTANGULAR CROSS SECTION

APPENDIX A

RADIUS OF CURVATURE EFFECTS IN DIELECTRIC
IMAGE GUIDES OF RECTANGULAR CROSS SECTION

1. INTRODUCTION

To realize, in practice, various circuit functions using a transmission medium, curved waveguide sections must be made part of a circuit pattern. In fact, not only are curved waveguide sections essential in the design of circuit components, i.e., filters, couplers, hybrids, etc., but also in designing compact integrated systems. It is well known, however, that any curved open waveguide, such as the dielectric image guide, loses energy into the surrounding medium by radiation. The amount of radiation loss is a strong function of the guide's radius of curvature R. Thus, the basic design problem becomes that of estimating the minimum allowable radius of curvature for a specified radiation loss (dB/radian). Moreover, knowledge of radiation due to curvature effects is essential in calculating the isolation (crosstalk) between circuit components in close proximity to each other.

In an attempt to obtain the above design information, this Appendix is devoted to the problem of curvature effects in curved dielectric image guides of rectangular cross section.

2. THE BOUNDARY-VALUE PROBLEM

Figure A-1 depicts the basic geometry of the curved guide with a mean radius of curvature R. For convenience, two coordinate systems are employed in the analysis of this boundary-value

162

Fig. A-I CURVED DIELECTRIC IMAGE GUIDE

163
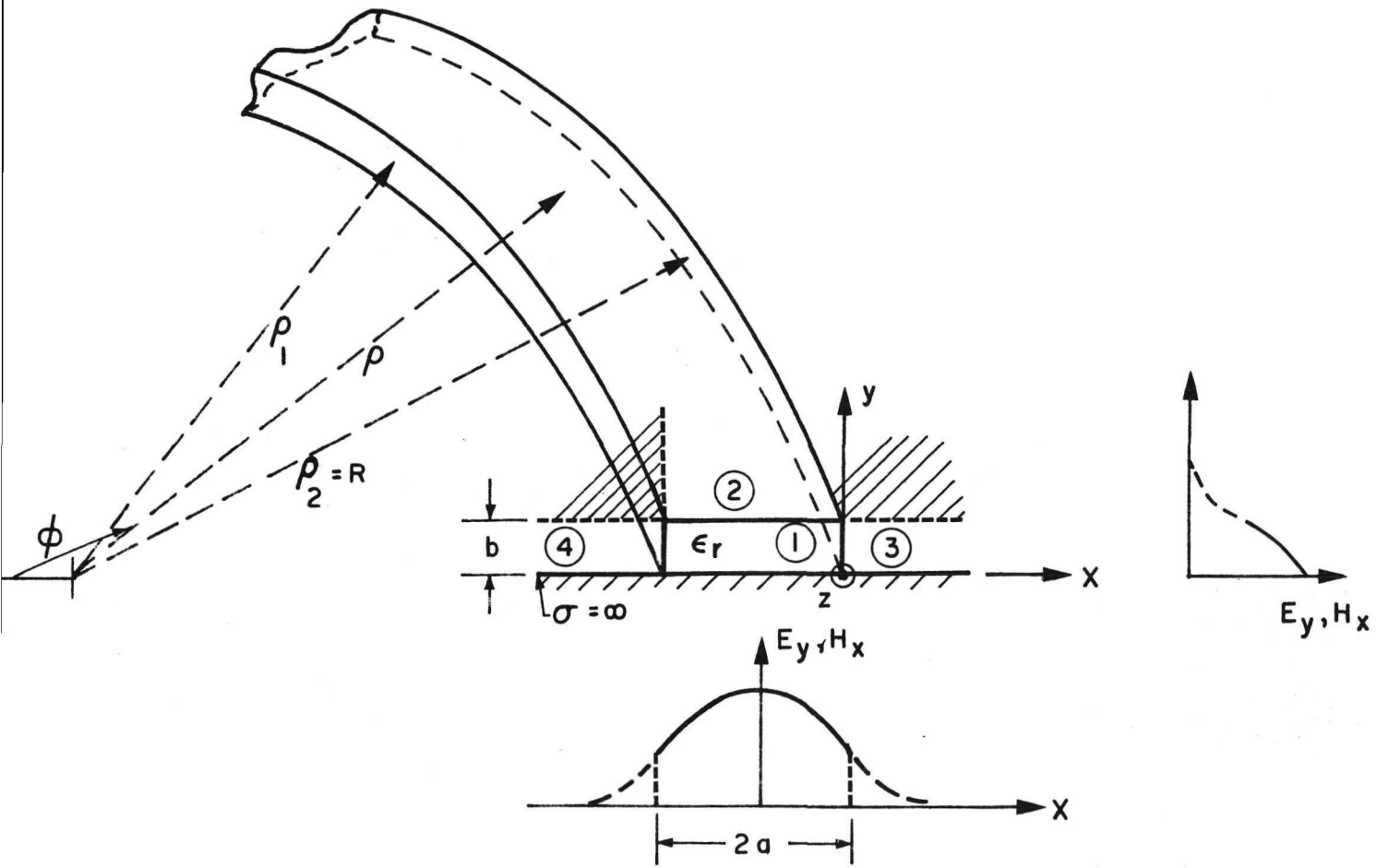
problem. The cross section is a rectangle whose sides are 2a and b. The relative dielectric constant of the guide is ϵ_r, and the surrounding medium is free space. The following analysis closely parallels that by Marcatili presented elsewhere.[24]

This boundary-value problem is solved approximately by introducing the same simplification used in solving the problem of transmission in the straight image guide.[15] The simplification arises from solving Maxwell's equations only for well-guided modes for which a small percentage of the total transmitted power flows through the shaded areas (see Figure A-1) and thus a negligible error is expected if matching is not performed at the edges of the fields.

As in the case of the straight guide, a family of hybrid modes propagates through this curved guide having, in general, six field components. Guidance occurs through total internal reflection when the plane wavelets that make up a mode impinge on the interfaces at angles greater than the crititical θ_c = $\sin^{-1}$ $(1/\sqrt{\epsilon_r})$, where θ_c is measured from the normal to an interface. For example, for an alumina image guide with ϵ_r = 9, the critical angle of incidence is about 19°. Thus, for well-guided modes, the angle of incidence θ_i would have to be $\theta_i > 19°$. Therefore, to a first order approximation, the only large field components are perpendicular to the curved z-axis (Figure A-1) especially for smaller dielectric constants. Past experience with straight dielectric waveguides has shown that the above

164

assumption is valid even for large dielectric constants, provided the mode under consideration is a well-guided one.

The modes are then of the quasi-TEM kind and are designated as E_{mn}^y. The main field components of this family of modes are E_y and H_x. Virtually every one of these components varies sinusoidally along x and y within the guiding medium 1 and decays exponentially in the surrounding medium. The subindices m and n represent the number of maxima of each field component in the x and y directions, respectively. The field configuration of the fundamental mode E_{11}^y is shown in Figure A-1. The following section describes the influence of a finite radius of curvature on this field configuration.

3. E_{mn}^y MODES IN A CURVED WAVEGUIDE

In general, the field components in each region of Figure A-1 should be written as summation expressions[24] but, as discussed above, the power propagating through the shaded areas is neglected and field matching is applied only along the sides of region 1. Therefore, the field expressions need not be so general.

In cylindrical coordinates and assuming variations with time and ϕ to be given by exp $(j\omega t-j\nu\phi)$, Maxwell's equations yield[26]

$$h^2 E_\rho = \frac{\partial^2 E_y}{\partial_y \partial_\rho} - \frac{\omega\mu_o}{\rho} \nu H_y$$

$$h^2 E_\phi = \frac{-j\nu}{\rho} \frac{\partial E_y}{\partial_y} + j\omega\mu_o \frac{\partial H_y}{\partial\rho}$$

$$\left.\begin{array}{l}\\\\\\\\\\\\\end{array}\right\} \quad \text{(A-1)}$$

$$h^2 H_\rho = \frac{\partial^2 H_y}{\partial_y \partial_\rho} + \frac{\omega\varepsilon}{\rho} \nu E_y$$

$$h^2 H_\phi = - \frac{j\nu}{\rho} \frac{\partial H_y}{\partial_y} - j\omega\varepsilon \frac{\partial E_y}{\partial\rho}$$

where

$$h^2 = k^2 - k_y^2$$

k_y = propagation constant in the y-direction

$$k = \omega \sqrt{\mu_o \varepsilon_o \varepsilon_r} \quad \text{(in medium 1)}$$

$$= \omega \sqrt{\mu_o \varepsilon_o} \quad \text{(in surrounding medium)}$$

μ_o = permeability of free space

ε_o = **permittivity of free space**

ω = radian frequency.

ν = propagation constant in the ϕ direction

It is now assumed that the H_y field component is very nearly equal to zero because of the presence of the infinitely conducting ground plane, which tends to cause the magnetic field lines to lie on planes parallel to it. Under this assumption, Equations (A-1) become

$$h^2 E_\rho = \frac{\partial^2 E_y}{\partial_y \partial_\rho}$$

$$h^2 E_\phi = \frac{-j\nu}{\rho} \frac{\partial E_y}{\partial_y}$$

$$h^2 H_\rho = \frac{\omega\epsilon}{\rho} \nu E_y \tag{A-2}$$

$$h^2 H_\phi = -j\omega\epsilon \frac{\partial E_y}{\partial_\rho}$$

$$H_y \simeq 0$$

The wave equation in cylindrical coordinates is

$$\frac{\partial^2 E_y}{\partial\rho^2} + \frac{1}{\rho} \frac{\partial E_y}{\partial\rho} + \frac{\partial^2 E_y}{\partial_y^2} + (k^2 - \frac{\nu^2}{\rho^2}) E_y = 0 \tag{A-3}$$

This equation can be solved by the usual technique of assuming a product solution. The procedure leads to two ordinary differential equations, the solutions of which are known. Let

167

$$E_y = R\,(\rho h)\,Y(yk_y) \tag{A-4}$$

Then

$$\frac{d^2Y}{d(yk_y)^2} + Y = 0 \tag{A-5}$$

$$\frac{d^2R}{d(\rho h)^2} + \frac{1}{(\rho h)}\frac{dR}{d(\rho h)} + \left[1 - \frac{\nu^2}{(\rho h)^2}\right]R = 0 \tag{A-6}$$

and

$$Y = \begin{cases} A_1\,\cos\,(yk_y) & (0 \le y \le b) \\[2mm] A_1\,\cos\,(bk_y)\,e^{-(y-b)\,k_{y_0}} & (y \ge b) \end{cases} \tag{A-7}$$

$$R = \begin{cases} B_1 J_\nu(\rho h) + C_1 Y_\nu(\rho h) & (\rho_1 \le \rho \le \rho_2) \\[2mm] A_3 H_\nu^{(2)}(\rho h_o) & (\rho \ge \rho_2) \\[2mm] A_4 J_\nu(\rho h_o) & (\rho \le \rho_1) \end{cases} \tag{A-8}$$

where

$$h^2 = \varepsilon_r k_o^2 - k_y^2 \tag{A-8a}$$

$$h_o^2 = k_o^2 - k_y^2 \tag{A-8b}$$

$$k_o = 2\pi/\lambda_o$$

$$\lambda_o = \text{free-space wavelength}$$

168

J_ν = Bessel function of the first kind of order ν

Y_ν = Bessel function of the second kind of order ν

$H_\nu^{(2)}$ = Hankel function of the second kind of order ν

Now, field matching of the tangential E and H components along the boundaries of medium 1 yields the following two characteristic equations:

$$bk_y = \frac{n\pi}{Z} - \tan^{-1} \frac{k_y}{\varepsilon_r k_{y_o}} \qquad (\eta = 1,2,3, \ldots) \tag{A-9a}$$

$$\frac{Q_1 J_\nu(\rho_1 h) - J_\nu{}'(\rho_1 h)}{Q_1 Y_\nu(\rho_1 h) - Y_\nu{}'(\rho_1 h)} = \frac{Q_2 J_\nu(\rho_2 h) - J_\nu{}'(\rho_2 h)}{Q_2 Y_\nu(\rho_2 h) - Y_\nu{}'(\rho_2 h)} \tag{A-9b}$$

where

$$Q_1 = \frac{h}{\varepsilon_r h_o} \frac{J_\nu{}'(\rho_1 h_o)}{J_\nu(\rho_1 h_o)} \tag{A-10a}$$

$$Q_2 = \frac{h_1}{\varepsilon_r h_o} \frac{H_\nu^{(2)}{}'(\rho_2 h_o)}{H_\nu^{(2)}(\rho_2 h_o)} \tag{A-10b}$$

$$k_{y_o} = \left[(\varepsilon_r - 1) k_o{}^2 - k_y{}^2 \right]^{1/2} \tag{A-10c}$$

169

It is noted that Equation (A-9a) is the same characteristic equation that is obtained in solving the straight waveguide case and that its eigenvalues are independent from those associated with the ρ-variation of the fields. The $\tan^{-1}$ function appearing in (A-9a) is to be taken in the first quadrant, and the arbitrary integer η is the order of the mode, i.e., the number of half-cycle variations of each field component within the guiding rod in the y-direction. Equation (A-9a) is easily programmable for a digital computer by employing numerical techniques.

Let us consider the numerical solution of the characteristic Equation (A-9b) whose unknown is the order ν of the Bessel functions. Because of radiation in a curved guide, the order ν is a complex eigenvalue and, as such, programming Equation (A-9b) becomes a formidable task, since there are no standard subroutines available for Bessel functions of complex order. However, for guided modes, both the arguments and the order of the Bessel and Hankel functions involved in Equation (A-9b) are large compared with unity, and consequently they can be replaced by their first term approximations as[24]

$$J_\nu(z) = 1/2 \left[\frac{2}{\pi(\nu^2-z^2)^{1/2}} \right]^{1/2} \exp\left[-\frac{(\nu^2-z^2)^{3/2}}{3\nu^2} \right] \text{ for } \nu > z$$

$$J_\nu (z) = \left[\frac{2}{\pi (z^2-\nu^2)^{1/2}} \right]^{1/2} \sin \left[\frac{(z^2-\nu^2)^{3/2}}{3\nu^2} + \frac{\pi}{4} \right] \quad \text{for } z > \nu$$

$$Y_\nu (z) = - \left[\frac{2}{\pi (\nu^2-z^2)^{1/2}} \right]^{1/2} \exp \left[\frac{(\nu^2-z^2)^{3/2}}{3\nu^2} \right] \quad \text{for } \nu > z$$

$$Y_\nu = - \left[\frac{2}{\pi (z^2-\nu^2)^{1/2}} \right]^{1/2} \cos \left[\frac{(z^2-\nu^2)^{3/2}}{3\nu^2} + \frac{\pi}{4} \right] \quad \text{for } z > \nu$$

$$H_\nu^{(2)} = J_\nu - j Y_\nu \tag{A-11}$$

which are valid if

$$\left| \frac{\nu^2}{(z^a-\nu^2)^{3/2}} \right| << 1. \tag{A-12}$$

Introducing these approximations for the Bessel functions in Equation (A-9b), one obtains the following approximate characteristic equation:

$$\frac{1}{3\nu^2}\left[\left(\rho_2^2 h^2 - \nu^2\right)^{3/2} - \left(\rho_1^2 h^2 - \nu^2\right)\right]^{3/2}$$

$$= m\pi - \tan^{-1}\left[\varepsilon_r \frac{h_o^2}{h^2}\left(\frac{\rho_1^2 h^2 - \nu^2}{\nu^2 - \rho_1 h_o^2}\right)^{1/2}\right]$$

$$- \tan^{-1}\left\{\varepsilon \frac{h_o^2}{h^2}\left(\frac{\rho_1^2 h^2 - \nu^2}{\nu^2 - \rho_1 h_o^2}\right)^{1/2}\left(1 - j\ \exp\left[-\frac{2}{3}\frac{(\nu^2 - \rho_2^2 h_o^2)^{3/2}}{\nu^2}\right]\right)\right\} \quad \text{(A-13)}$$

in which m is an arbitrary integer larger than zero which deter-mines the order of the mode in the ρ-direction (or x-direction, see Figure A-1), and the $\tan^{-1}$ functions are to be taken in the first quadrant.

In order to relate the curved guide analysis to that of the straight guide, let

$$\nu = Rk_z \qquad \text{(A-14)}$$

and

$$k_z = (\varepsilon_r k_o^2 - k_y^2 - k_x^2)^{1/2} \qquad \text{(A-15)}$$

where k_x, k_y, and k_z are the transverse and axial propagation constants at x = 0 (Figure A-1).

To find the eigenvalues of the curved image guide, Equations (A-9a) and (A-13) were programmed for a digital computer. Unfor-tunately, in running various cases, numerical difficulties were

172

encountered in the search routine that solves for the eigenvalues of Equation (A-13). It was discovered that this difficulty is due to the fact that the real part of ν is much larger than its imaginary part for guided modes, i.e.,

$$\nu' \gg \nu''$$

where

$$\nu = \nu' + j\nu'' \tag{A-16}$$

The computer program did, however, find the real part of the eigenvalue, ν', correctly. On the basis of ν' and Equation (A-14), the velocity of propagation in a curved guide may be calculated, This information is important in determining the guide wavelength in a curved dielectric image guide. As expected it was found that, in all cases considered, the guide velocity, and thus the guide wavelength, increased due to the waveguide curvature. Two typical examples that were run on a digital computer are given below

$$\underline{\text{Example} \quad \#1} \quad (E_{11}^y \text{ Mode})$$

Straight Guide

$$a/b = 1$$
$$\varepsilon_r = 9$$
$$R/2a = \infty$$
$$B = 1$$
$$\lambda_o/\lambda_z = 1.075$$

Curved Guide

$$a/b = 1$$
$$\varepsilon_r = 9$$
$$R/2a = 8.8$$
$$B = 1$$
$$\lambda_o/\lambda_z = 1.014$$
$$\nu' = 25.15$$
$$\nu'' = -1.7 \times 10^{-4}$$
$$(\text{nep/rad.})$$

173

where

$$B = \frac{4b}{\lambda_o} \sqrt{\varepsilon_r - 1}$$

$$\nu = \nu' + j\nu''$$

<u>Example #2</u> (E_{11}^y Mode)

<u>Straight Guide</u>   <u>Curved Guide</u>

$a/b = 1$ $a/b = 1$

$\varepsilon_r = 9$ $\varepsilon_r = 9$

$R/2a = \infty$ $R/2a = 6$

$B = 1$ $B = 1$

$\lambda_o/\lambda_z = 1.28$ $\lambda_o/\lambda_z = 1.15$

$\nu' = 7.7$

$\nu'' = -1.15 \times 10^{-8}$

(nep/rad.)

The above calculations clearly indicated the difficulty in solving
for the imaginary part, ν'', of the eigenvalue ν. There is no rea-
son to believe that this numerical difficulty cannot be resolved,
by employing appropriate and efficient eigenvalue search routines.
At the time this work was being conducted, the above approach
was considered too costly to continue. An alternate solution
to calculating ν'', and thus radiation losses, was considered
and is presented in Appendix B. This second approach, however,
cannot be used to predict the velocity or guide wavelength
in a curved waveguide.

174

APPENDIX B

RADIATION LOSSES IN

DIELECTRIC IMAGE GUIDES

OF RECTANGULAR CROSS SECTION

175

APPENDIX B

RADIATION LOSSES IN DIELECTRIC IMAGE GUIDES

OF RECTANGULAR CROSS SECTION

1. INTRODUCTION

In general, any curved dielectric waveguide loses energy
into the surrounding medium by radiation. The amount of radia-
tion loss in a strong function of the mean radius of curvature R.
The problem, thus, is to estimate the minimum allowable radius
of curvature for a specified insertion loss due to radiation.

In an attempt to provide an answer to this problem, this
Appendix is devoted to curvature effects in curved image guides.

2. ANALYSIS

Figure B-1 shows a representation of a curved dielectric
image guide (top view). The shaded wave-guiding region has a
dielectric constant larger than that of the surrounding region,
resulting in a transverse field distribution for the guided mode
$F(x)$ which decays exponentially but remains finite. To obtain
an approximate expression for radiation loss (dB/radian) as a
function of bending radius R, this may be visualized as a two-
dimensional guide with an isotropic surrounding region capable
of supporting a free-space radiating wave. Note that at some
transverse distance x_r the maintenance of a pure guided mode with
equiphase fronts on radial planes required energy propagating at
the speed of light, and for $x > x_r$ a pure guided mode implies
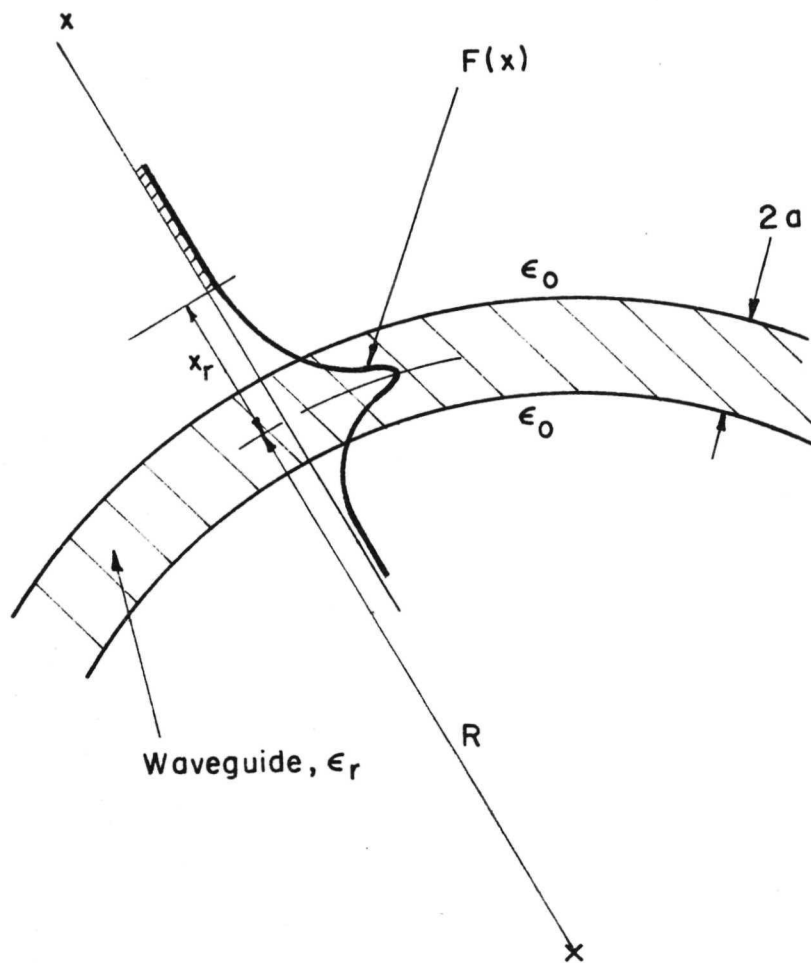energy propagating at greater than the velocity of light. This

176

Fig. B-I A CURVED DIELECTRIC WAVEGUIDE

is true at some value of x_r for any finite bend radius R, since F(x) extends indefinitely in the x-direction. To a first approximation, it is assumed here that the transverse field distribution F(x) is virtually the same in the curved region as in a straight guide for large R. The fraction of energy in the guided mode at $x > x_r$ is assumed to be lost to radiation; this loss is taken to occur in a longitudinal distance equal to the collimated-beam length associated with the field F(x). All these assumptions imply that any mode propagating along the curved open guide radiates.

It is shown elsewhere[25] that the attenuation constant (due to radiation) for the fundamental mode (E_{11}^y) of the bend region is given by

$$\alpha_r = \frac{1}{2Z_c} \frac{E_\ell}{E_T} \tag{B-1}$$

where

$$E_\ell = \frac{1}{2k_{xo}} \cos^2 (ak_x) \exp\left[-2k_{xo} (x_r-a)\right] \tag{B-2}$$

$$E_T = a + \frac{\sin(2ak_x)}{2k_x} + \frac{\cos^2(ak_x)}{k_{xo}} \tag{B-3}$$

$$Z_c = \frac{2\left[a+\cos(ak_x)/k_{xo}\right]^2}{\lambda_o} \tag{B-4}$$

$$X_r = \left(\frac{k_z-k_o}{k_o}\right) R \tag{B-5}$$

178

k_x = propagation constant in the x-direction

$$k_{xo} = \left[(\varepsilon_{re}-1) \; k_o^2 - k_x^2 \right]^{1/2} \tag{B-6}$$

$$\varepsilon_{re} = \varepsilon_r - \frac{k_y^2}{k_o^2} \tag{B-7}$$

k_y = propagation constant in the transverse y-direction

$$k_z = \varepsilon_r k_o^2 - k_y^2 - k_x^2 \tag{B-8}$$

$$k_o = 2\pi/\lambda_o$$

λ_o = free-space wavelength.

The transverse propagation constants k_x and k_y are obtained by solving the following characteristic equations:

$$bk_y = \frac{\pi}{2} - \tan^{-1} \left(\frac{k_y}{\varepsilon_r k_{yo}} \right) \tag{B-9}$$

179

$$ak_x = \frac{\pi}{2} - \tan^{-1}\left(\frac{k_x}{k_{xo}}\right) \tag{B-10}$$

Equations (B-9) and (B-10) result from applying the appropriate boundary conditions at the image guide interfaces.

3. NUMERICAL RESULTS

Equations (B-1) through (B-10) were programmed for a digital computer and typical results are shown in Figure B-2 for an image guide with $\varepsilon_r = 9$ and an aspect ratio of $a/b = 1$. The cross section of the guide is 2axb, and the attenuation constant α_r in dB/radian is plotted versus the normalized height of the image guide defined as

$$B = \frac{4b}{\lambda_o}\sqrt{\varepsilon_r - 1}$$

These results clearly indicate the extremely rapid variation of the radiation loss with frequency, which is typical for curved dielectric waveguides.[24]
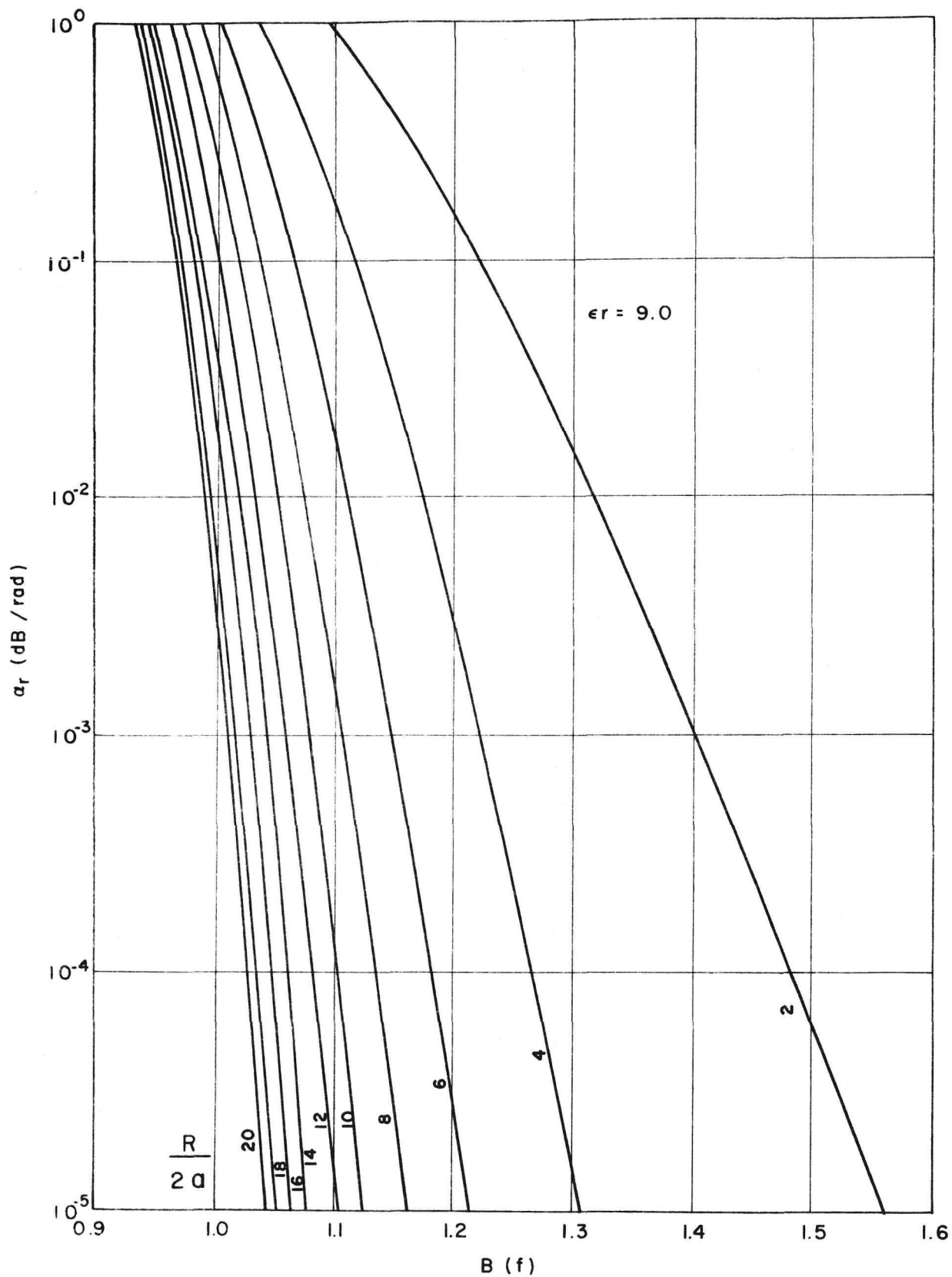
Fig. B-2 ATTENUATION CONSTANT DUE TO RADIATION

REFERENCES

1. D. D. King, "Dielectric Image Line," *Journal of Applied Physics*, V. 23, June 1952, pp. 699-700.

2. D. D. King, "Properties of Dielectric Image Lines," *IRE Trans. on Microwave Theory and Techniques*, V. MTT-3, March 1955, pp. 75-81

3. D. D. King and S. P. Schlesinger, "Losses in Dielectric Image Lines," *IRE Trans. on Microwave Theory and Techniques*, V. MTT-3, December 1955, pp. 35-39.

4. C. H. Chandler, "An Investigation of Dielectric Rod as Waveguide," *Journal of Applied Physics*, V. 20, December 1949, pp. 1188-1192.

5. W. M. Elsasser, "Attenuation in a Dielectric Circular Rod," *Journal of Applied Physics*, V. 20, December 1949, p. 1192.

6. R. H. DuHamel and J. W. Duncan, "Launching Efficiency of Wires and Slots for a Dielectric Waveguide," *IRE Trans. on Microwave Theory and Techniques*, V. MTT-6, July 1958, pp. 277-284.

7. R. H. DuHamel, "The Efficiency of Excitation of a Surface Wave on a Dielectric Cylinder," *IRE Trans. on Microwave Theory and Techniques*, V. MTT-7, April 1959, pp. 257-268.

8. J. W. Duncan and R. H. DuHamel, "A Technique for Controlling the Radiation from Dielectric Rod Waveguides," *IRE Trans. on Antennas and Propagation*, V. AP-5, July 1957, pp. 284-289.

9. A. Okaya and L. F. Bardsi, "The Dielectric Microwave Resonator," *Proc. of the IRE*, V. 50, October 1962, pp. 2081-2091.

10. R. V. D'Aiello and H. J. Proger, "Dielectric Resonators for Microwave Applications," *IEEE Trans. on Microwave Theory and Techniques*, V. MTT-12, September 1964, p. 549.

11. R. D. Richtmeyer, "Dielectric Resonator," *Journal of Applied Physics*, V. 10, June 1930, p. 391.

12. D. D. King, "Circuit Components in Dielectric Image Lines," *IRE Trans. on Microwave Theory and Techniques*, V. MTT-3, December 1955, pp. 35-39.

REFERENCES (cont.)

13. H. G. Fox, "Dielectric Waveguide Techniques for Milli-
     meter Waves," presented at the IRE Convention, New York,
     N.Y., 1952.

14. D. D. King and S. P. Schlesinger, "Dielectric Image
     Lines," IRE Trans. on Microwave Theory and Techniques,
     V. MTT-8, July 1958, pp. 291-299.

15. R. M. Knox and P. P. Toulios, "Integrated Circuits for
     the Millimeter through Optical Frequency Range," pre-
     sented at the Symposium on Millimeter Waves, New York,
     N.Y., March 1970.

16. R. M. Knox and P. P. Toulios, "Rectangular Dielectric
     Image Lines for Millimeter Integrated Circuits," Western
     Electronic Show and Convention, Los Angeles, California,
     August 25-28, 1970.

17. P. P. Toulios, "Image Line Millimeter Integrated Cir-
     cuits - Directional Coupler Design," Proc. of the National
     Electronics Conference, Chicago, Illinois, December 7-9,
     1970.

18. R. M. Knox and P. P. Toulios, "Alumina Image Guides for
     Millimeter Integrated Circuits," IIT Research Institute
     Technical Note FT/RFD-109, February 1971.

19. R. A. Pucel, et al., "Losses in Microstrip," IEEE Trans.
     on Microwave Theory and Techniques, Vol. MTT-16, No. 6,
     June 1966, pp. 342-350.

20. W. S. Jones, "A Survey of Some Conditions Limiting the
     Application of Hybrid Microstripline Techniques at Milli-
     meter-Wave Frequencies," Texas Instruments Technical
     Report 03-68-85, December 9, 1968.

21. H. Sobol, "Applications of Integrated Circuit Technology
     to Microwave Frequencies," Proc. IEEE, V. 59, August 1971,
     pp. 1200-1211.

22. T. C. Reissing, "An Overview of Today's Thick Film Tech-
     nology," Proc. IEEE, V. 59, October 1971, pp. 1448-1454.

23. M. Caulton, "Film Technology in Microwave Integrated
     Circuits," Proc. IEEE, V. 59, October 1971, pp. 1481-
     1489.

REFERENCES (cont.)

24. E. A. J. Marcatili, "Bends in Optical Dielectric Guides,"
    Bell System Technical Journal, V. 48, September 1969,
    pp. 2103-2132.

25. E. A. J. Marcatili and S. E. Miller, "Improved Relations
    Describing Directional Control in Electromagnetic Wave
    Guidance," Bell System Technical Journal, V. 48, September 1969, pp. 2161-2188.

26. E. C. Jordan, Electromagnetic Waves and Radiating Systems, Prentice-Hall, Inc., Englewood Cliffs, N.J., 1950.